NASA TN D-1002

TECHNICAL NOTE

D-1002

AERODYNAMIC CHARACTERISTICS OF A CANARD AND AN OUTBOARD-TAIL AIRPLANE MODEL AT HIGH SUBSONIC SPEEDS

By Paul G. Fournier

Langley Research Center
Langley Air Force Base, Va.

NATIONAL AERONAUTICS AND SPACE ADMINISTRATION
WASHINGTON
November 1961

NATIONAL AERONAUTICS AND SPACE ADMINISTRATION

TECHNICAL NOTE D-1002

AERODYNAMIC CHARACTERISTICS OF A CANARD AND AN OUTBOARD-TAIL AIRPLANE MODEL AT HIGH SUBSONIC SPEEDS

By Paul G. Fournier

SUMMARY

An investigation has been made in the Langley high-speed 7- by 10-foot tunnel through a range of Mach numbers from 0.60 to 0.95 of the static longitudinal and lateral stability and control characteristics of a canard airplane configuration and an outboard-tail configuration. The canard model had a twisted wing with approximately 67° of sweepback and an aspect ratio of 2.91 and was tested with three trapezoidal canard surfaces having ratios of exposed area to wing area of 0.032, 0.076, and 0.121. The canard model had a single body-mounted vertical tail. The outboard-tail model had its horizontal- and vertical-tail surfaces mounted on slender bodies attached to the wing tips and located to the rear and outboard of the 67° sweptback wing of aspect ratio 1.00. The data, which are presented with limited analysis, provide information at high subsonic speeds on these two types of high-speed airplanes which have previously been tested at supersonic speeds and reported in NACA RM L58B07 and NACA RM L58E20.

INTRODUCTION

Problems of trim drag and of maintaining adequate longitudinal and lateral stability throughout the operational angle-of-attack range for high-speed airplanes have stimulated research on many different types of airplane configurations. A study of these problems is presented in reference 1 and some configurations designed to alleviate these problems are suggested in references 1 and 2. The present investigation, which is presented with limited analysis, was undertaken to provide stability and

control information at high subsonic speeds on two different types of high-speed airplanes previously tested at supersonic speeds as reported in references 3 and 4.

The outboard-tail model and the canard model tested in the present investigation were related in that both models used the same body and the wings had the same leading-edge and trailing-edge sweep angles and the same root-chord length. The present canard configuration was tested with three different sizes of canard surfaces in combination with the twisted wing used in the investigation of reference 4. Test results at subsonic speeds for these models were obtained in the Langley high-speed 7- by 10-foot tunnel at Mach numbers from 0.60 to 0.95 and the corresponding test Reynolds number range varied from 2.1×10^6 to 3.4×10^6 based on the mean aerodynamic chord. Both static longitudinal and lateral stability data were obtained for a maximum angle-of-attack range of approximately -2° to 22°.

COEFFICIENTS AND SYMBOLS

The axis system used and the direction of positive forces, moments, and angles are presented in figure 1. The basic reference area, span, and mean aerodynamic chord used for the reduction of the outboard-tail model data were based on the composite geometry of the wing plus horizontal-tail surfaces whereas the geometry of the wing alone was used for the canard model. The reference center of moments (center-of-gravity positions) are indicated in figures 2 and 3 for the respective models. Coefficients and symbols are defined as follows:

C_L lift coefficient, $\frac{\text{Lift}}{qS}$

C_D drag coefficient, $\frac{\text{Drag}}{qS}$

C_m pitching-moment coefficient, $\frac{\text{Pitching moment}}{qS\bar{c}}$

C_l rolling-moment coefficient, $\frac{\text{Rolling moment}}{qSb}$

C_n yawing-moment coefficient, $\frac{\text{Yawing moment}}{qSb}$

C_Y lateral-force coefficient, $\frac{\text{Lateral force}}{qS}$

C_{l_β}	rolling moment due to sideslip, $\frac{\partial C_l}{\partial \beta}$, per deg
C_{n_β}	yawing moment due to sideslip, $\frac{\partial C_n}{\partial \beta}$, per deg
C_{Y_β}	lateral force due to sideslip, $\frac{\partial C_Y}{\partial \beta}$, per deg
b	span of wing for canard model or wing plus horizontal tail for outboard-tail model, ft
c	wing chord, ft
$\bar{c}$	mean aerodynamic chord of wing for canard model or wing plus horizontal tail for outboard-tail model, ft
i_t	incidence of outboard horizontal-tail surface, positive when trailing edge is down, deg
q	free-stream dynamic pressure, $\frac{\rho V^2}{2}$, lb/sq ft
L/D	lift-drag ratio
M	Mach number
S	area of wing for canard model or wing plus horizontal tail for outboard-tail model, sq ft
V	free-stream velocity, ft/sec
α	angle of attack, deg
β	angle of sideslip, deg
δ_c	canard control deflection, positive when trailing edge is down, deg
ρ	mass density of air, slugs/cu ft
Λ	sweep angle, deg

Subscripts:

le	leading edge
te	trailing edge

Configuration designation:

W	wing not including outboard-tail surface, outboard-tail model
W_1	twisted wing, canard model
F	fuselage
B	outer bodies
V	twin vertical-tail surface
V_1	single vertical tail
H	outboard horizontal-tail surface
C_1	medium canard
C_2	small canard
C_3	large canard

MODEL, APPARATUS, AND TESTS

Details of the outboard-tail model and the canard model are shown in figures 2 and 3, respectively, and the geometric characteristics are given in tables I and II. The outboard-tail model used in the present investigation is the same model as that of reference 3 which was tested in the Langley 4-foot supersonic pressure tunnel. The wing had NACA 65A004 airfoil section at the wing root and NACA 65A003.5 airfoil section at 0.60 semispan, whereas the horizontal panel had a 0.40-chord hexagonal section. All airfoil sections given were parallel to the plane of symmetry. The wing had an aspect ratio of 1.00, a taper ratio of 0.33, and had a leading-edge sweepback angle of 67° (fig. 2). Each outboard body had a conical nose section, a cylindrical center section, and was arbitrarily faired into a square cross section in the vicinity of the tails. The vertical tails had a 0.40-chord hexagonal section.

The canard configuration was the same model with the twisted wing which was tested in the Langley 4-foot supersonic pressure tunnel (ref. 4). The model had a wing with linear twist to 4° washout at the tip and was composed of NACA 65A series sections with thickness ratios of 4 percent at the root, 3.5 percent at the 50-percent semispan, and 3 percent at the tip. The wing had a sweep of about 67° and an aspect ratio of 2.91 (fig. 3). The vertical tail and canard surfaces had hexagonal sections and a thickness ratio of 3 percent. Three sizes of canard surfaces were tested; these three were designated as small, medium, and large and had ratios of exposed area to wing area of 0.032, 0.076, and 0.121, respectively.

The coordinates for the elliptical cross-section fuselage used for both models are found in references 3 and 4; the fuselage was indented by the area-rule method for $M = 1.4$.

The models were tested on the sting-support system of the Langley high-speed 7- by 10-foot tunnel which was remotely operated through an angle-of-attack range from -2° to 22°. The tests were made through a Mach number range of 0.60 to 0.95, which corresponds to a Reynolds number range from approximately 2.1×10^6 to 3.4×10^6 based on the wing mean aerodynamic chord. Photographs of the two models tested are presented in figure 4.

Some tests of the outboard-tail model as well as the canard model were made with transition strips of 0.10-inch width located at 10 percent of the body length and wing chord. The particles used to make up the roughness of the transition strips were of such size as to have a Reynolds number based on roughness height in excess of the minimum critical value based on the criteria presented in reference 5.

CORRECTIONS

Blockage corrections determined by the method of reference 6 were applied to the data. Jet-boundary corrections to angle of attack and drag were determined from reference 7 and added to the angle-of-attack and drag coefficients.

Tares due to the sting support, which past experience has shown to be negligible, have not been applied. The drag has been adjusted to correspond to free-stream static pressure acting on the base of the model.

The angles of attack and sideslip have been corrected for deflection of the sting support and balance under load. No attempt has been made to correct the data for aeroelastic distortion of the wing.

PRESENTATION OF RESULTS

The static longitudinal and lateral aerodynamic stability characteristics for the outboard-tail model are presented in figures 5 to 10. The static longitudinal and lateral aerodynamic stability characteristics for the canard model are presented in figures 11 to 23. For convenience, an index to the data figures is presented in the following table:

SUMMARY OF RESULTS

A detailed discussion of results obtained in the investigation at Mach numbers from 0.60 to 0.95 of an outboard-tail airplane model and a canard airplane model has been omitted; however, a few general observations are made.

For the center-of-gravity location selected for the present tests, the data for the outboard-tail configuration indicate longitudinal stability and control up to moderate lift coefficients as well as lateral stability throughout the range of angles of attack.

The data for the canard configuration indicate that longitudinal stability and control up to moderate lift coefficients were obtained only with the small canard surface. As the canard-surface size increased, a forward movement in location of the center of gravity would be required, as expected, for the configuration with the larger canard surfaces to have longitudinal stability and control. In general, the data indicate lateral stability throughout the range of angle of attack for the model with the small canard surface. However, the range of angle of attack for stability decreased with increasing canard-surface size.

Langley Research Center,
National Aeronautics and Space Administration,
Langley Air Force Base, Va., June 26, 1961.

REFERENCES

1. Spearman, M. Leroy: Some Factors Affecting the Static Longitudinal and Directional Stability Characteristics of Supersonic Aircraft Configurations. NACA RM L57E24a, 1957.

2. Sleeman, William C., Jr.: Preliminary Study of Airplane Configurations Having Tail Surfaces Outboard of the Wing Tips. NACA RM L58B06, 1958.

3. Spearman, M. Leroy, and Robinson, Ross B.: Aerodynamic Characteristics of a Canard and an Outboard-Tail Airplane Model at a Mach Number of 2.01. NACA RM L58B07, 1958.

4. Spearman, M. Leroy, and Robinson, Ross B.: Longitudinal Stability and Control Characteristics at Mach Numbers of 1.41 and 2.01 of a 67° Swept-Wing Airplane Configuration With Canard Control Surfaces. NACA RM L58E20, 1958.

5. Von Doenhoff, Albert E., and Horton, Elmer A.: A Low-Speed Experimental Investigation of the Effect of a Sandpaper Type of Roughness on Boundary-Layer Transition. NACA Rep. 1349, 1958. (Supersedes NACA TN 3857.)

6. Herriot, John G.: Blockage Corrections for Three-Dimensional-Flow Closed-Throat Wind Tunnels, With Consideration of the Effect of Compressibility. NACA Rep. 995, 1950. (Supersedes NACA RM A7B28.)

7. Gillis, Clarence L., Polhamus, Edward C., and Gray, Joseph L., Jr.: Charts for Determining Jet-Boundary Corrections for Complete Models in 7- by 10-Foot Closed Rectangular Wind Tunnels. NACA WRL-123, 1945. (Formerly NACA ARR L5G31.)

TABLE I.- GEOMETRIC CHARACTERISTICS OF OUTBOARD-TAIL MODEL

Wing plus horizontal tail (used in reduction of data):	
Area, sq ft	1.278
Span, ft	1.667
Mean aerodynamic chord, ft	0.939
Aspect ratio	2.174
Taper ratio	0.222
Wing (inboard of outer body, including fuselage intercept):	
Area, sq ft	1.000
Span, ft	1.000
Mean aerodynamic chord, ft	1.083
Aspect ratio	1.000
Taper ratio	0.333
Leading-edge sweepback, deg	67.01
Trailing-edge sweepback, deg	19.65
Airfoil section parallel to plane of symmetry -	
Root	NACA 65A004
Tip	NACA 65A003.5
Body:	
Length, in.	39.000
Maximum cross-sectional area, sq in.	6.072
Diameter of equivalent circle, in.	2.78
Length-diameter ratio	14.03
Base area, sq in.	2.99
Vertical tail (exposed), each:	
Area, sq ft	0.104
Span, ft	0.279
Mean aerodynamic chord, ft	0.404
Taper ratio	0.33
Leading-edge sweep, deg	64.7
Aspect ratio	0.75
Airfoil section parallel to plane of symmetry	Hexagonal
Thickness, percent chord	4
Horizontal tail (exposed), each:	
Area, sq ft	0.099
Span, ft	0.250
Tip chord, ft	0.333
Root chord, ft	0.458
Leading-edge sweep, deg	61.7
Taper ratio	0.728
Airfoil section parallel to plane of symmetry	Hexagonal
Thickness, percent chord	4

TABLE II.- GEOMETRIC CHARACTERISTICS OF CANARD MODEL

Wing:		
Area, sq ft		1.375
Span, ft		2.000
Mean aerodynamic chord, ft		0.895
Taper ratio -		
Inboard		0.333
Outboard		0.500
Total		0.167
Sweep, deg -	Λ_{le}	Λ_{te}
Inboard	67.01	19.65
Outboard	61.70	53.61
Aspect ratio		2.91
Airfoil section parallel to plane of symmetry at -		
Root		NACA 65A004
0.5 semispan		NACA 65A003.5
Tip		NACA 65A003
Body:		
Length, in.		39.000
Maximum cross-sectional area, sq in.		6.072
Diameter of equivalent circle, in.		2.78
Length-diameter ratio		14.03
Base area, sq in.		2.99
Vertical tail:		
Area to fuselage center line, sq ft		0.279
Span, ft		0.478
Mean aerodynamic chord, ft		0.641
Taper ratio		0.29
Leading-edge sweep, deg		65.0
Aspect ratio		0.82
Airfoil section parallel to plane of symmetry		Hexagonal
Thickness, percent chord		3

Canard surfaces:	Small (C_2)	Medium (C_1)	Large (C_3)
Area, exposed, sq ft	0.044	0.104	0.166
Span, total, ft	0.387	0.548	0.666
Tip chord, ft	0.113	0.157	0.190
Root chord (to center line), ft	0.282	0.391	0.476
Taper ratio	0.410	0.410	0.410
Midchord sweep, deg	0	0	0
Ratio of exposed area to wing area	0.032	0.076	0.121

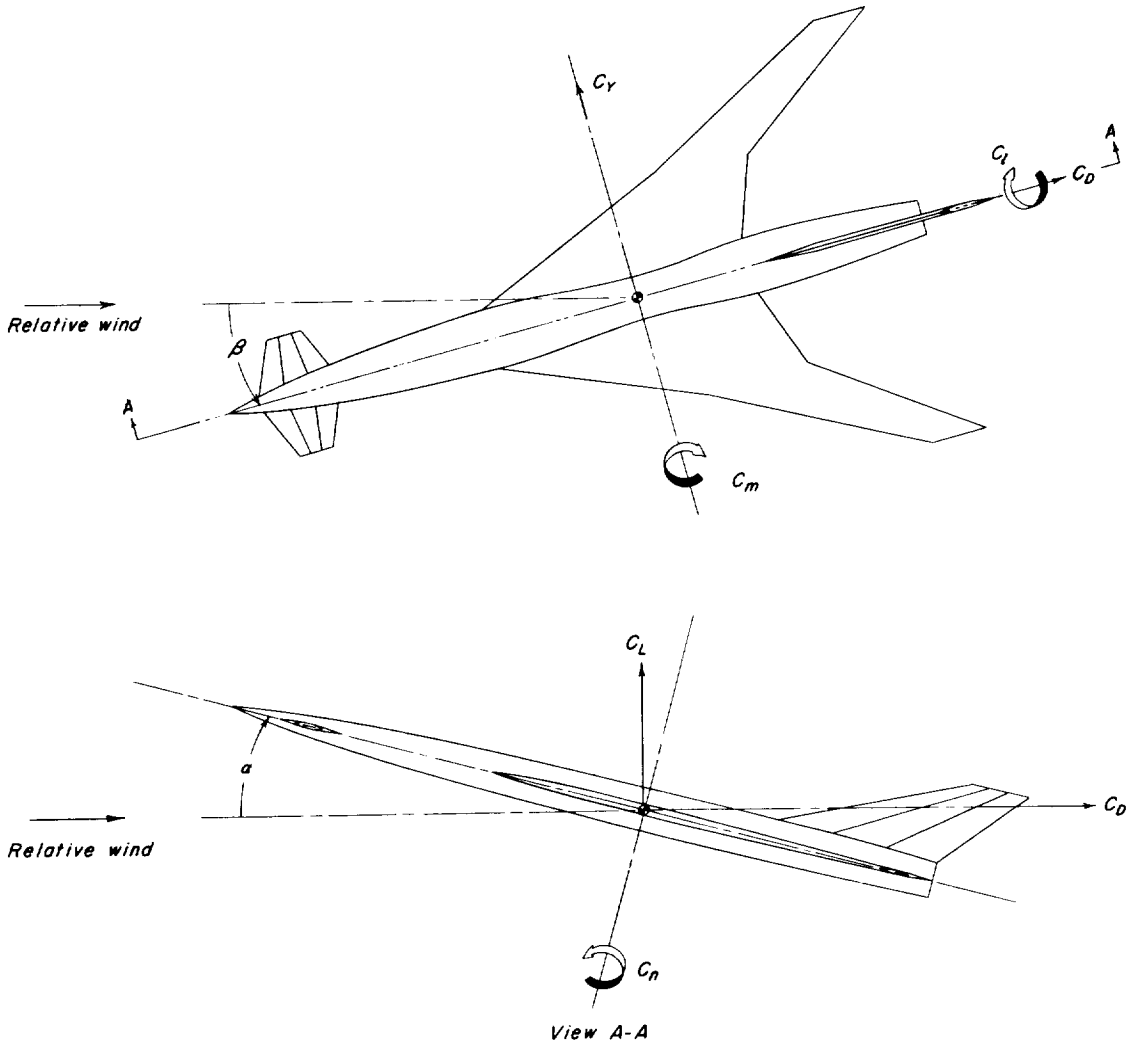

Figure 1.- Axes system and convention used to define positive sense of forces, moments, and angles.

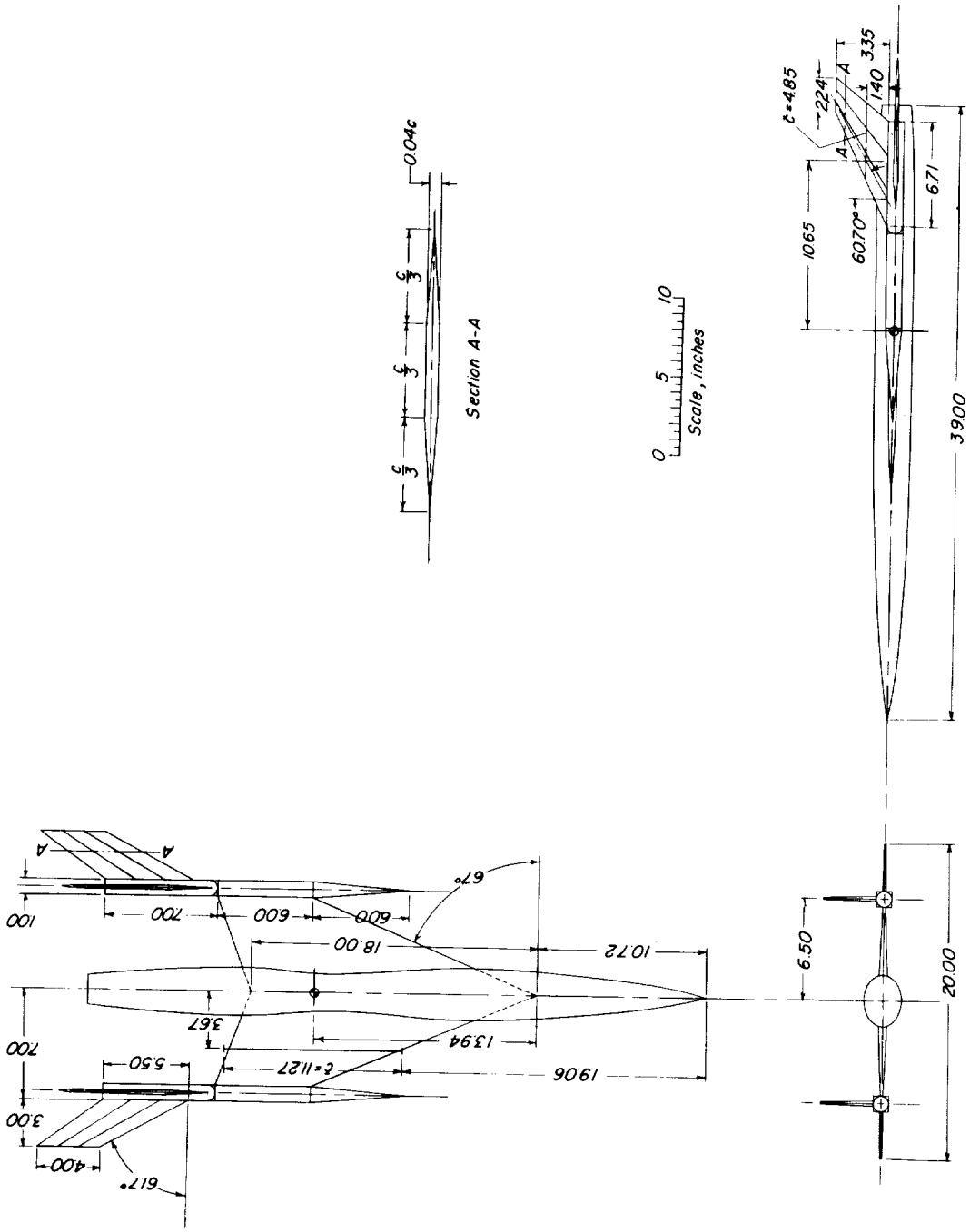

Figure 2.- Drawing of outboard-tail model.

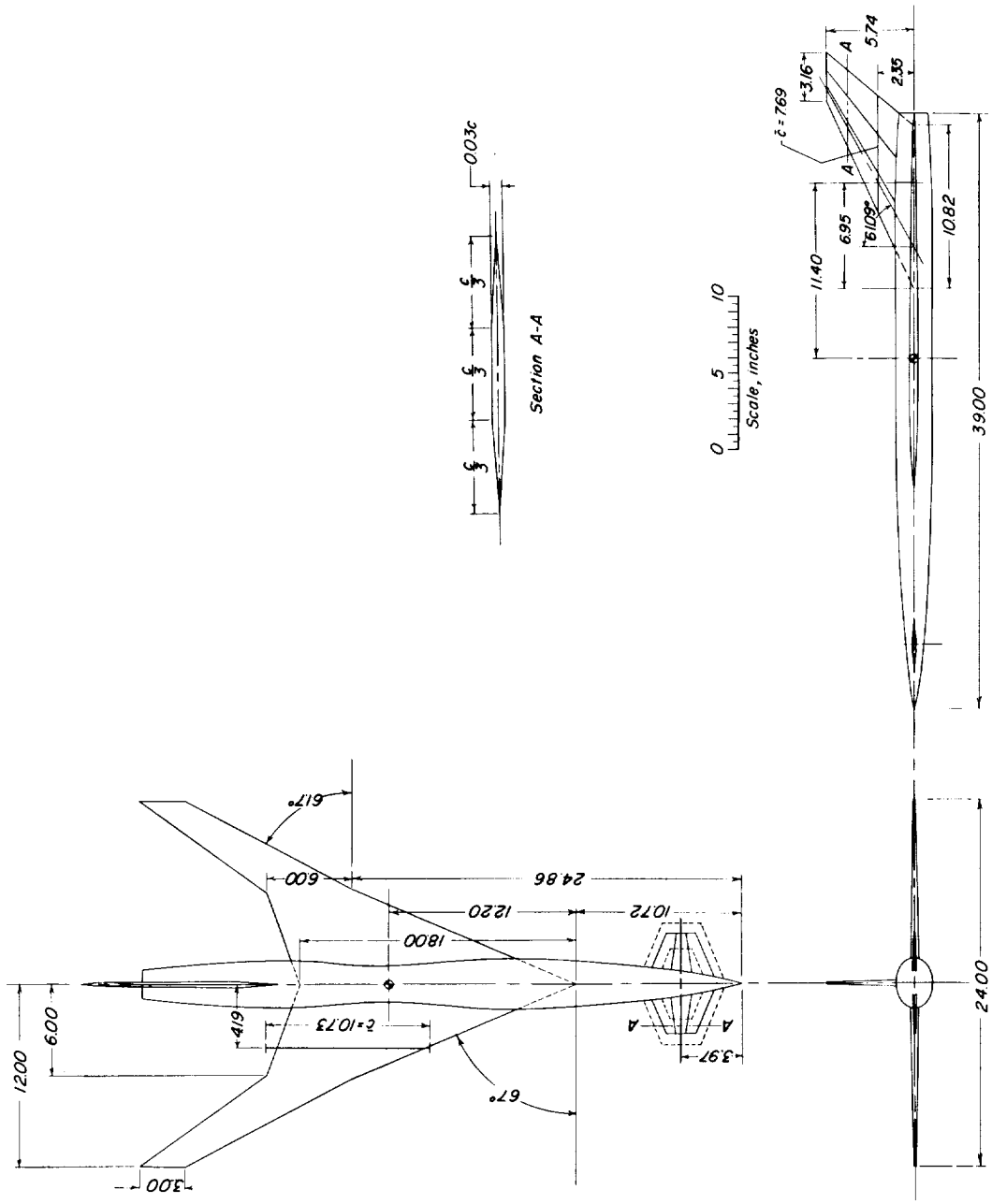

Figure 3.- Drawing of canard model.

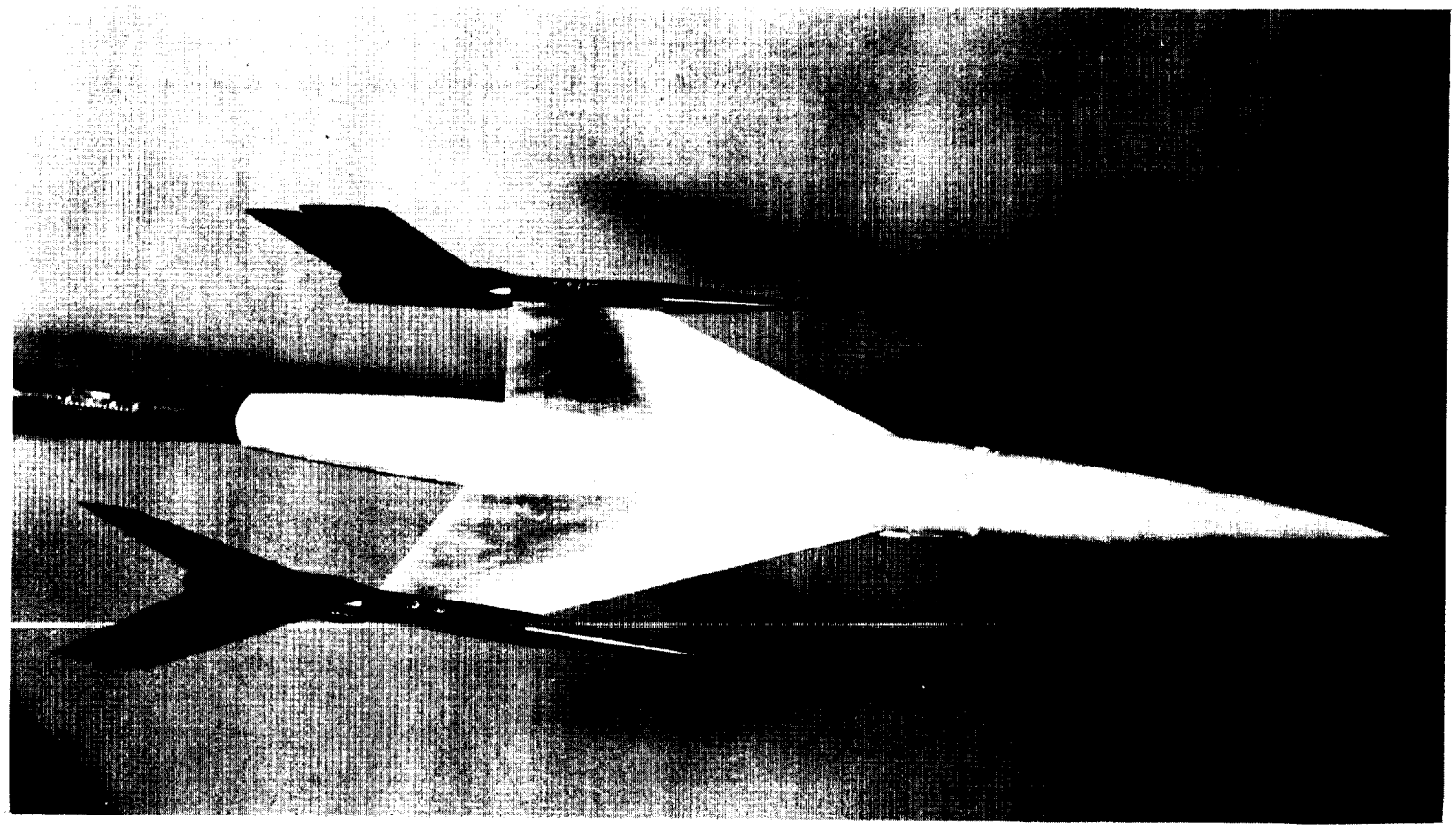

(a) Outboard-tail model. L-57-3253

Figure 4.- Photographs of models.

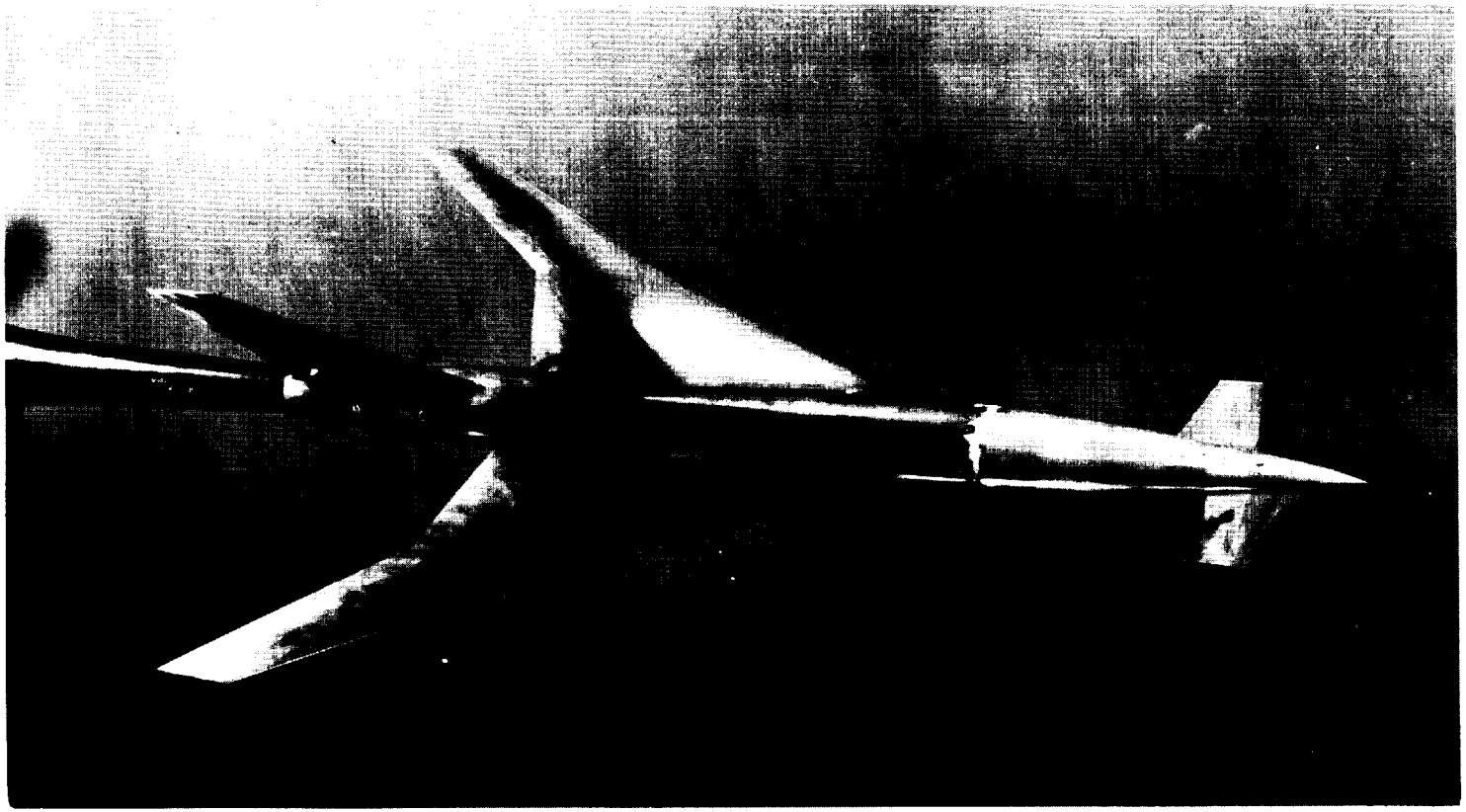

(b) Canard model. L-57-3254

Figure 4.- Concluded.

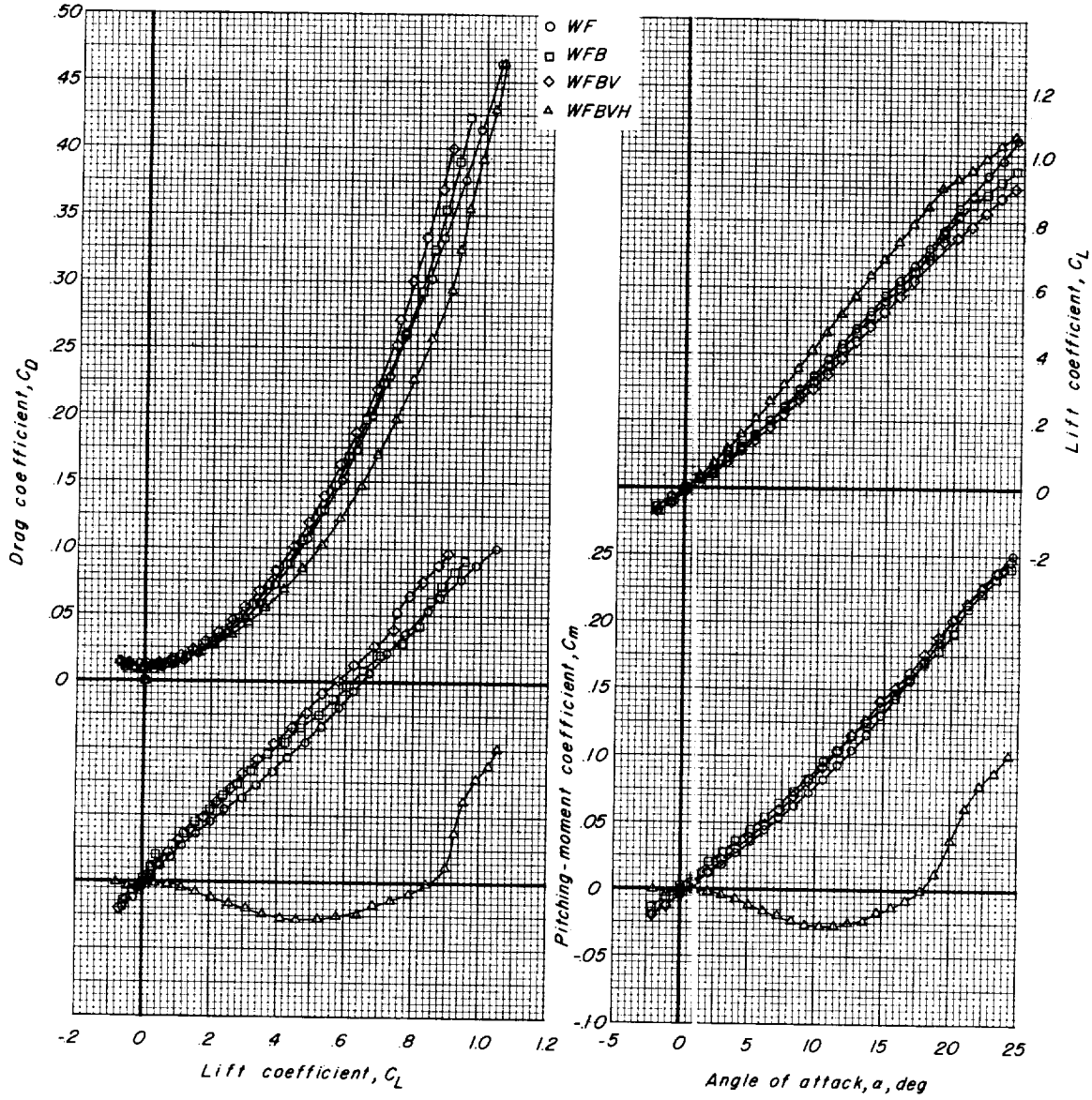

(a) M = 0.60.

Figure 5.- Static longitudinal stability characteristics for various component parts of outboard-tail model. Transition free; $i_t = 0^\circ$.

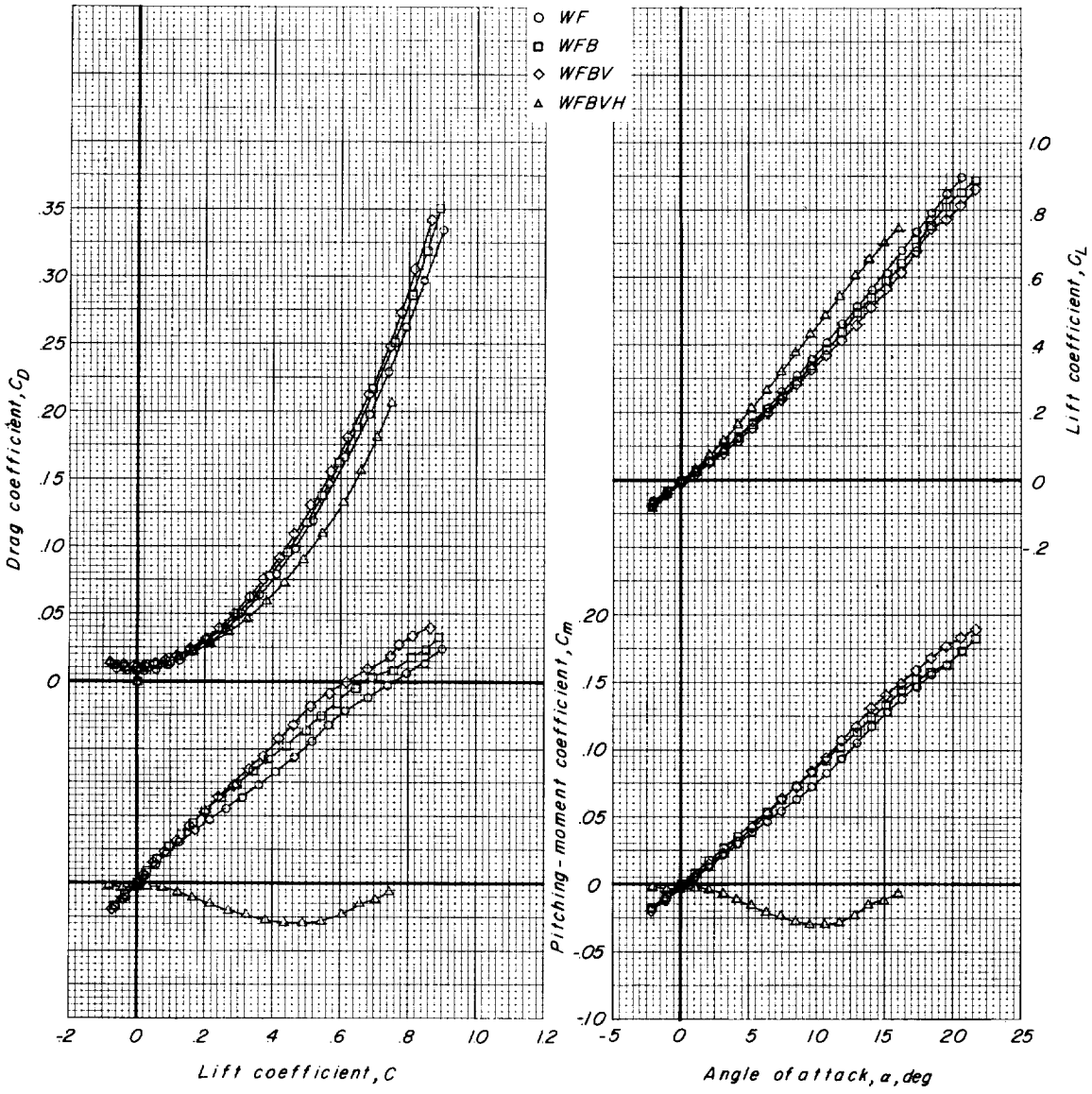

(b) M = 0.80.

Figure 5.- Continued.

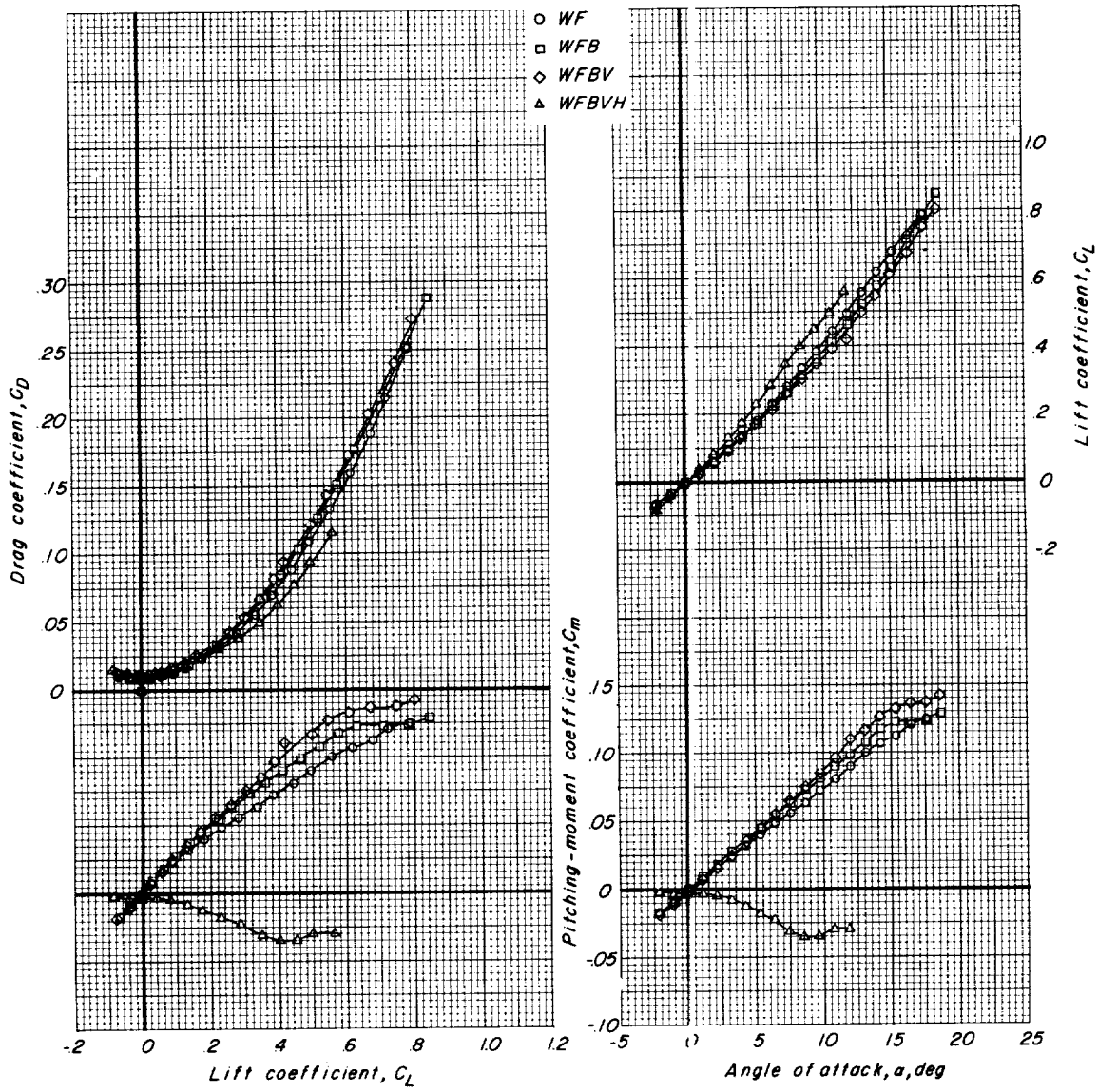

(c) M = 0.90.

Figure 5.- Continued.

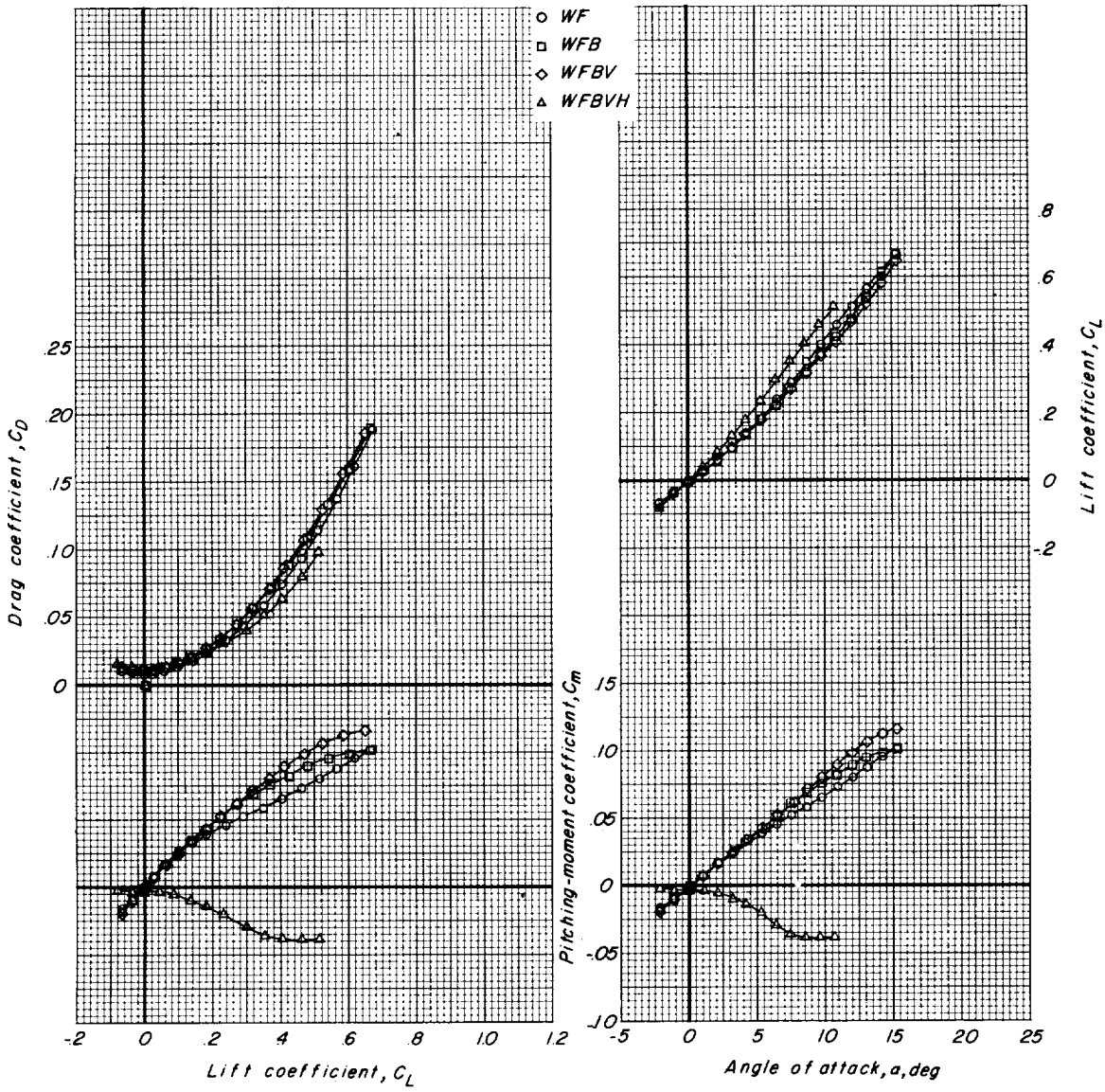

(d) M = 0.95.

Figure 5.- Concluded.

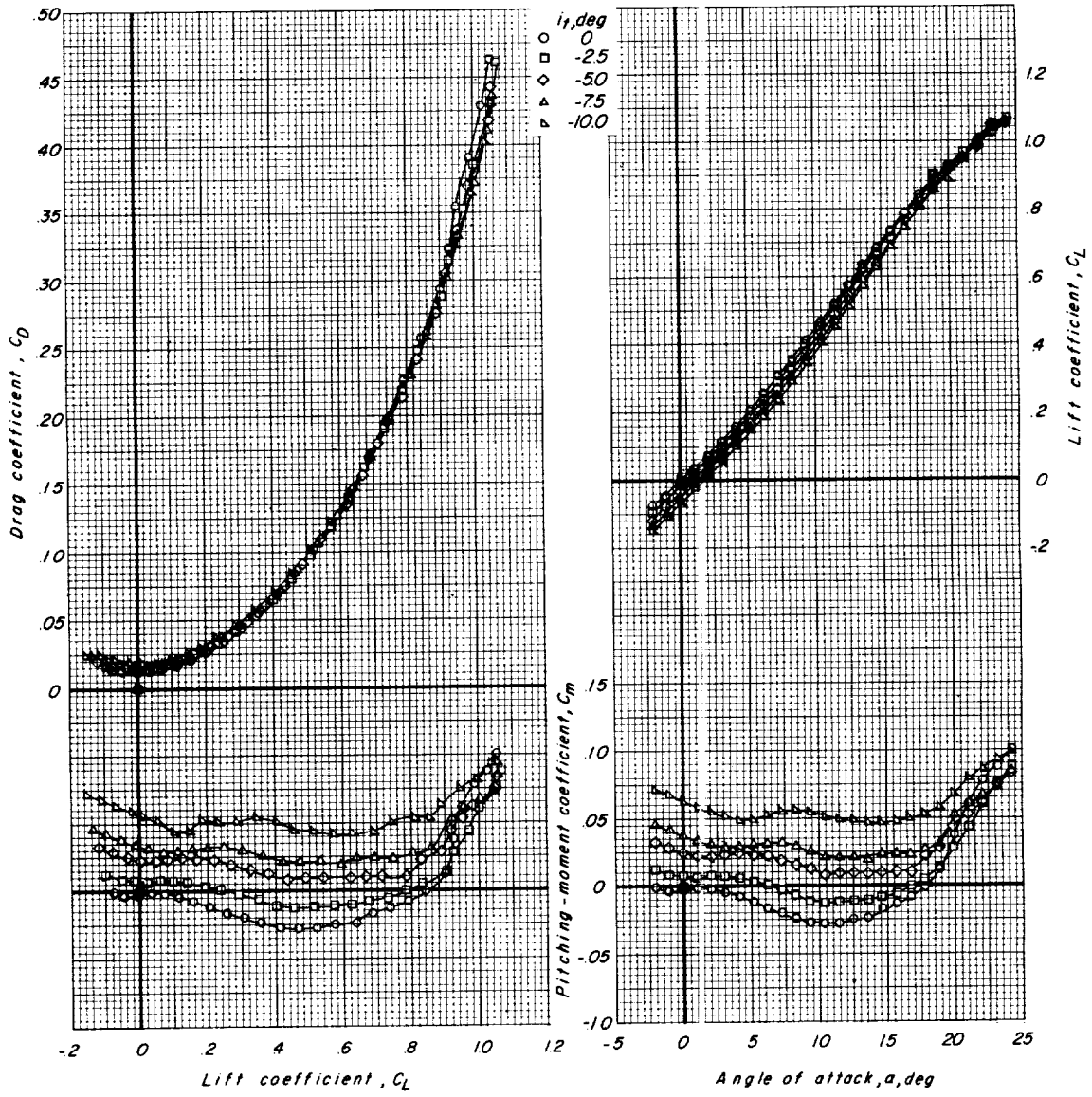

(a) M = 0.60.

Figure 6.- Static longitudinal stability characteristics for complete outboard-tail model with various control deflections. Transition free.

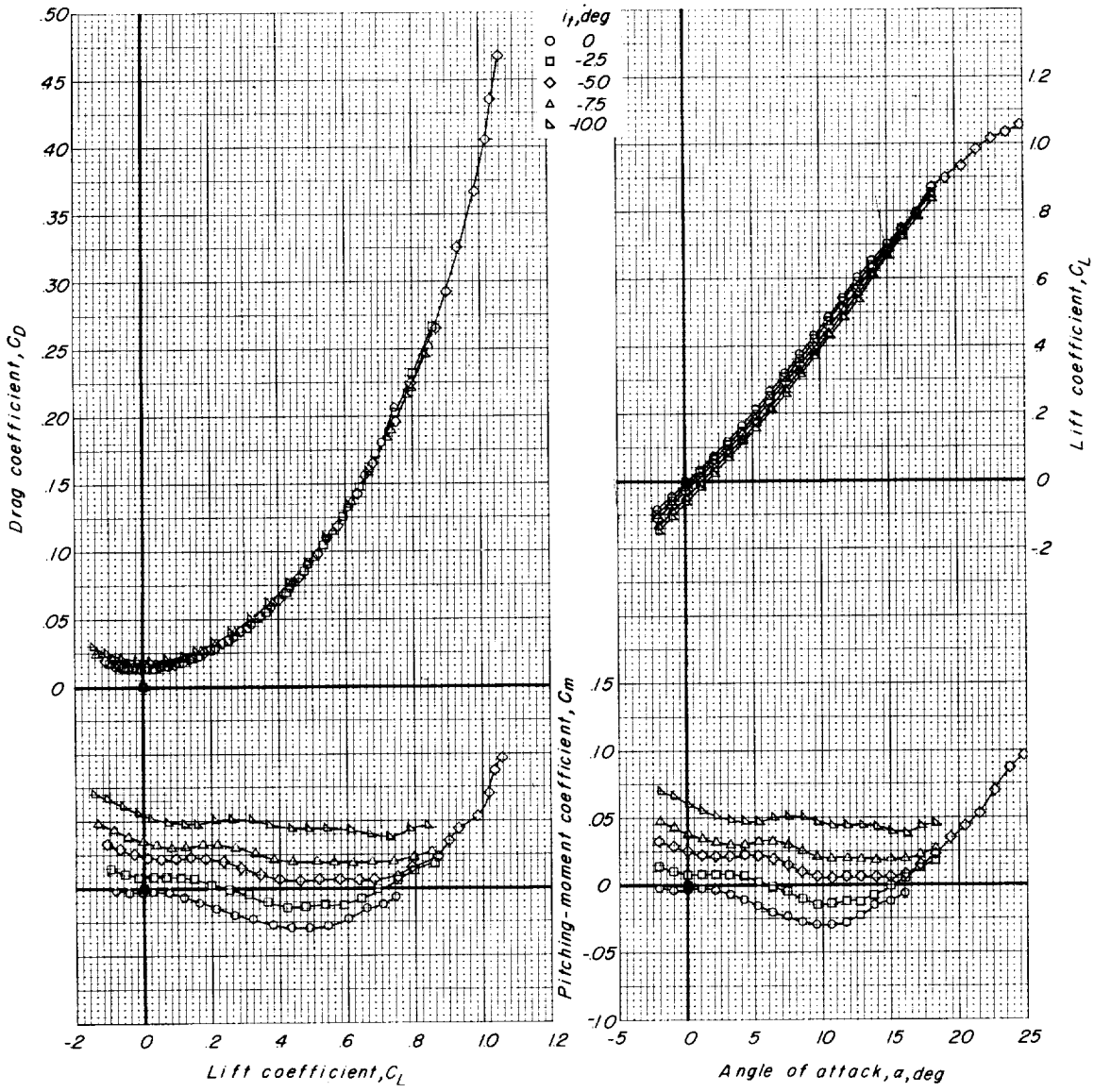

(b) M = 0.80.

Figure 6.- Continued.

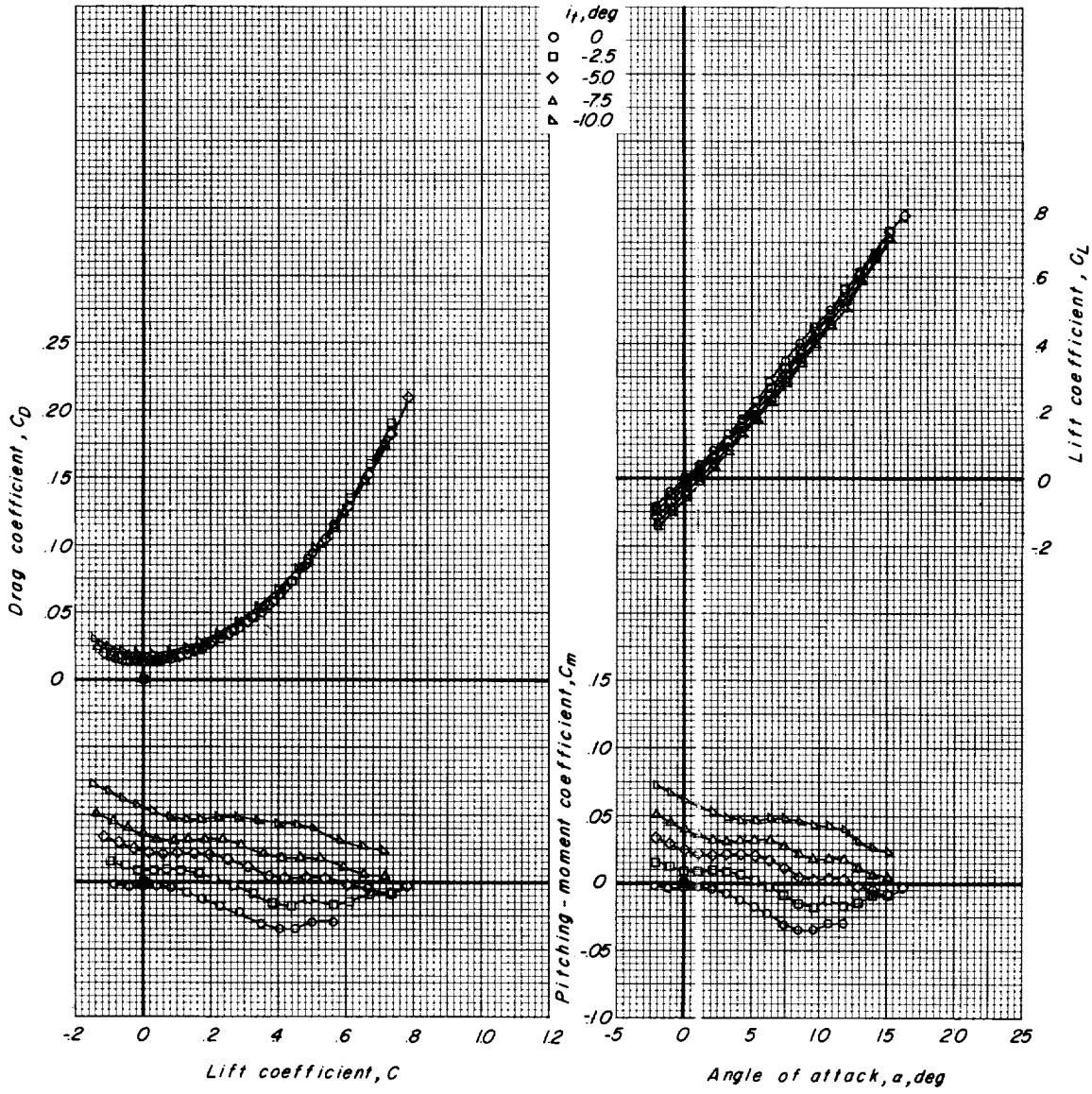

(c) M = 0.90.

Figure 6.- Continued.

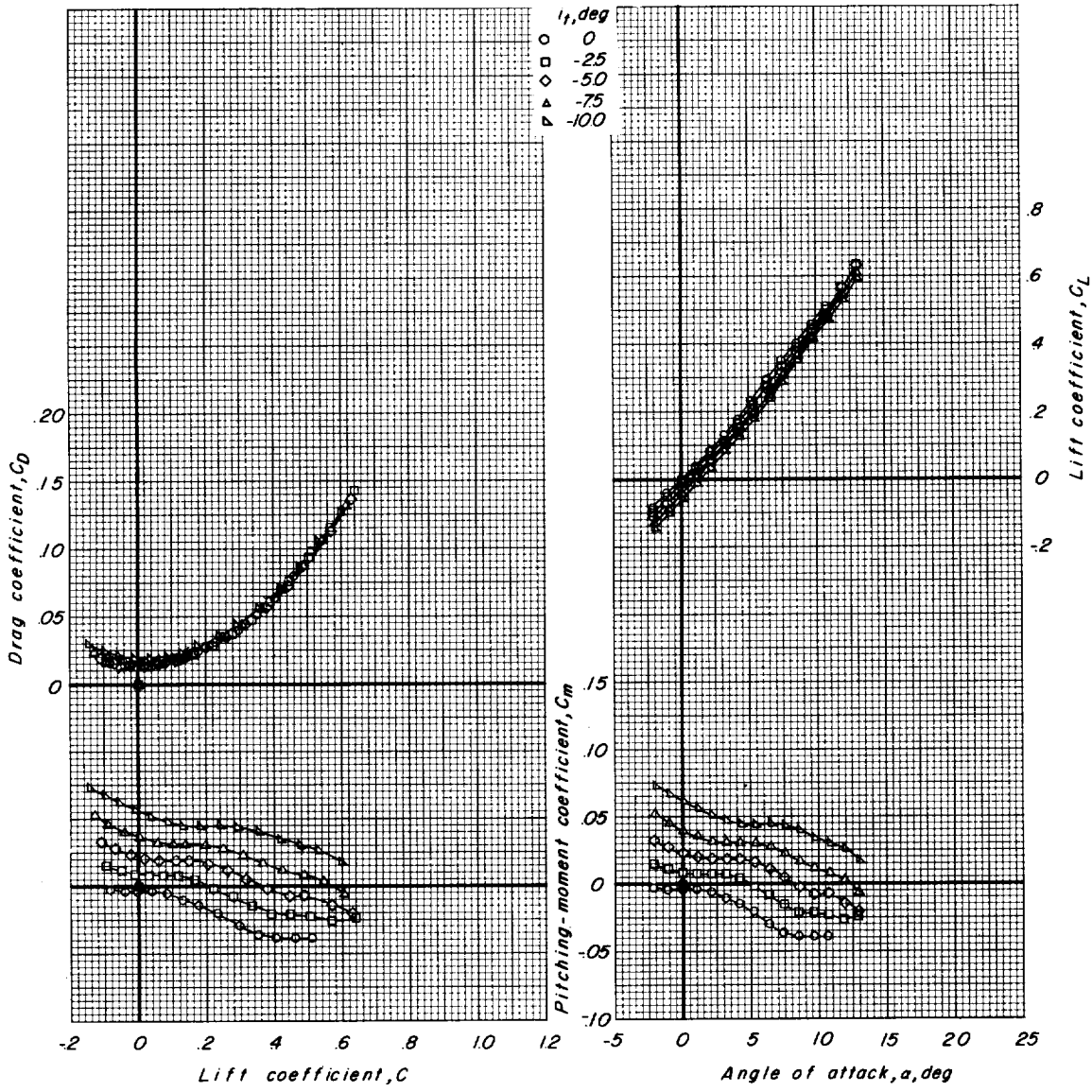

(d) M = 0.95.

Figure 6.- Concluded.

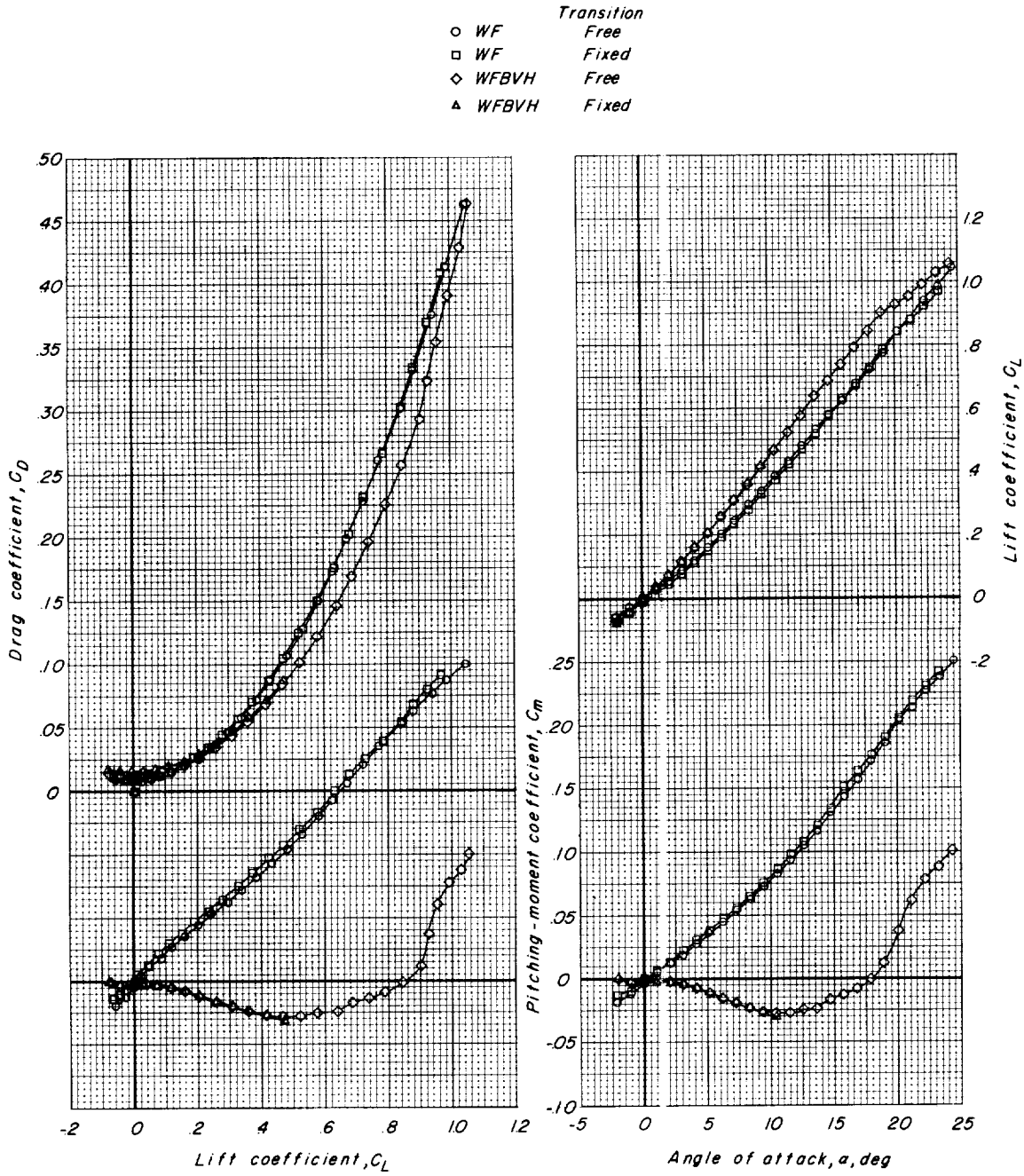

(a) M = 0.60.

Figure 7.- Static longitudinal stability characteristics for wing-fuselage and complete configurations of outboard-tail model with free and fixed transition. $i_t = 0^\circ$.

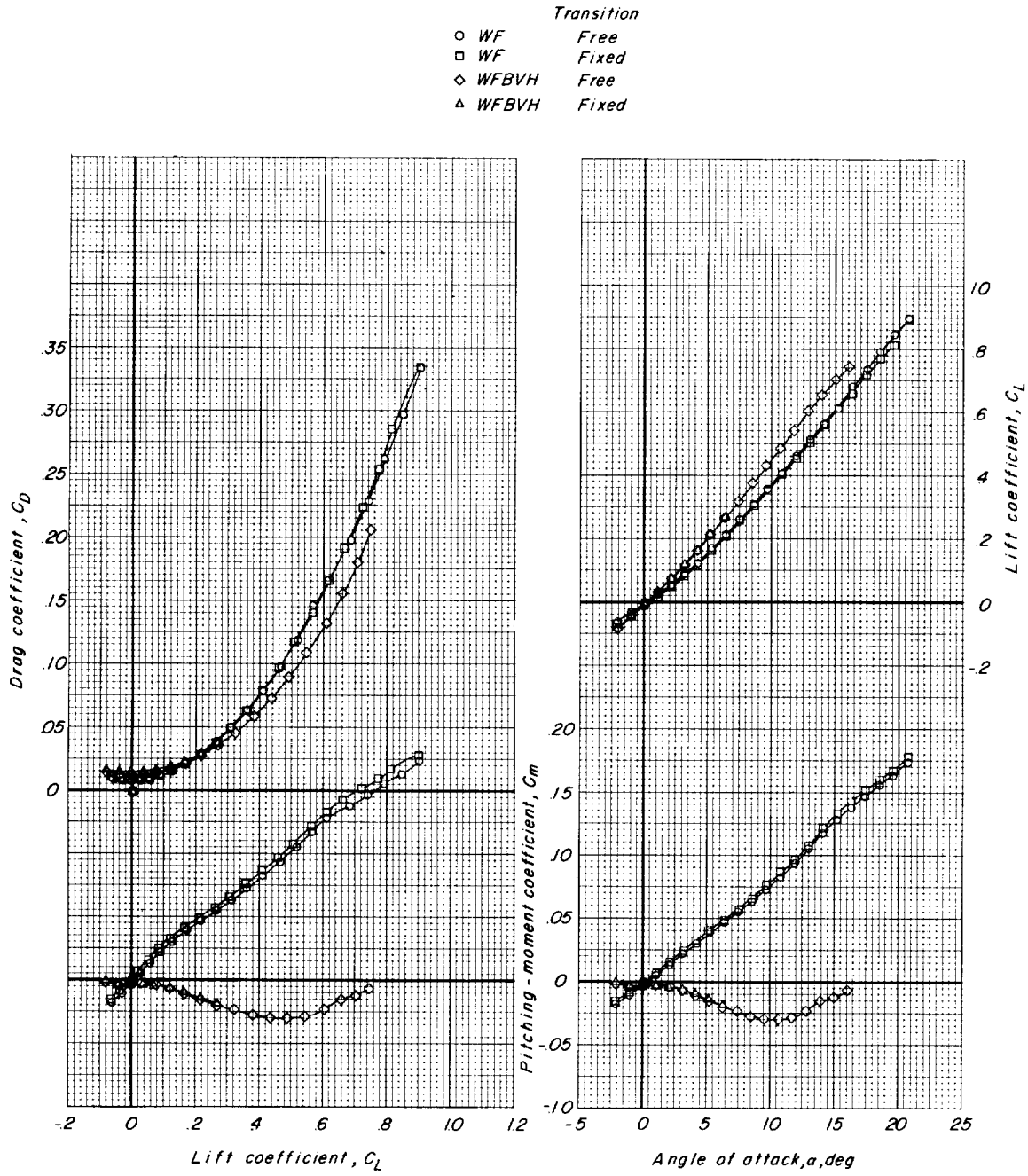

(b) M = 0.80.

Figure 7.- Continued.

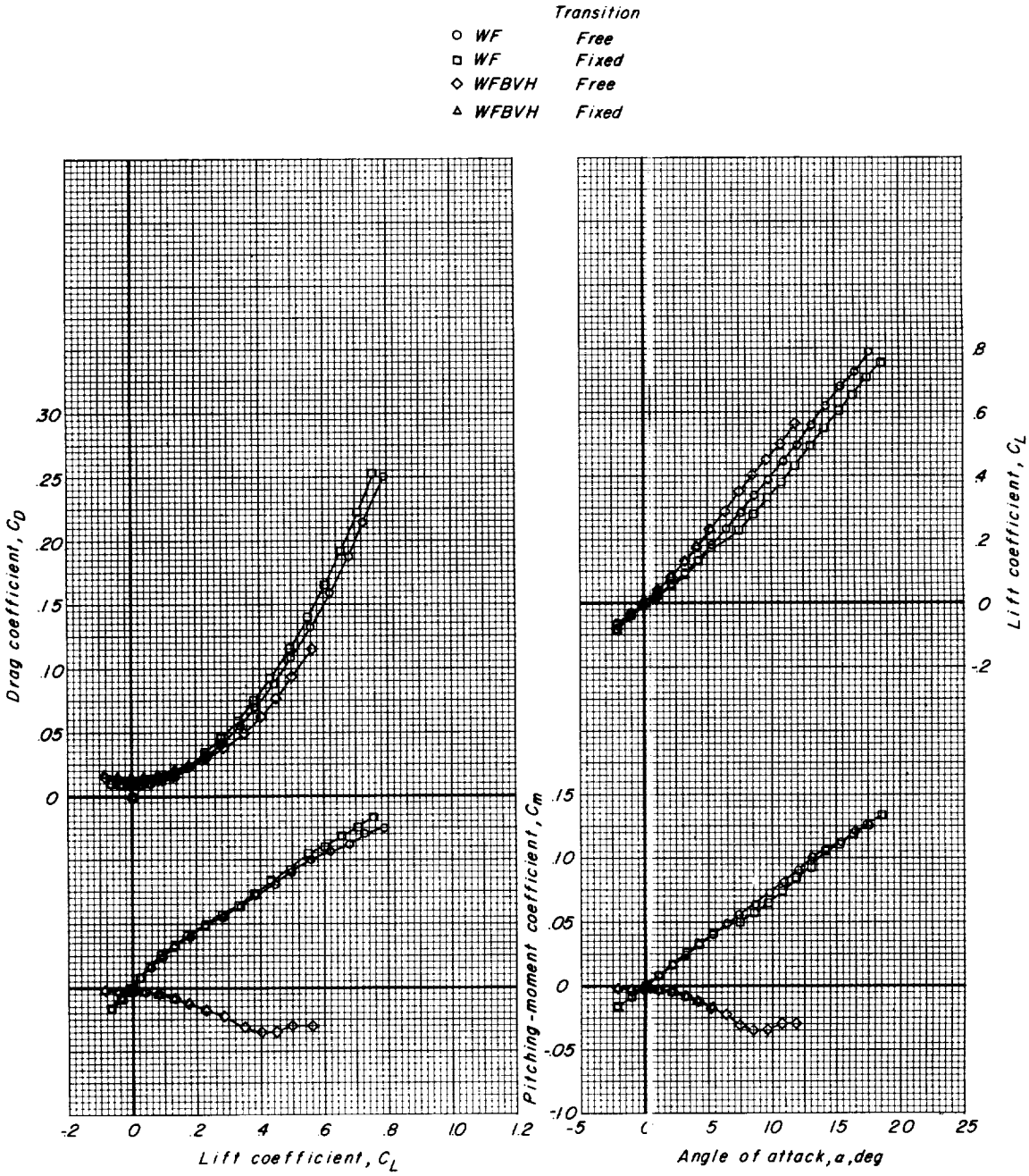

(c) M = 0.90.

Figure 7.- Continued.

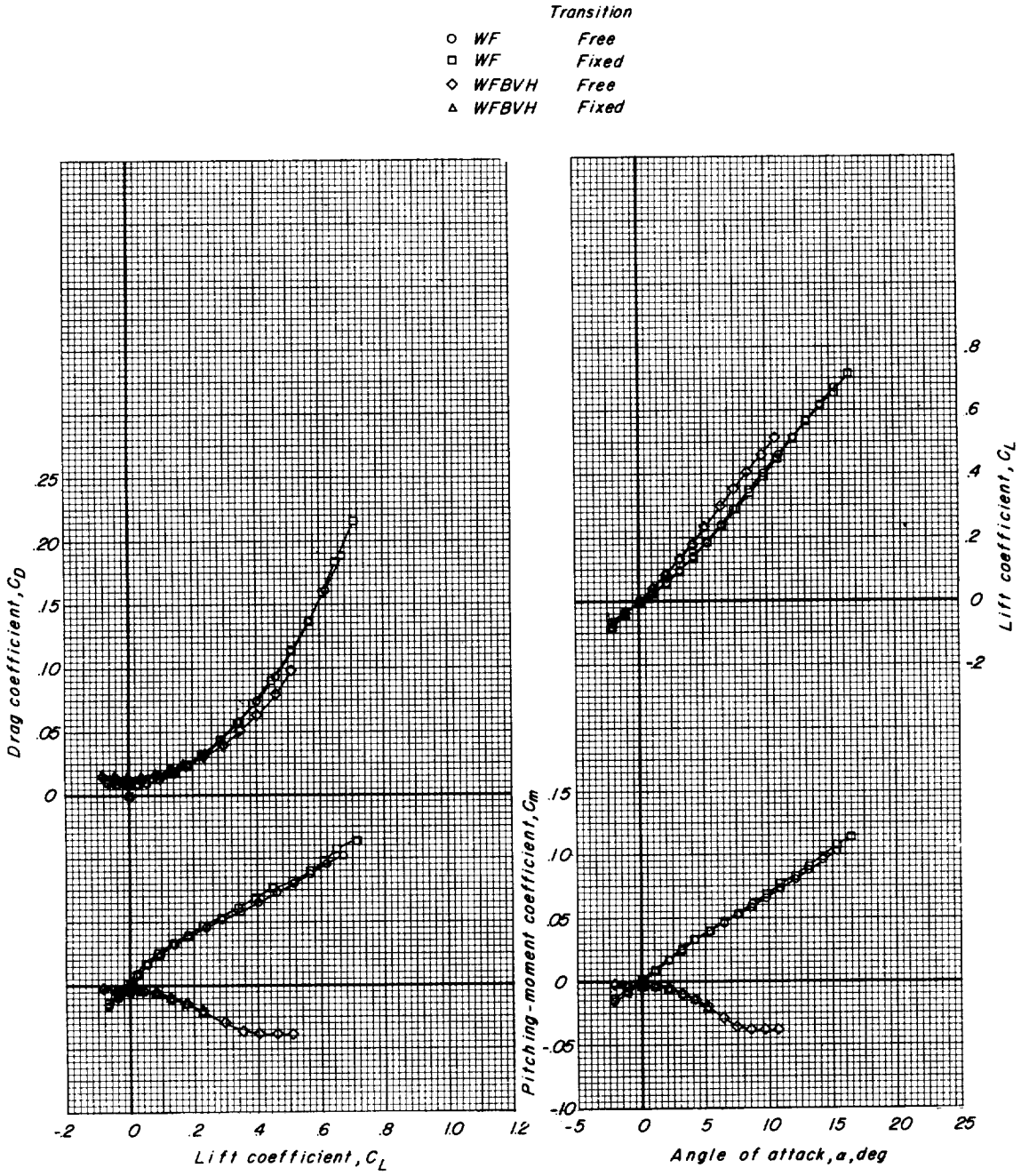

(d) M = 0.95.

Figure 7.- Concluded.

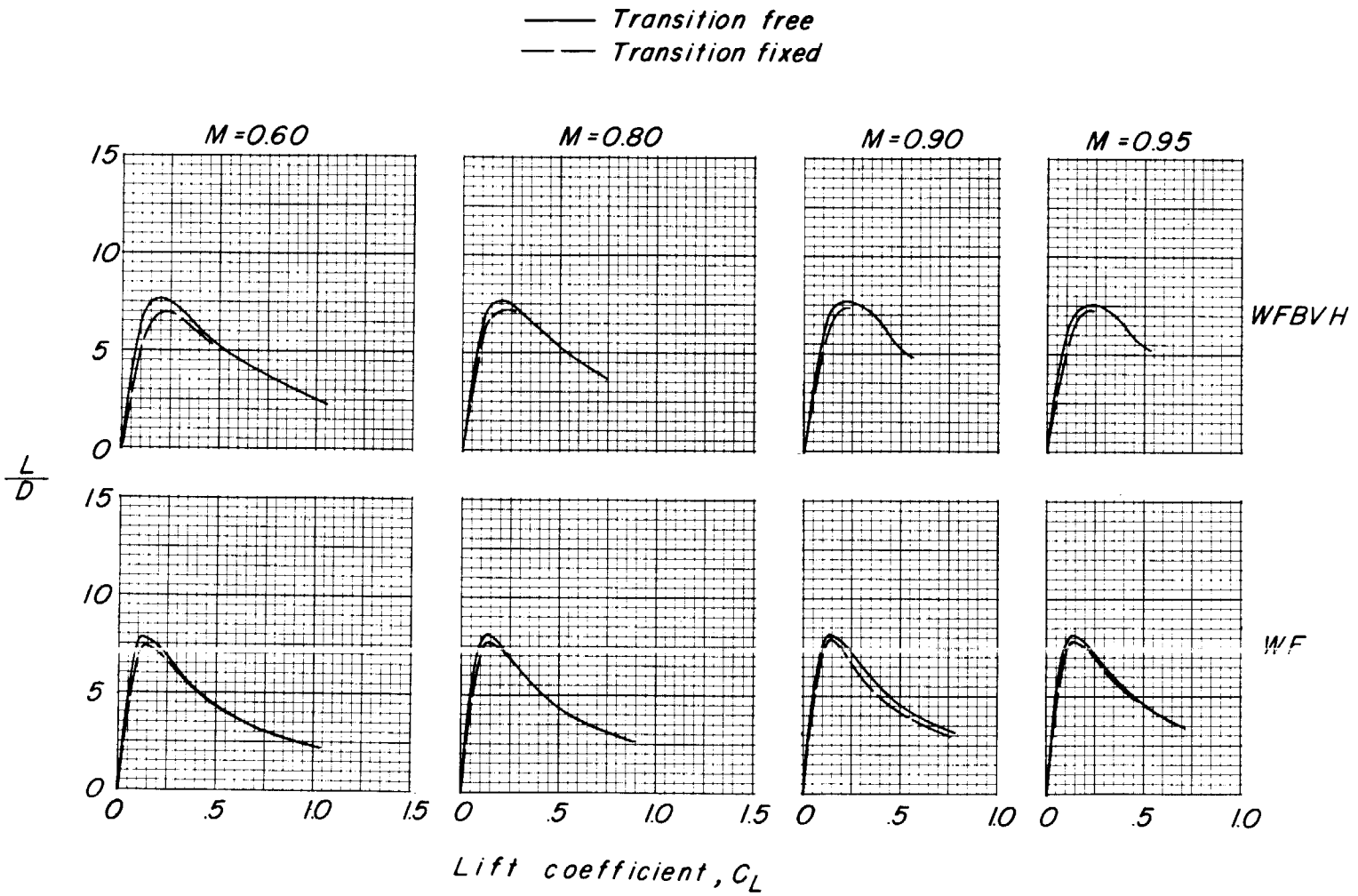

Figure 8.- Variation of lift-drag ratio with lift coefficient for wing-fuselage and complete configurations of outboard-tail model with free and fixed transition. $i_t = 0^\circ$.

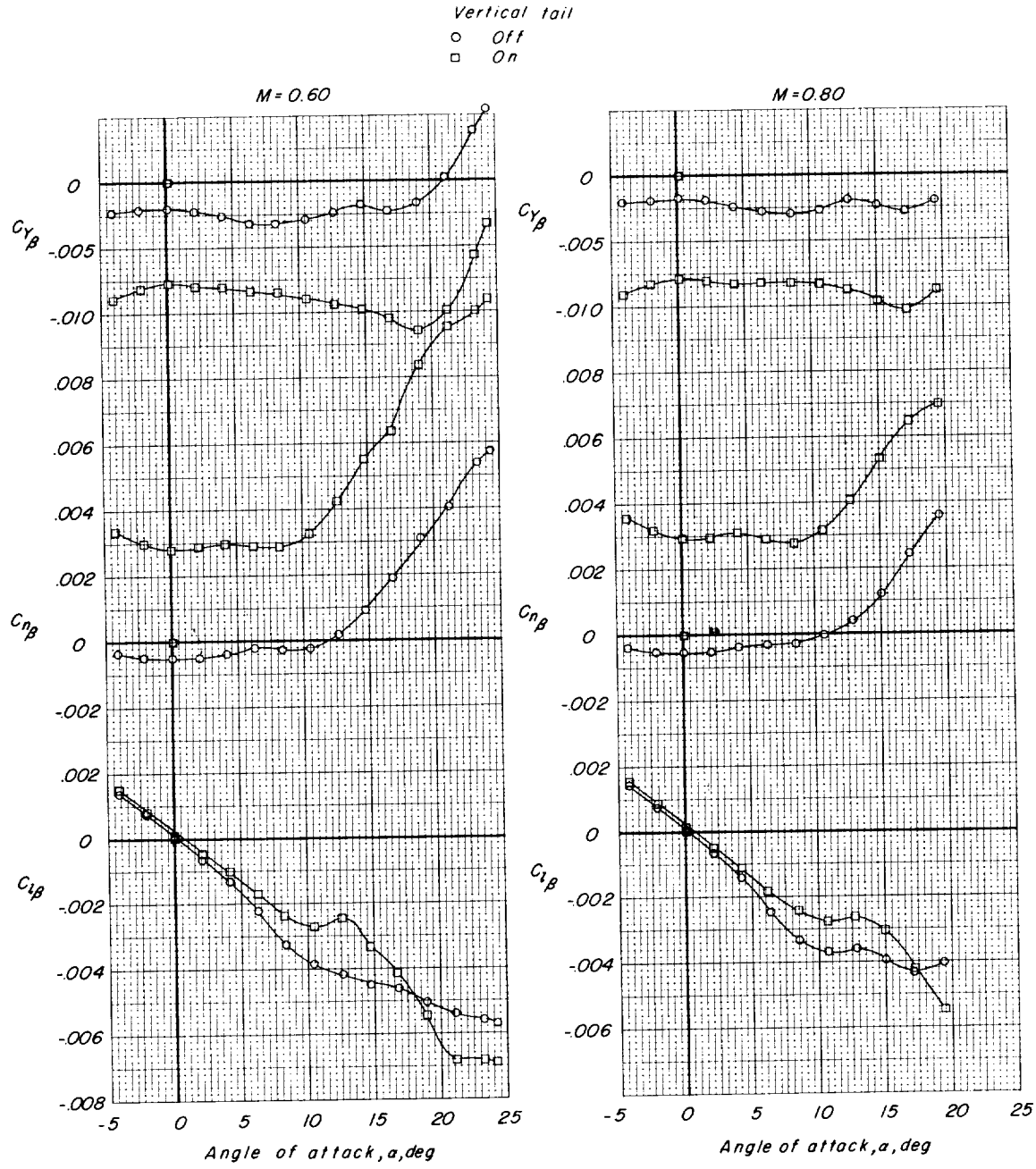

(a) M = 0.60 and 0.80.

Figure 9.- Variation of static lateral stability derivatives with angle of attack for outboard-tail model with and without vertical tail. Transition free; $i_t = 0^\circ$.

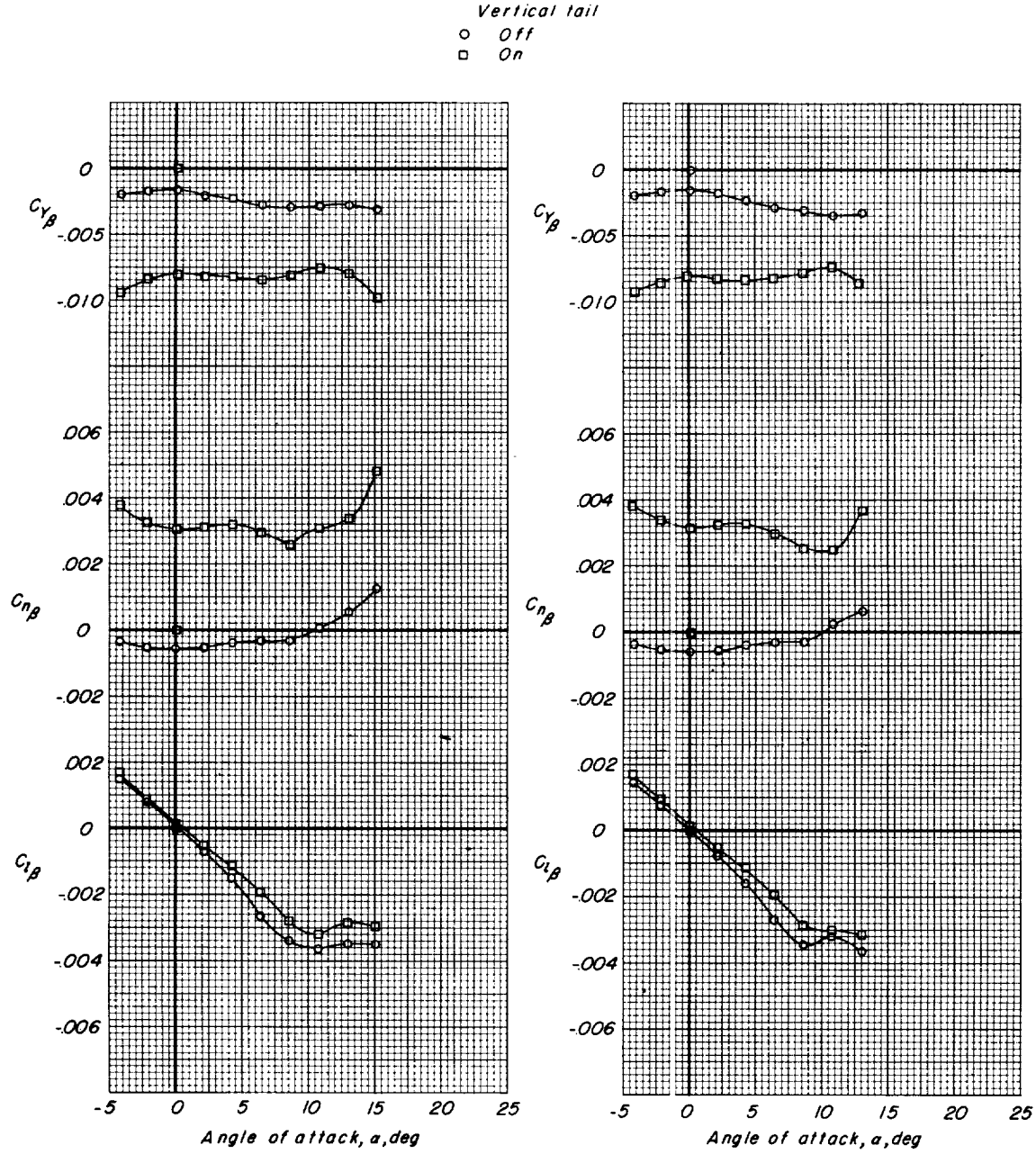

(b) M = 0.90 and 0.95.

Figure 9.- Concluded.

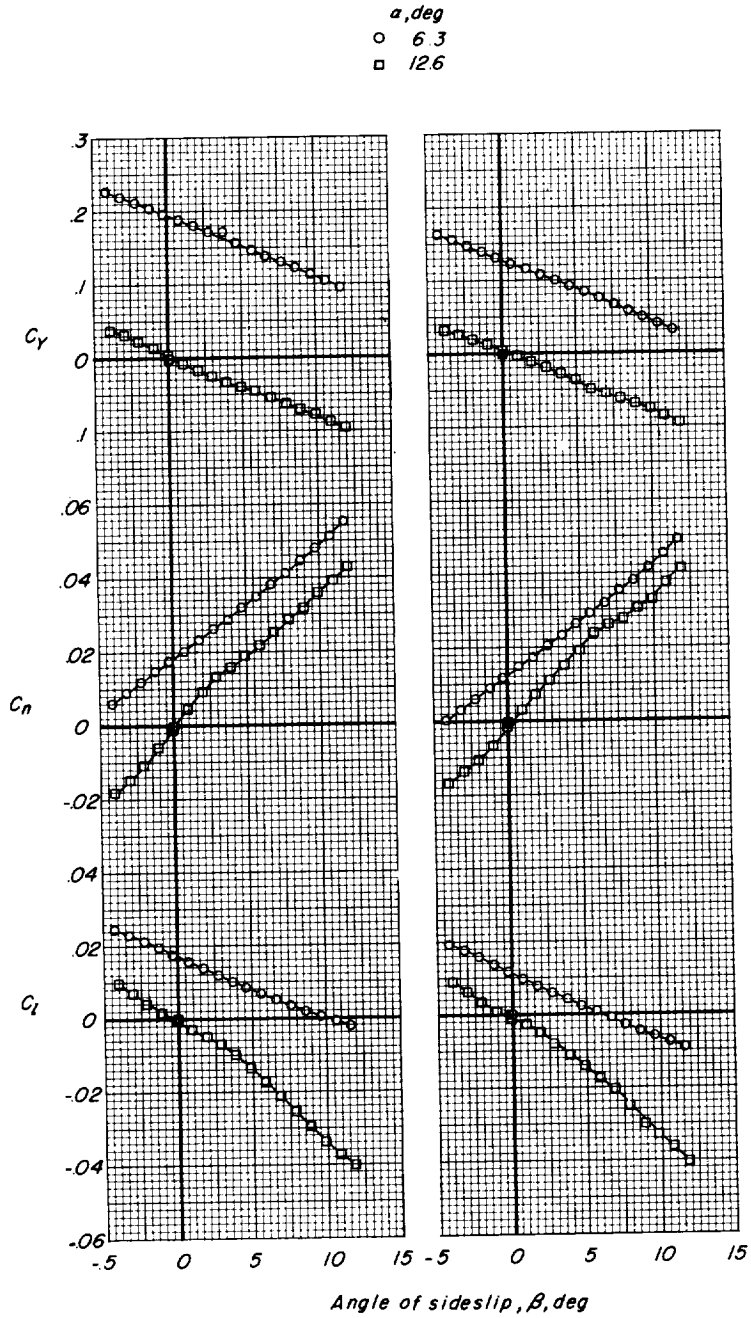

(a) M = 0.60 and 0.80.

Figure 10.- Static lateral stability characteristics for complete outboard-tail model at two angles of attack. Transition free; $i_t = 0^\circ$.

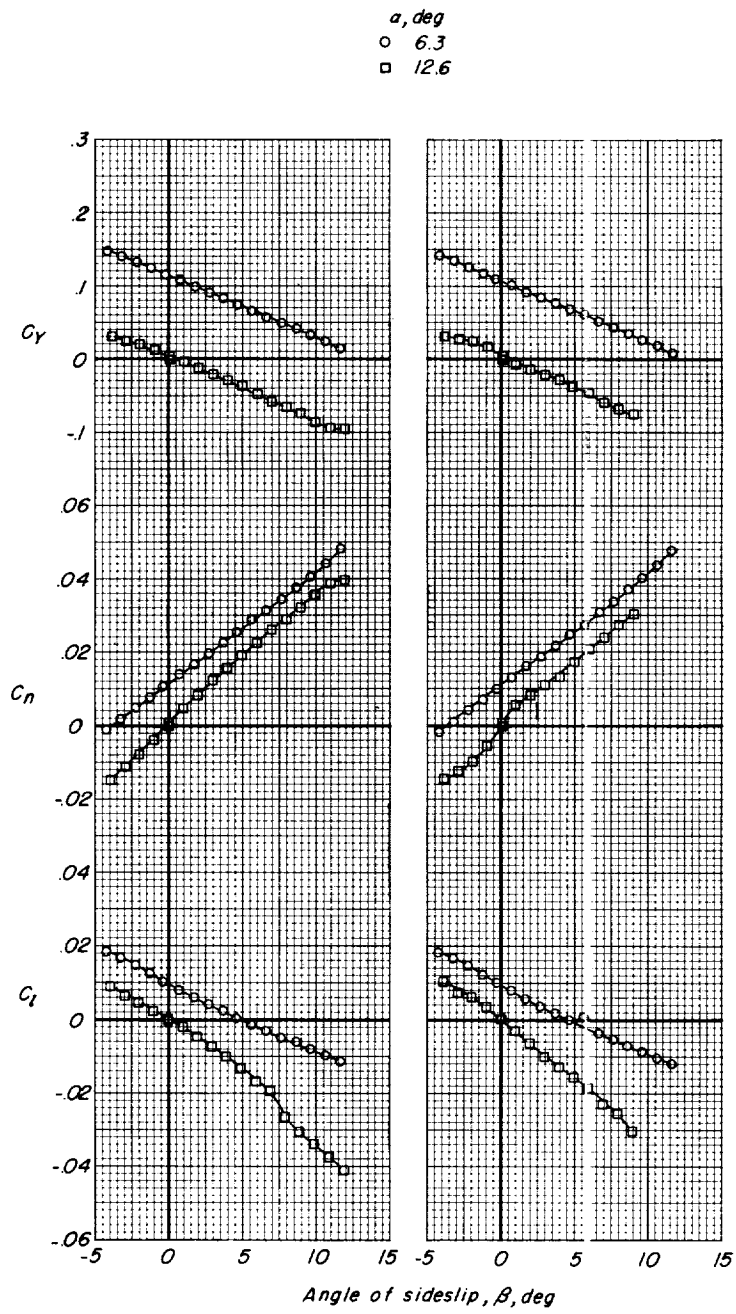

(b) M = 0.90 and 0.95.

Figure 10.- Concluded.

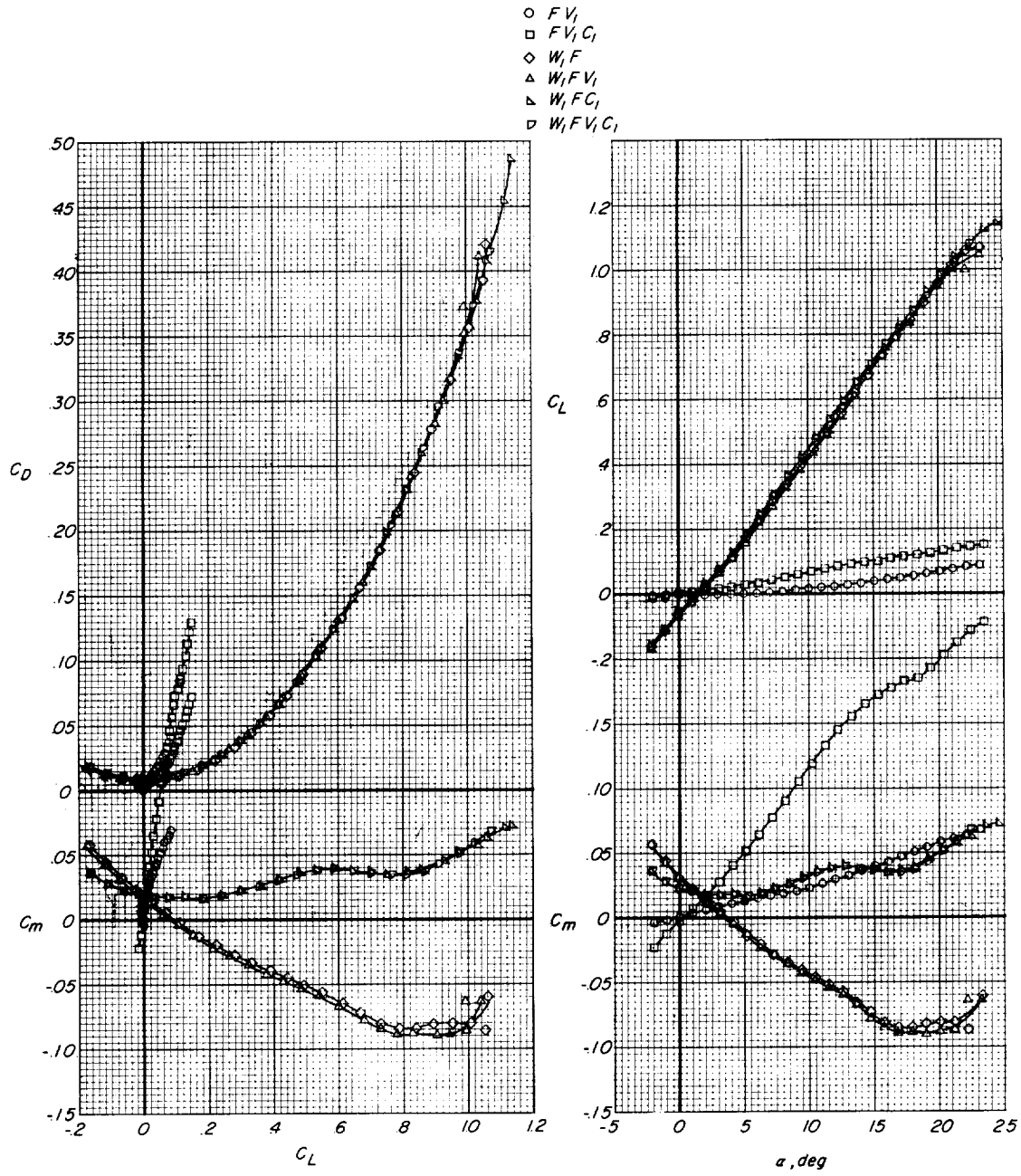

(a) M = 0.60.

Figure 11.- Static longitudinal stability characteristics for various component parts of canard model with medium canard surface. Transition free; $\delta_c = 0^o$.

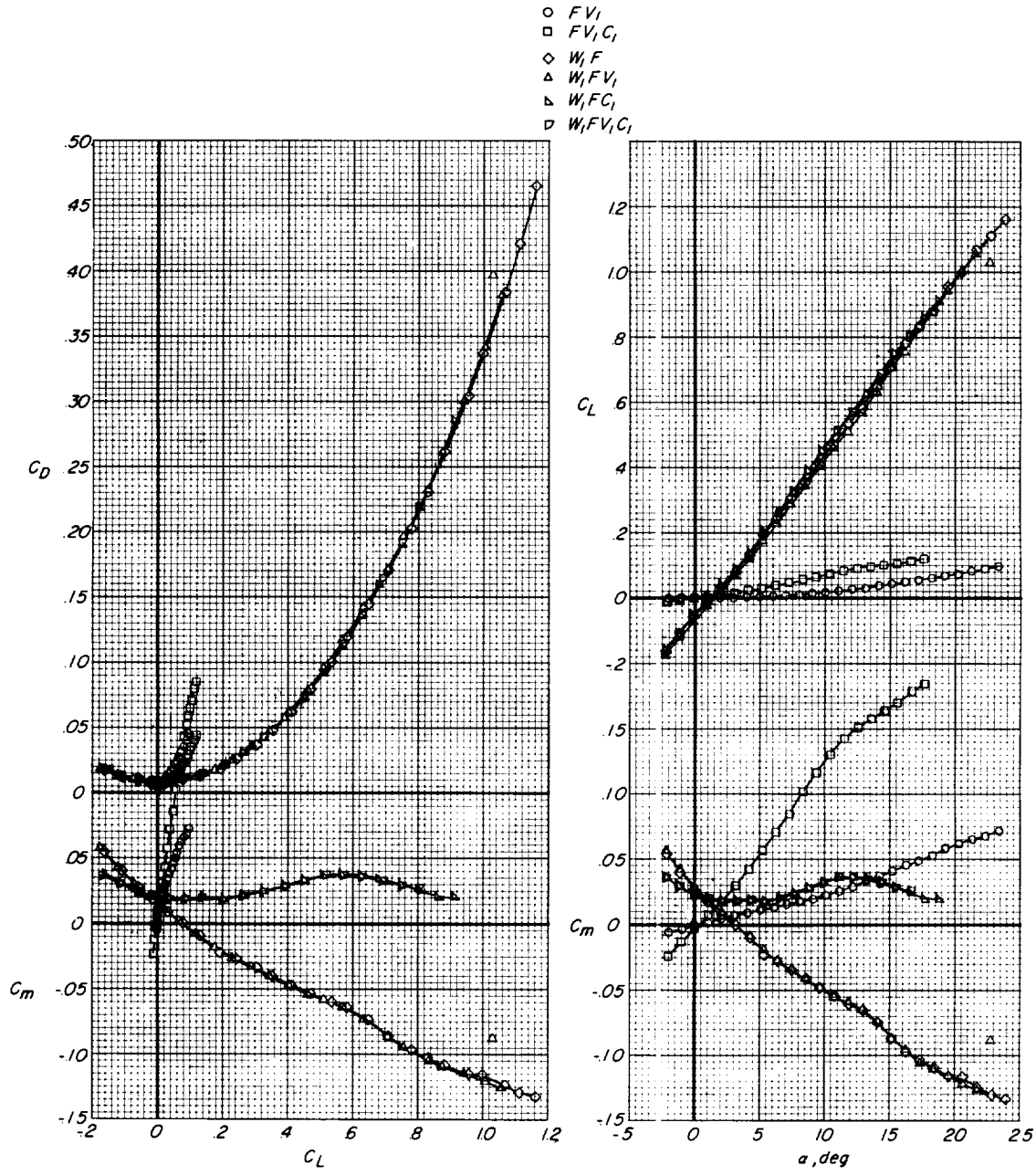

(b) M = 0.80.

Figure 11.- Contirued.

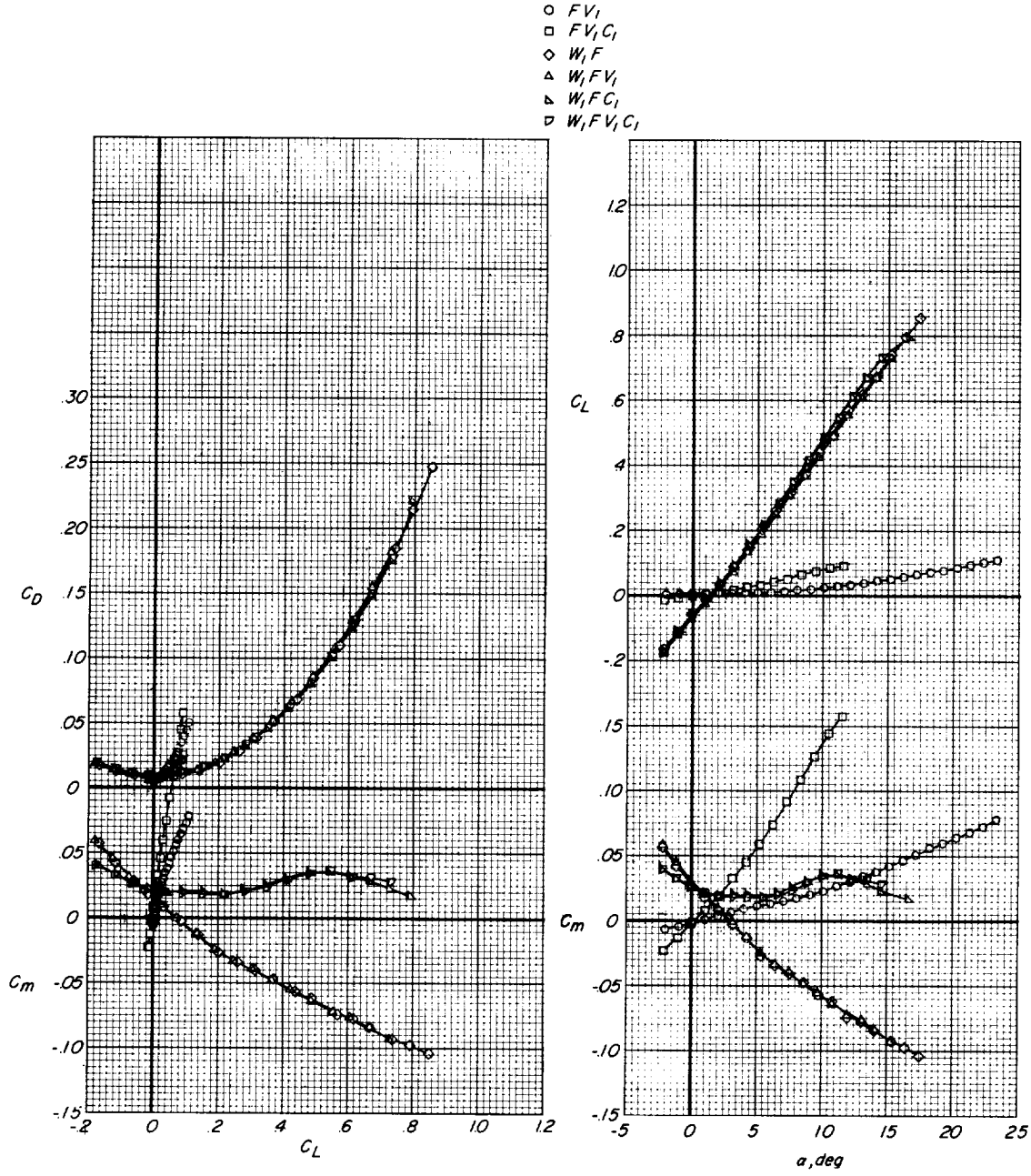

(c) M = 0.90.

Figure 11.- Continued.

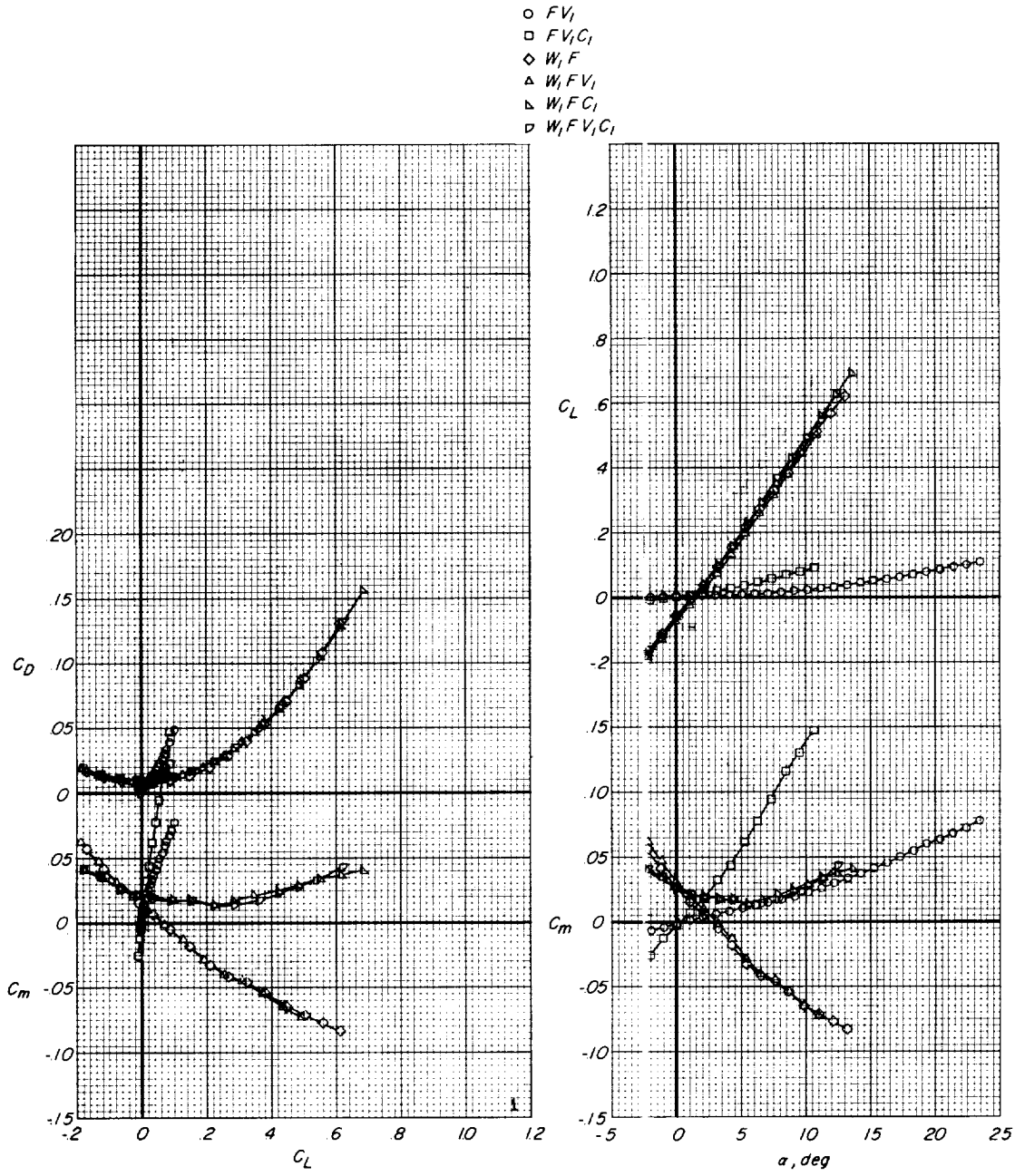

(d) M = 0.95.

Figure 11.- Concluded.

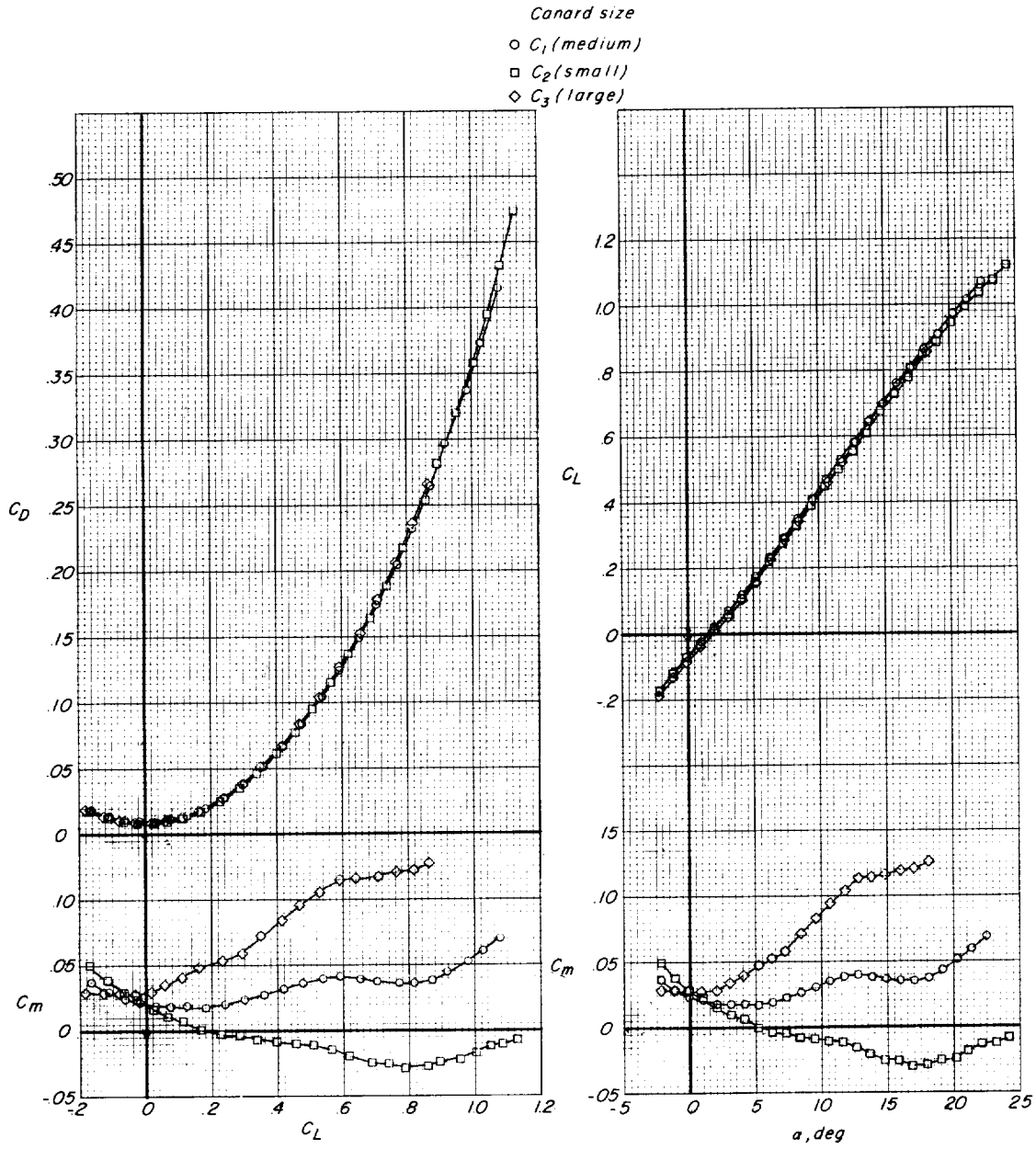

(a) M = 0.60.

Figure 12.- Static longitudinal stability characteristics for complete canard model with three canard-surface sizes. Transition free; $\delta_c = 0^\circ$.

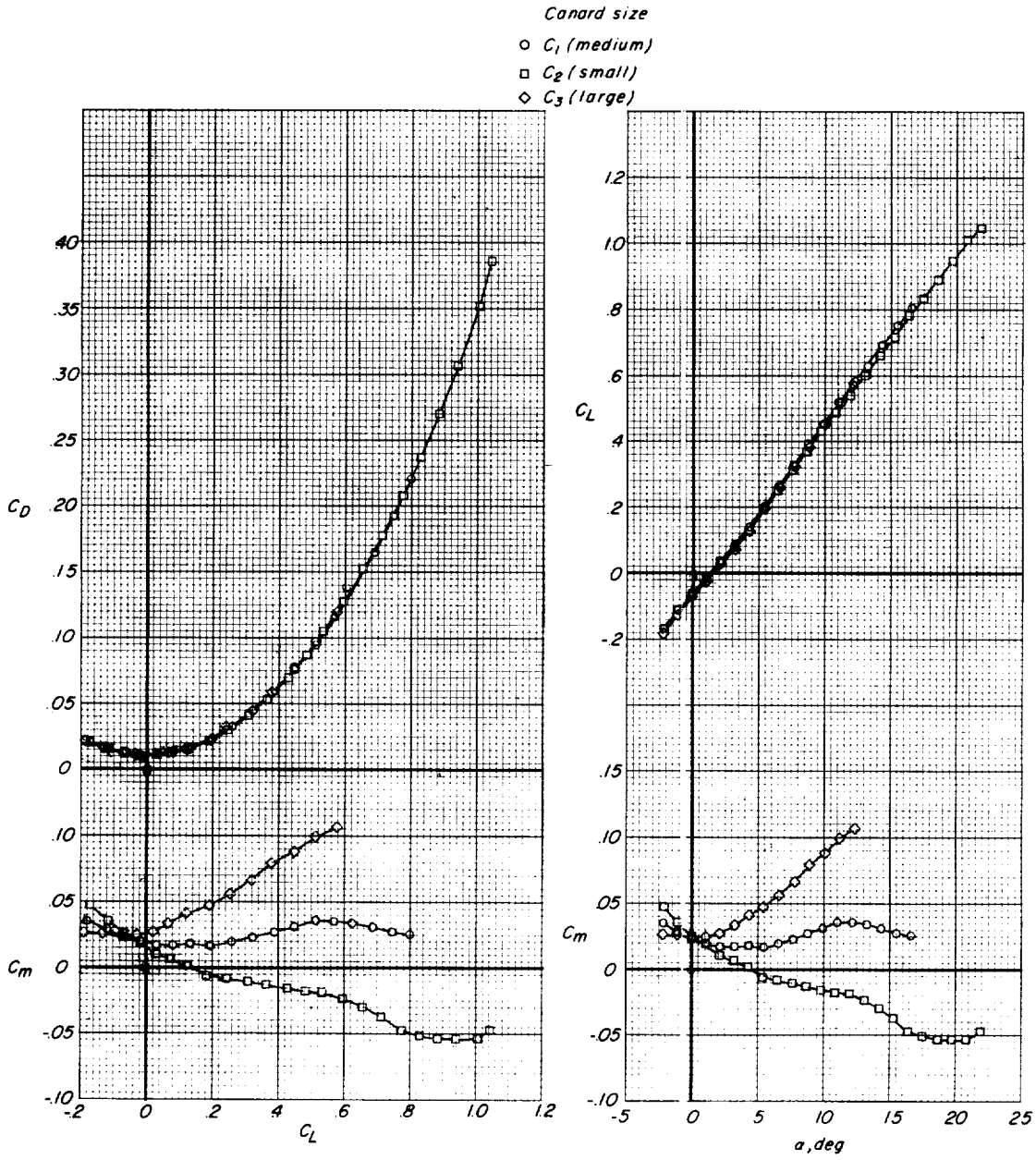

(b) M = 0.80.

Figure 12.- Continued.

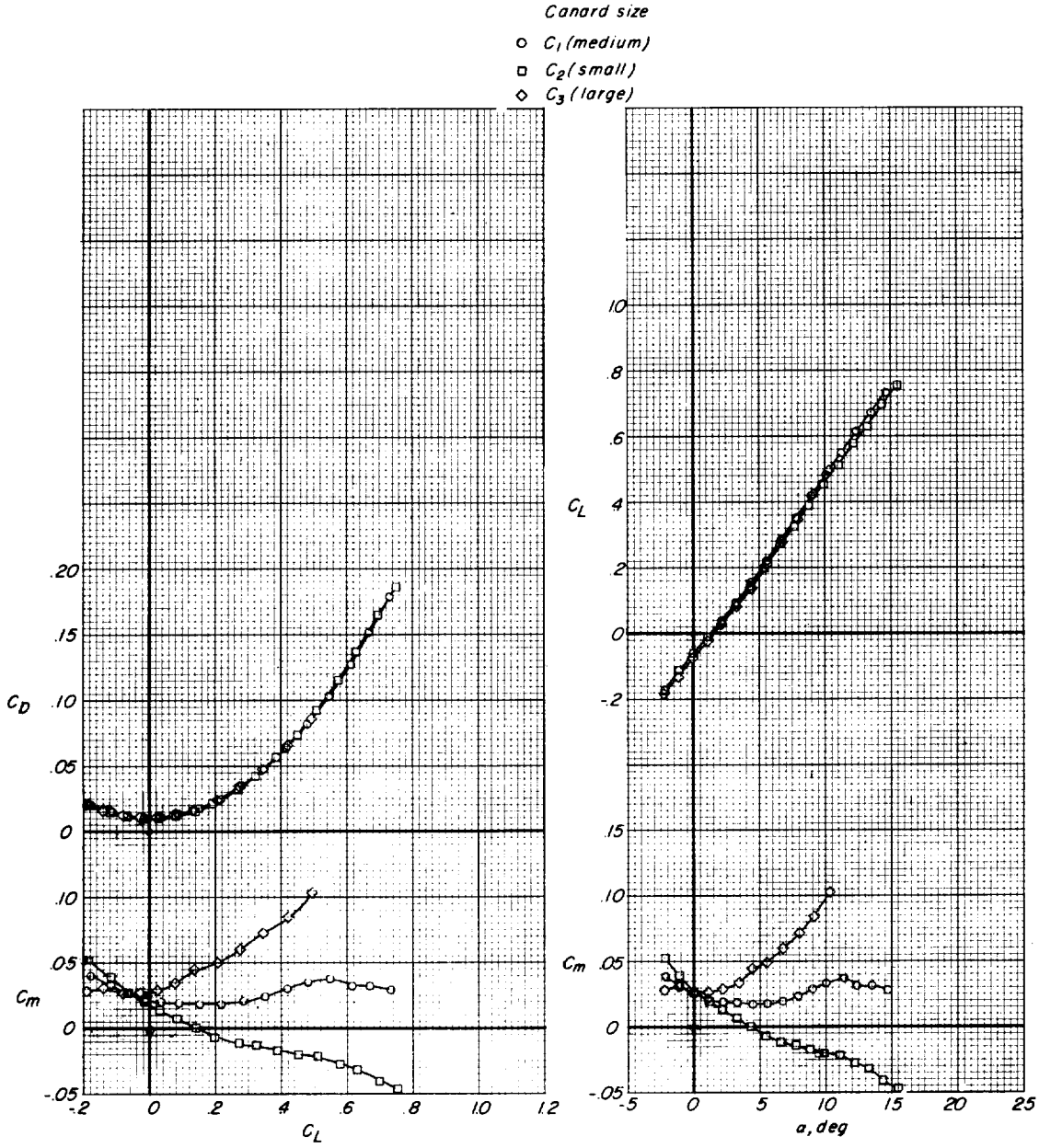

(c) M = 0.90.

Figure 12.- Continued.

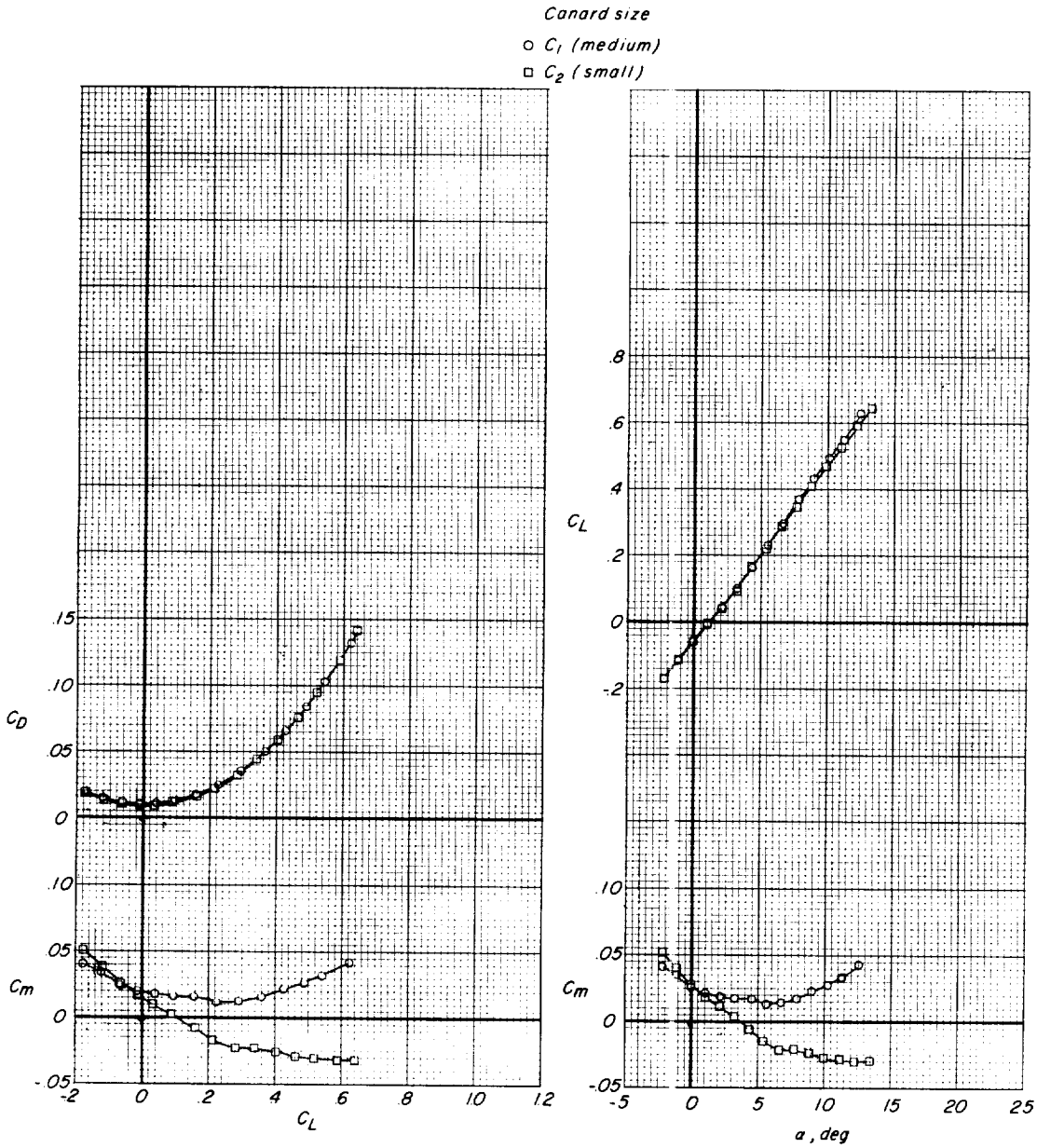

(d) M = 0.95.

Figure 12.- Concluded.

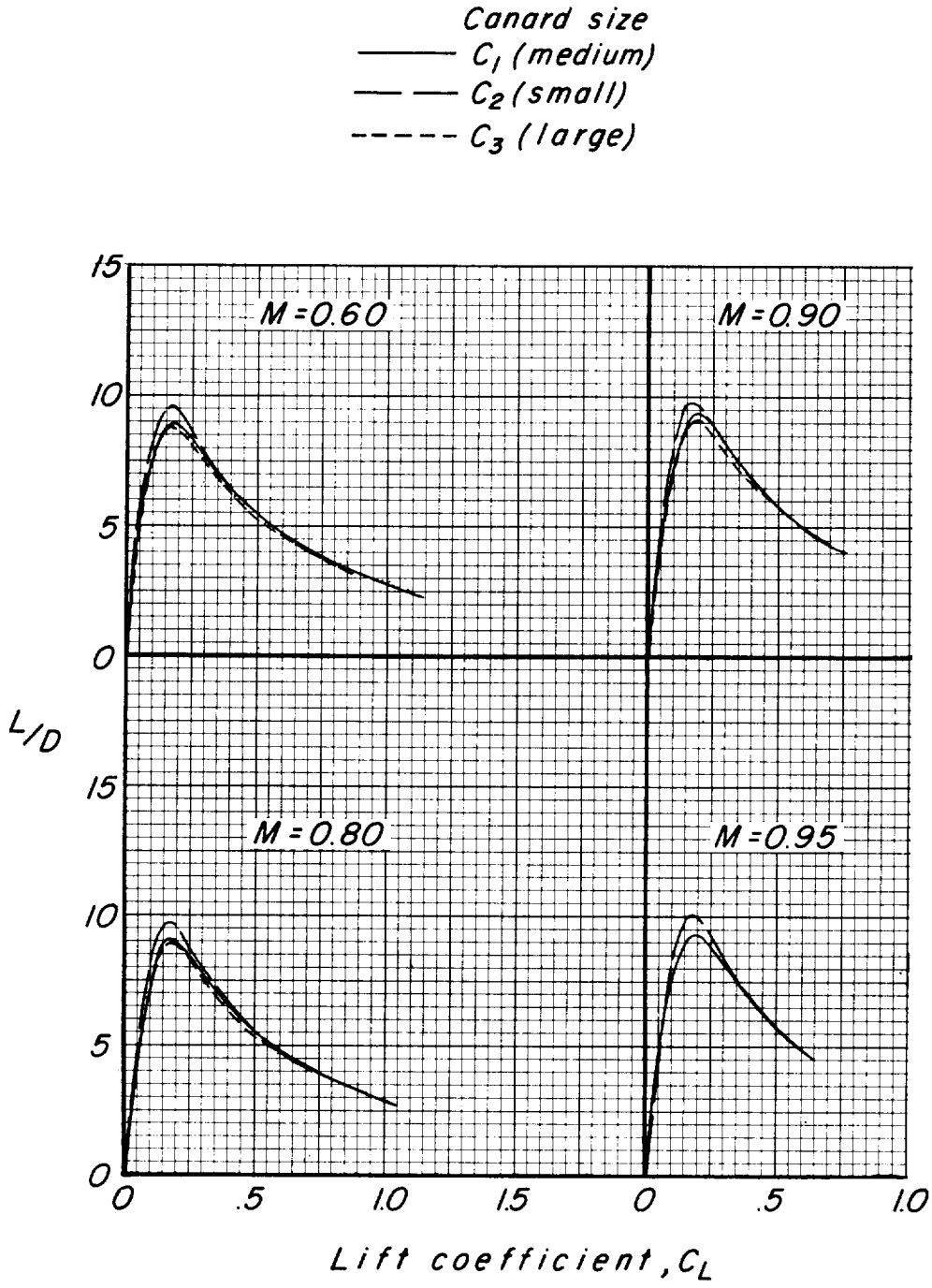

Figure 13.- Variation of lift-drag ratio with lift coefficient for complete canard model with three canard-surface sizes. Transition free; $\delta_c = 0^\circ$.

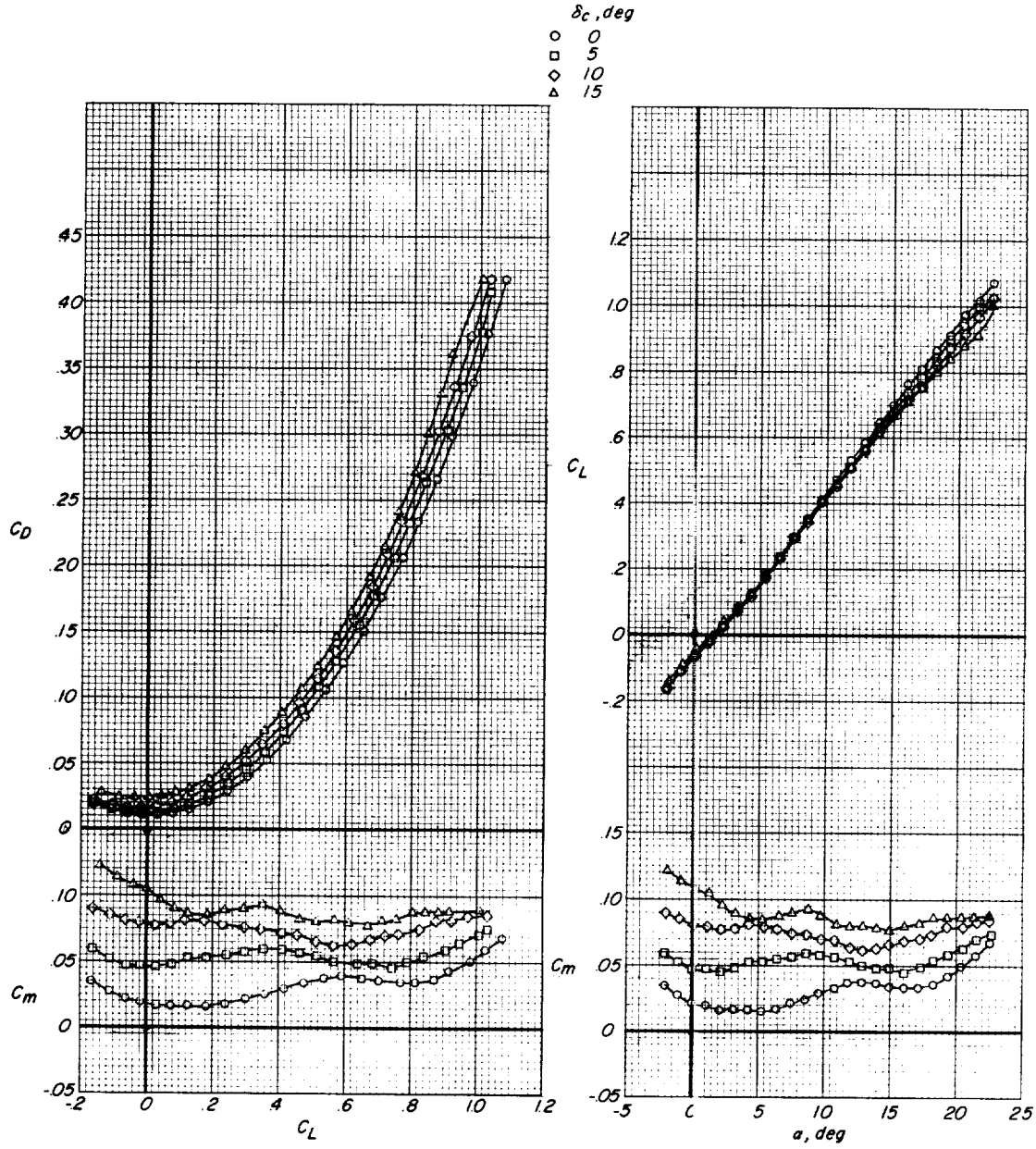

(a) M = 0.60.

Figure 14.- Static longitudinal stability characteristics for canard model with various control deflections of medium canard surface ($W_1FV_1C_1$). Transition free.

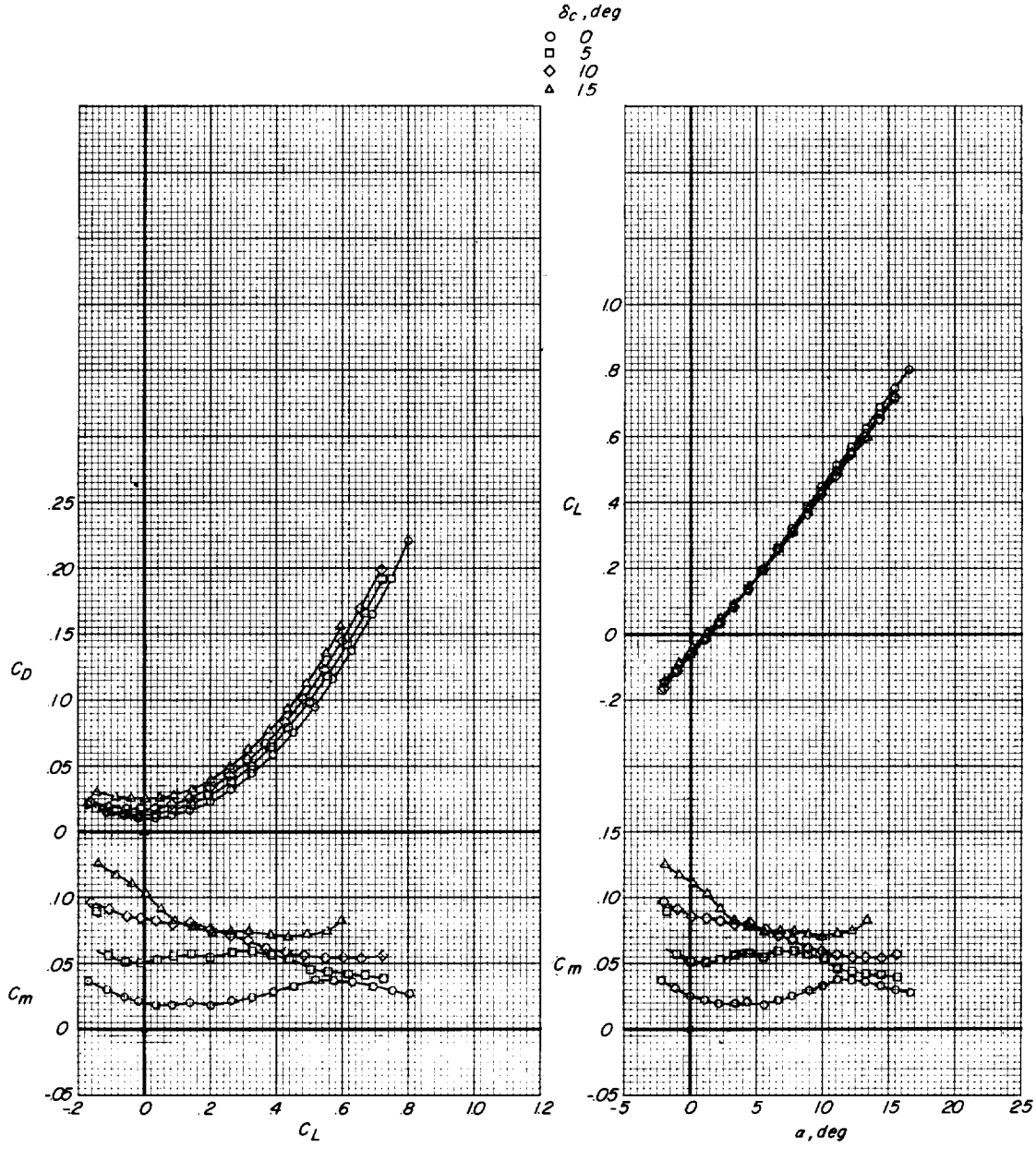

(b) M = 0.80.

Figure 14.- Continued.

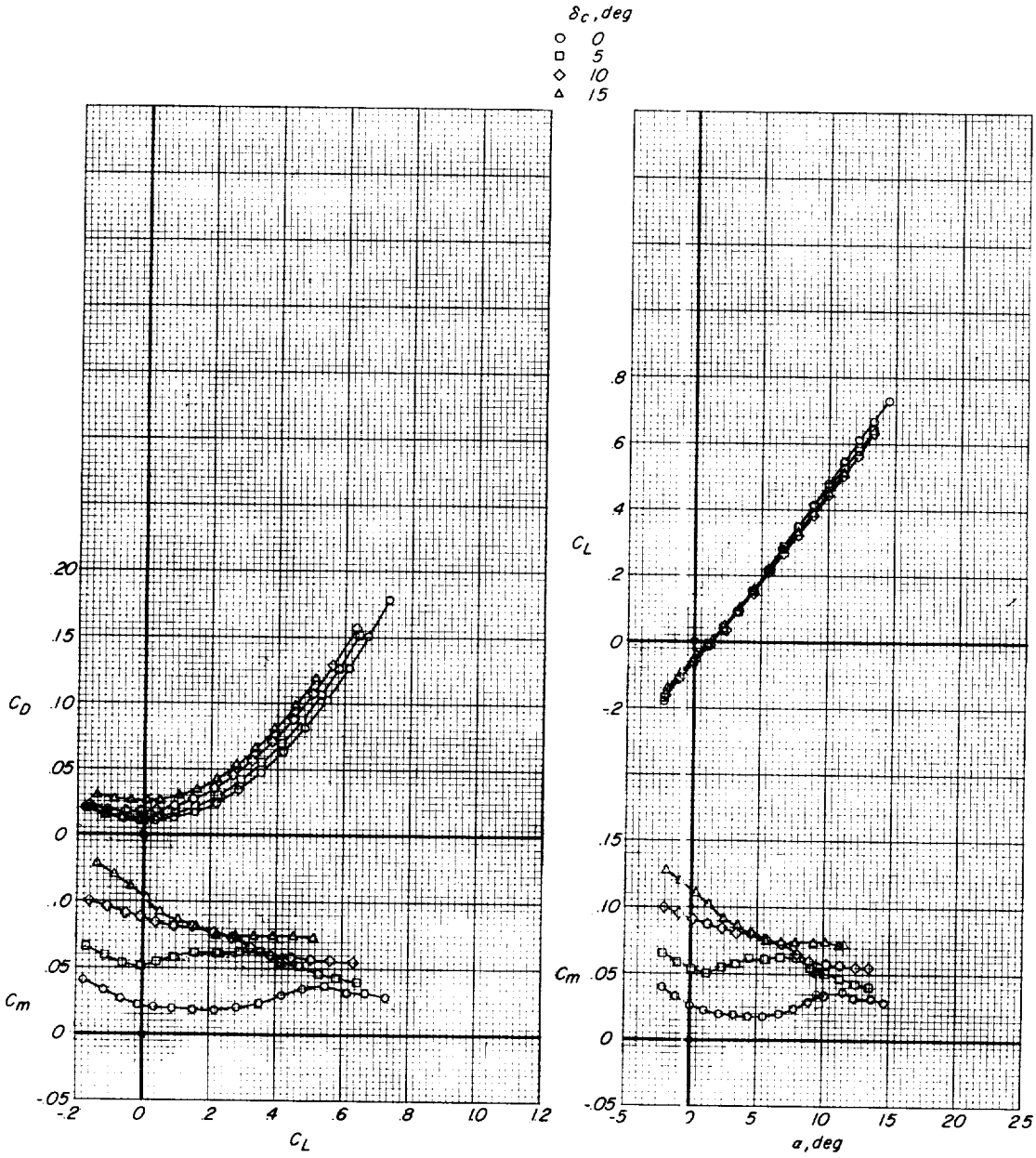

(c) M = 0.90.

Figure 14.- Continued.

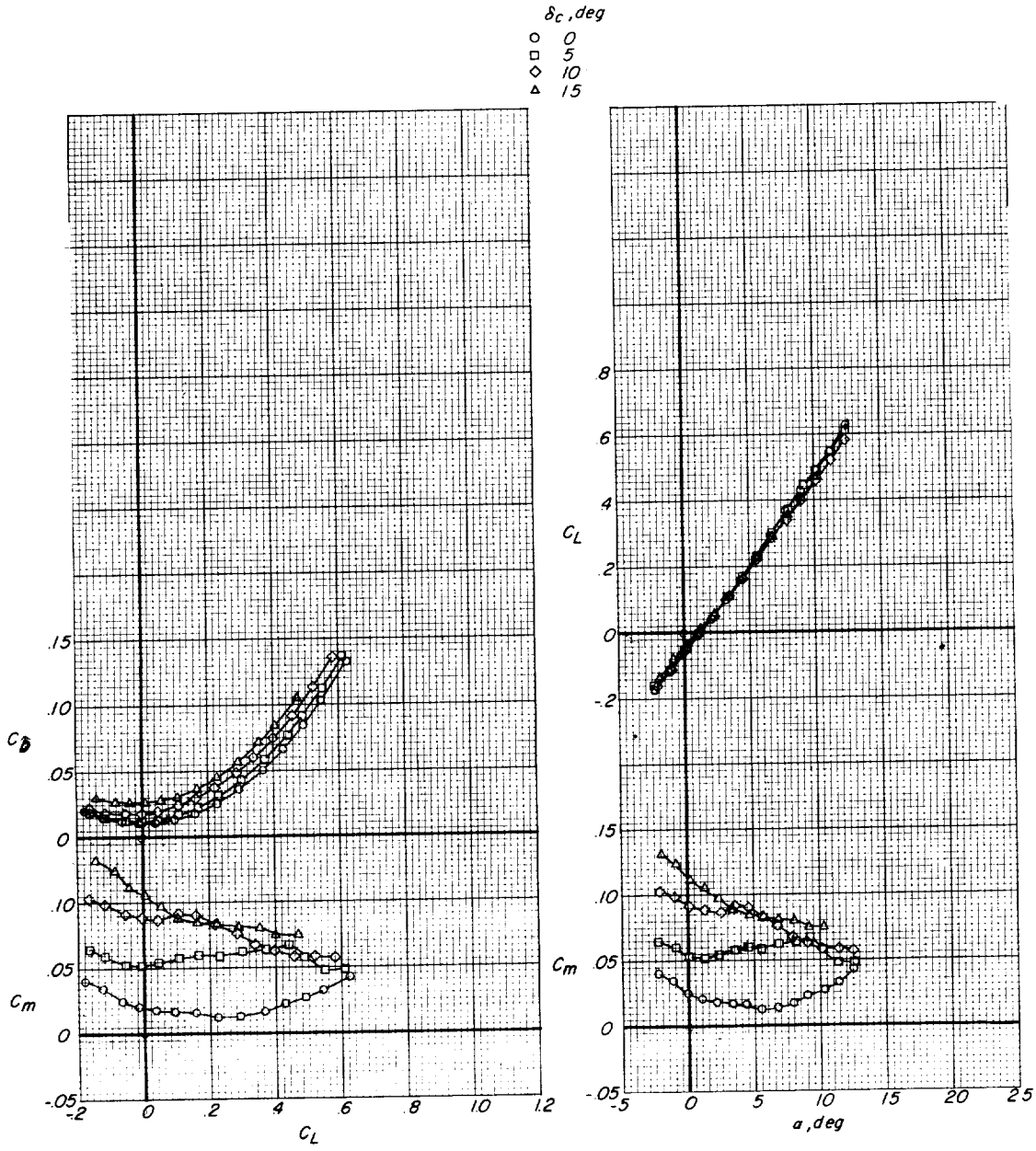

(d) M = 0.95.

Figure 14.- Concluded.

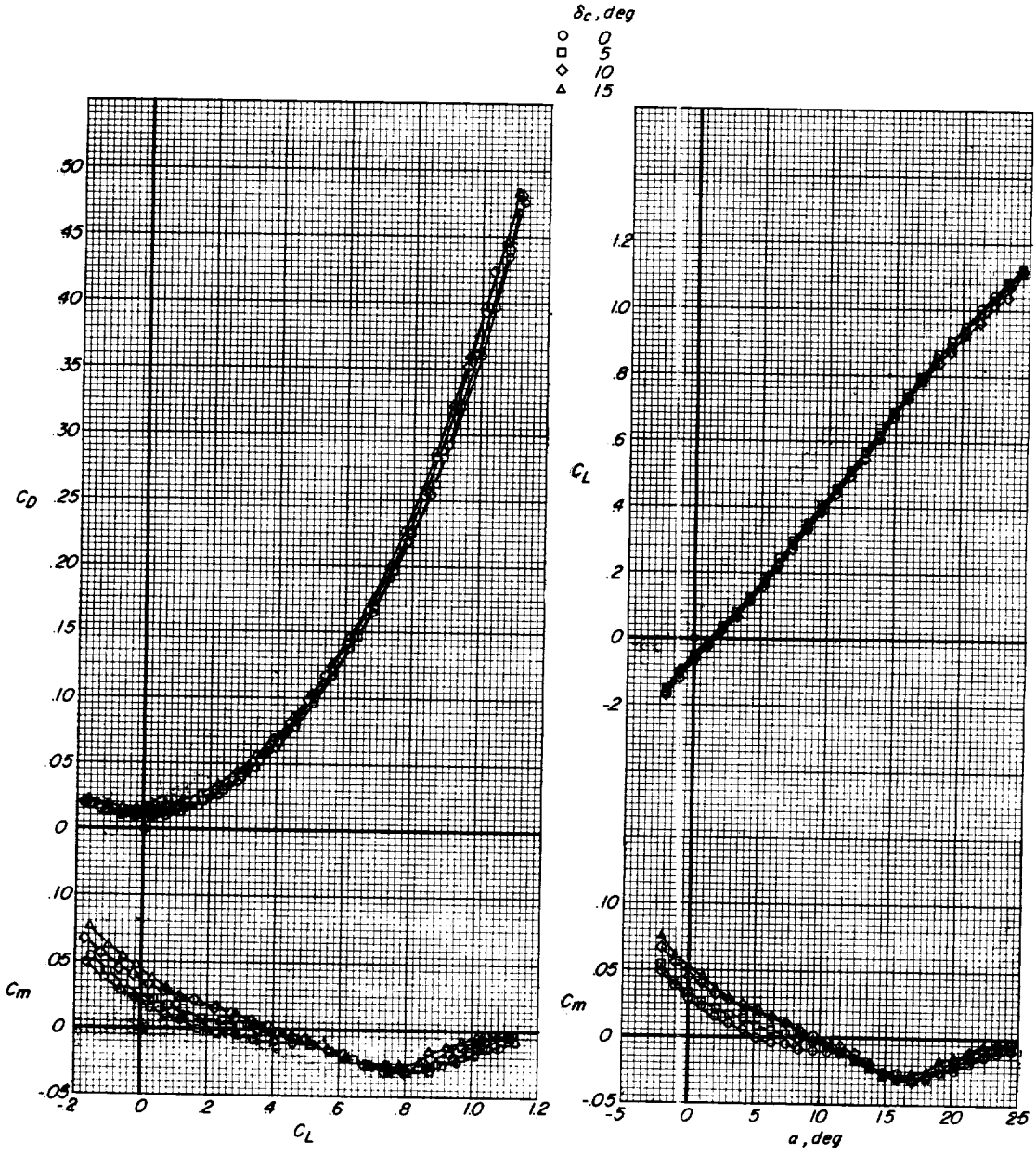

(a) M = 0.60.

Figure 15.- Static longitudinal stability characteristics for canard model with various control deflections of small canard surface ($W_1FV_1C_2$). Transition free.

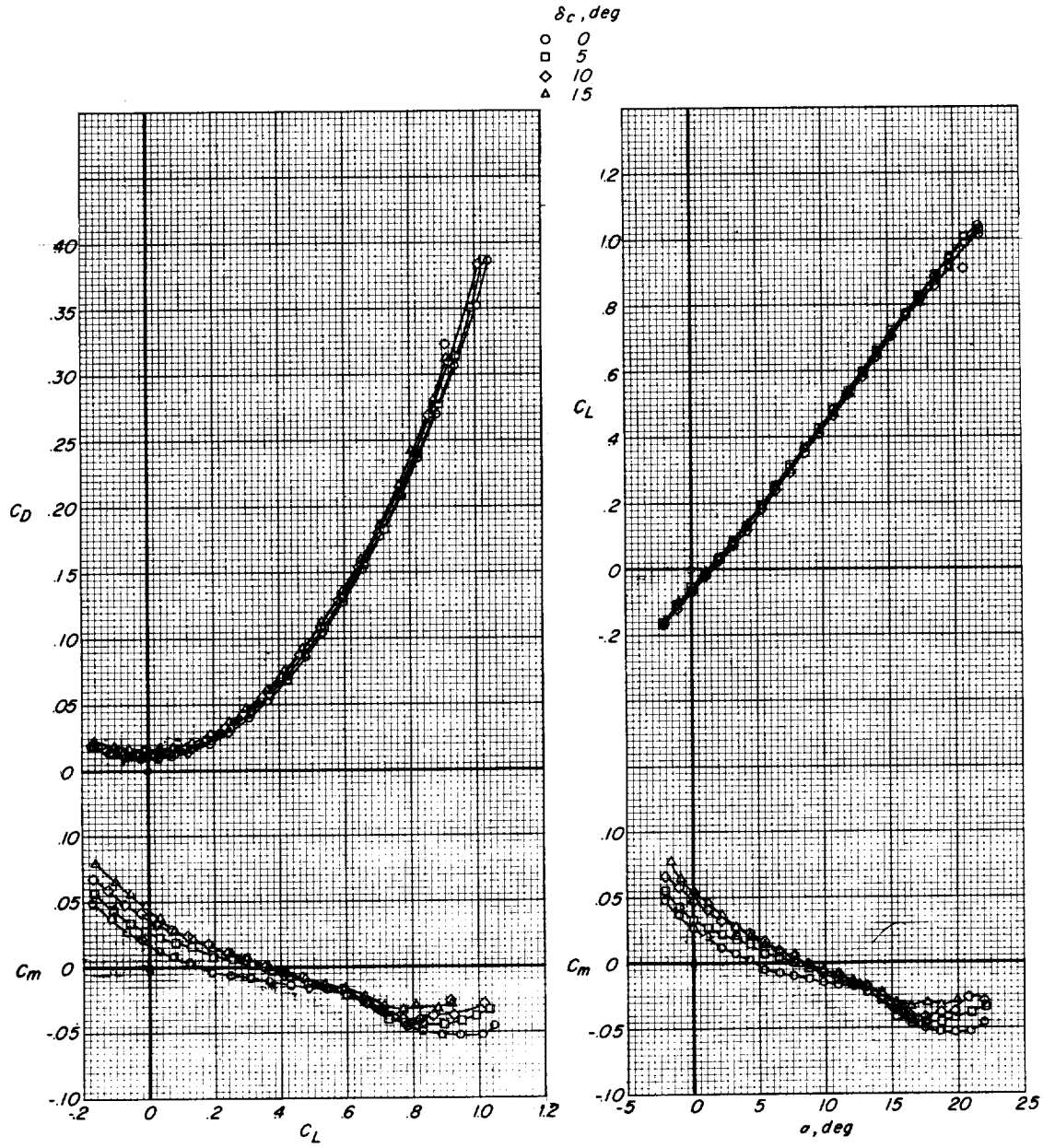

(b) M = 0.80.

Figure 15.- Continued.

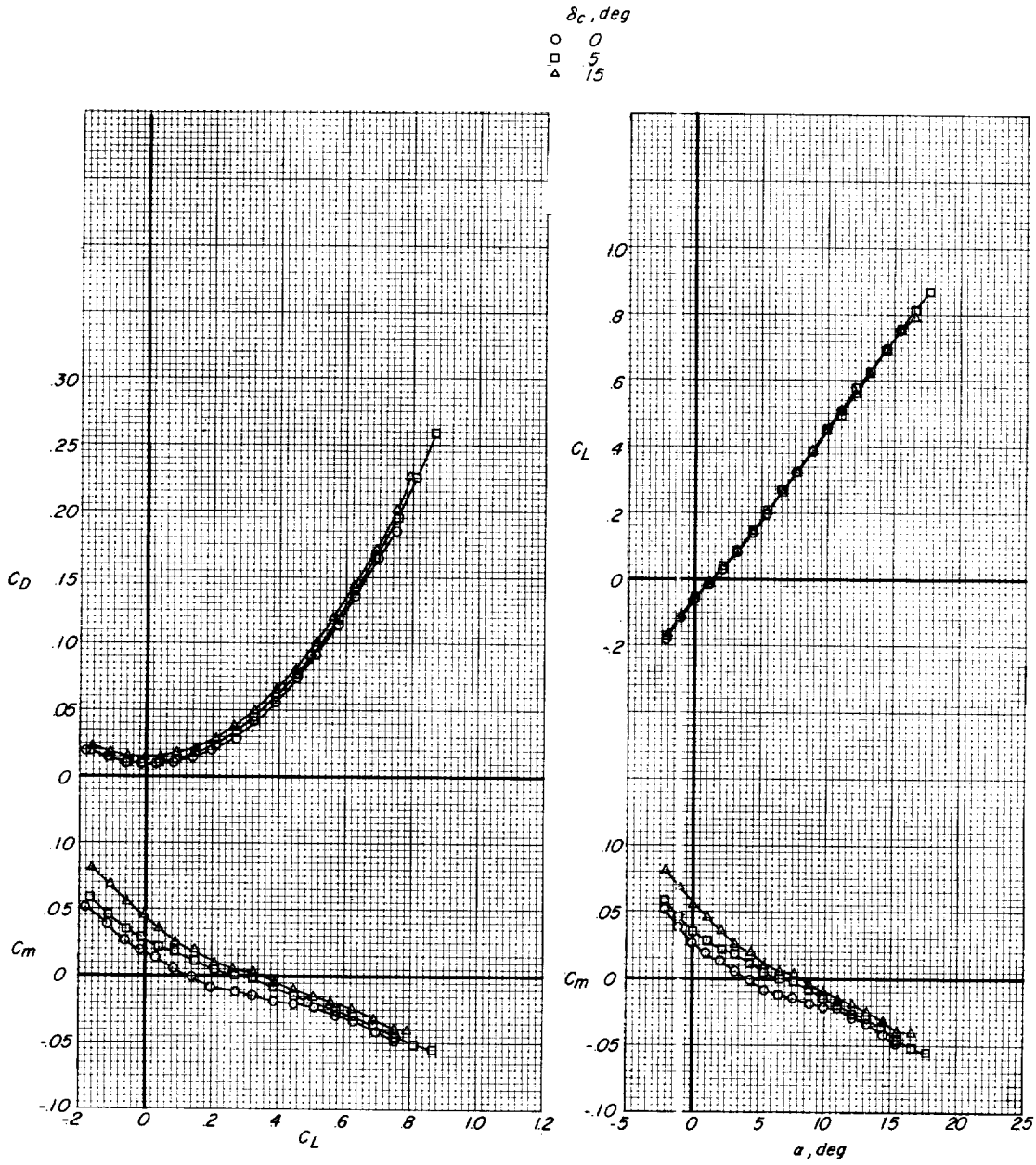

(c) M = 0.90.

Figure 15.- Continued.

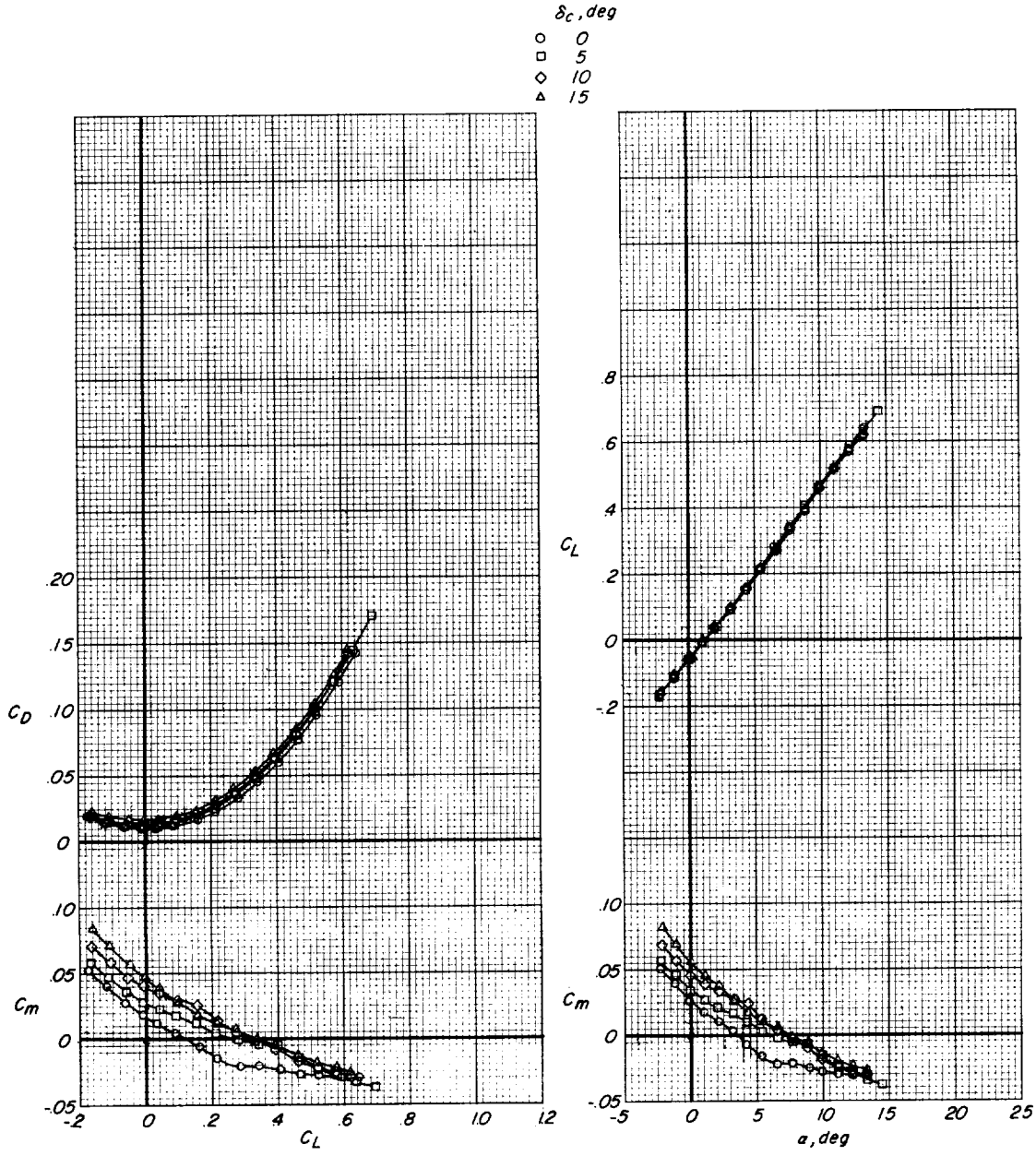

(d) M = 0.95.

Figure 15.- Concluded.

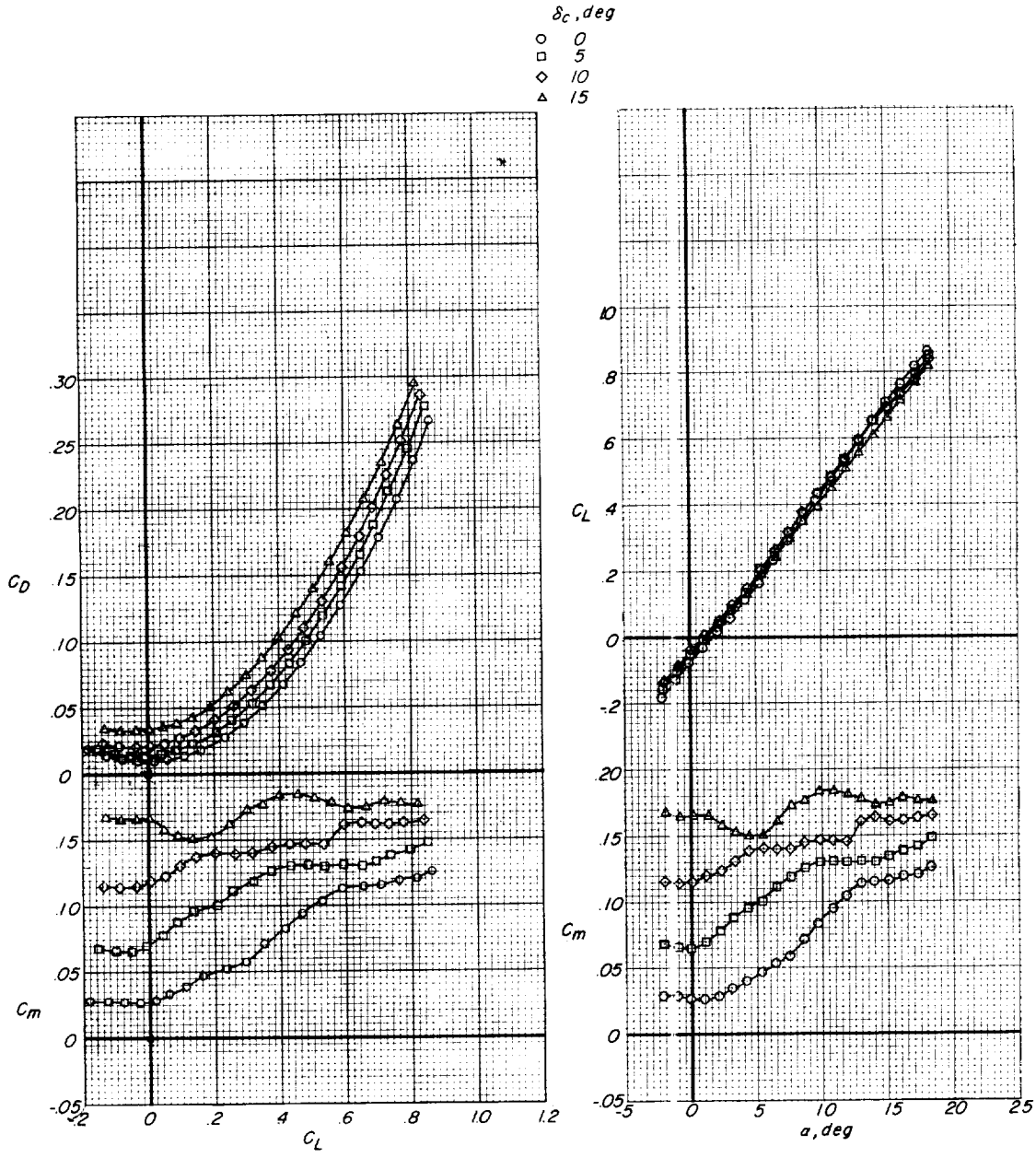

(a) M = 0.60

Figure 16.- Static longitudinal stability characteristics for canard model with various control deflections of large canard surface ($W_1FV_1C_3$). Transition free.

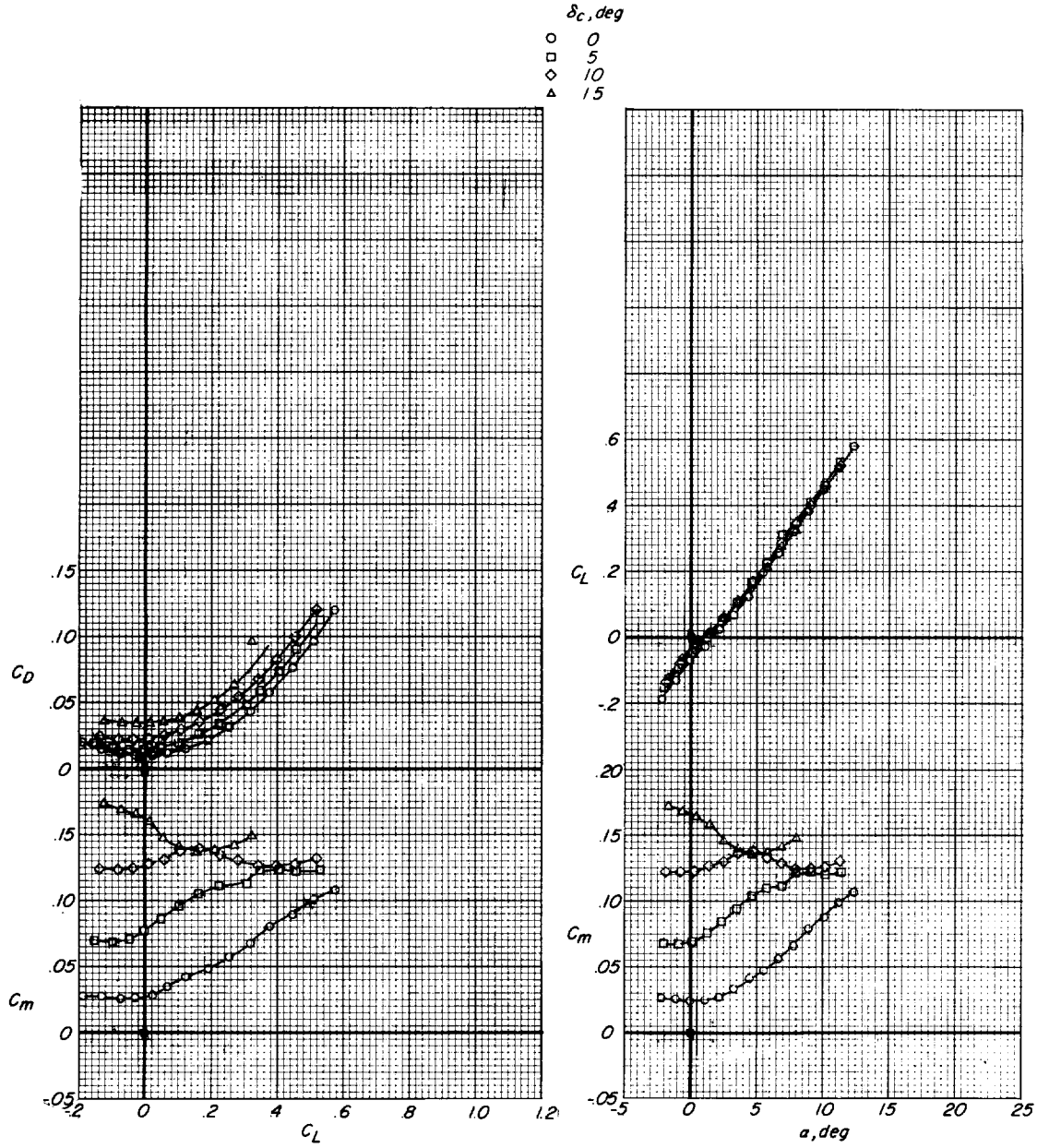

(b) M = 0.80.

Figure 16.- Continued.

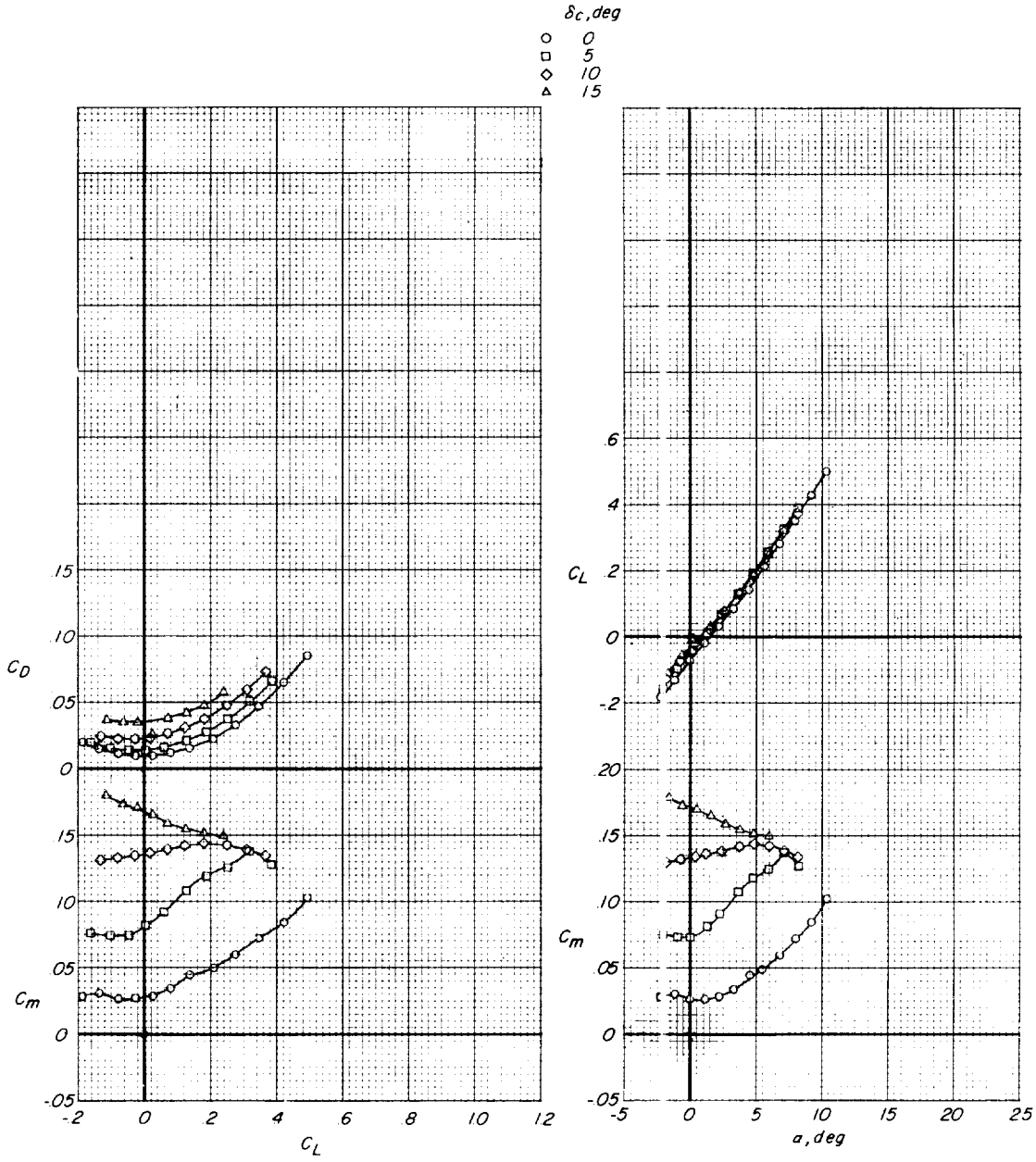

(c) M = 0.90.

Figure 16.- Concluded.

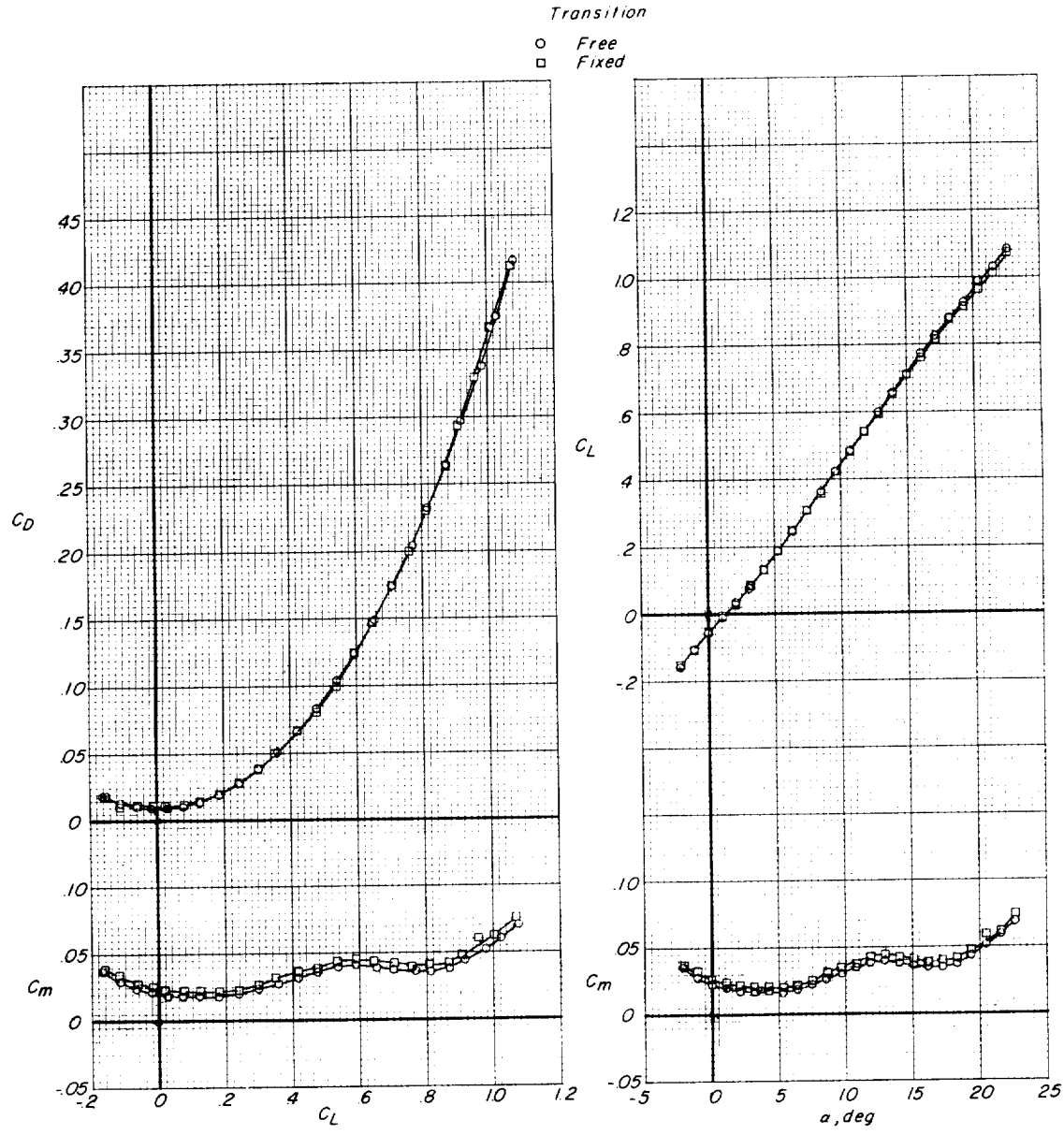

(a) M = 0.60.

Figure 17.- Static longitudinal stability characteristics for canard model having medium canard surface with free and fixed transition ($W_1FV_1C_1$). $\delta_c = 0^o$.

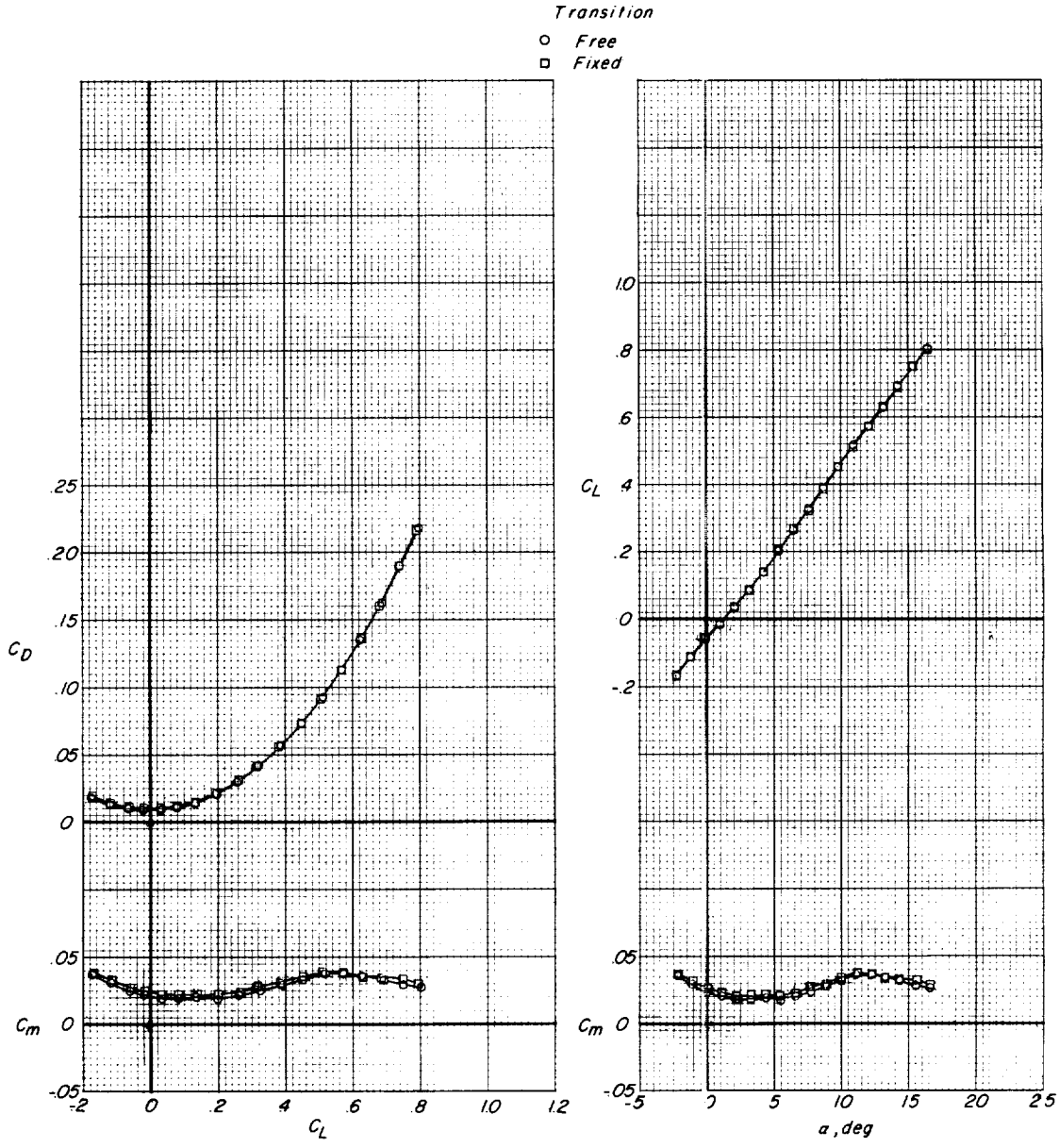

(b) M = 0.80.

Figure 17.- Continued.

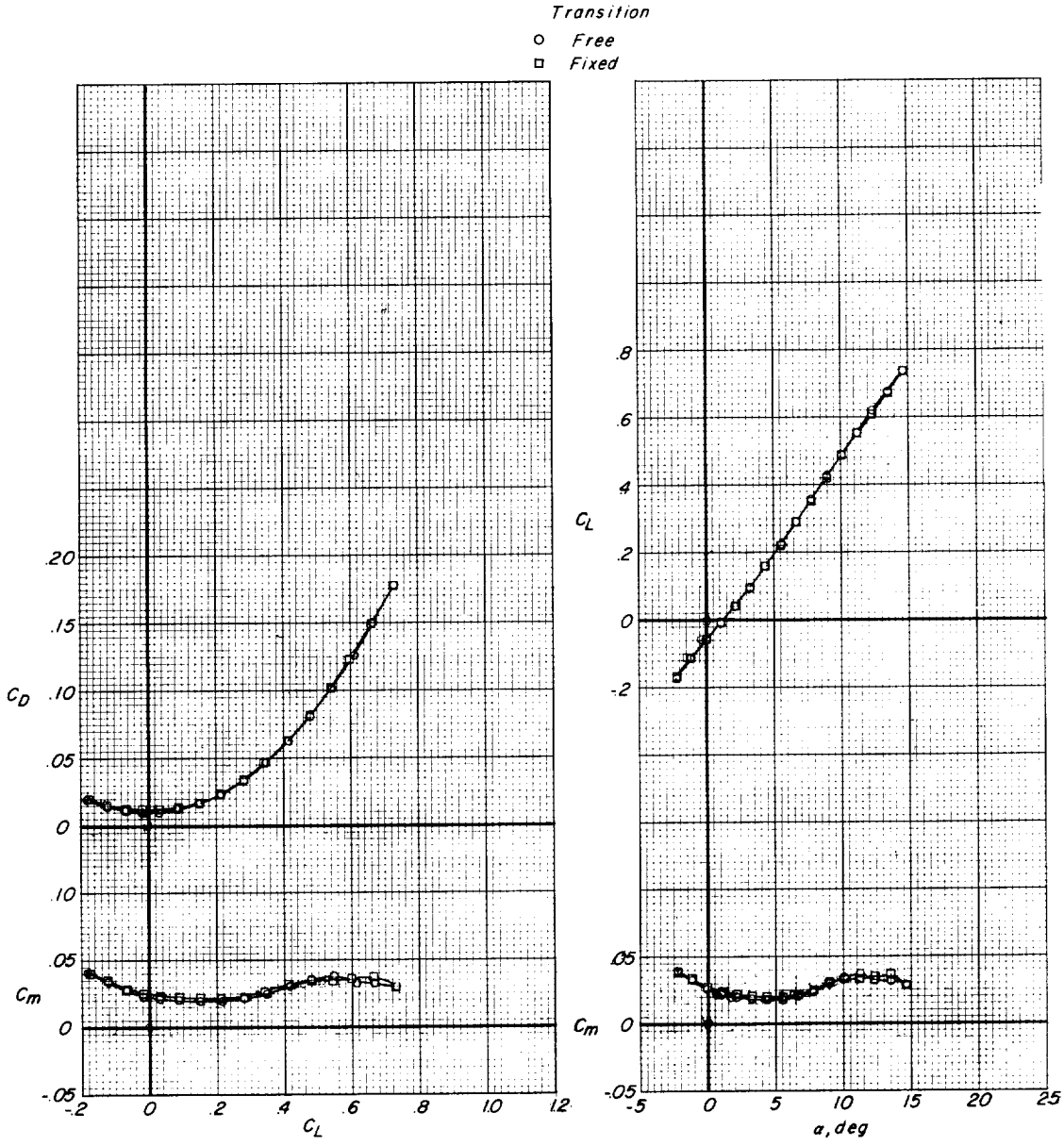

(c) M = 0.90.

Figure 17.- Continued.

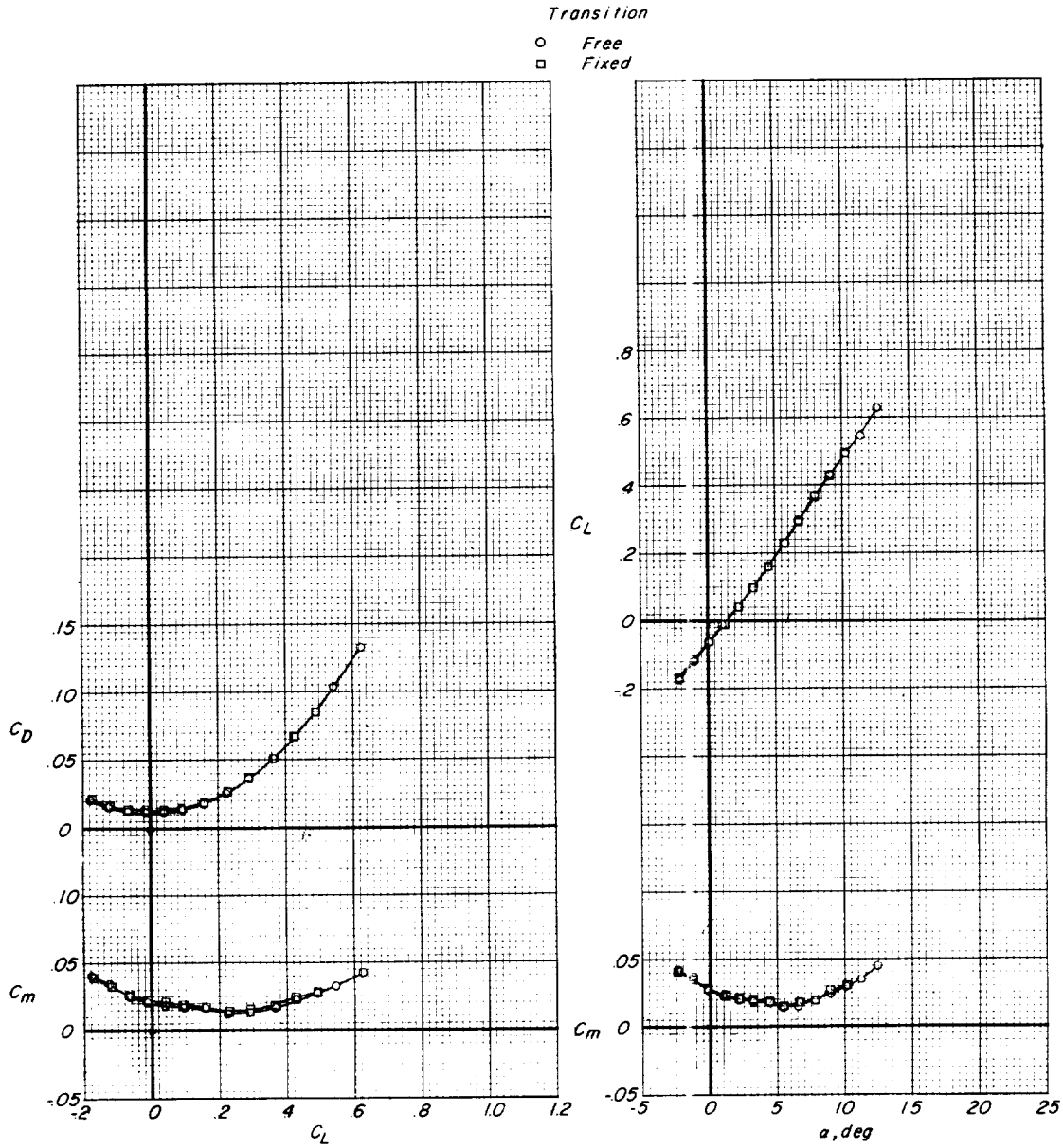

(d) M = 0.95.

Figure 17.- Concluded.

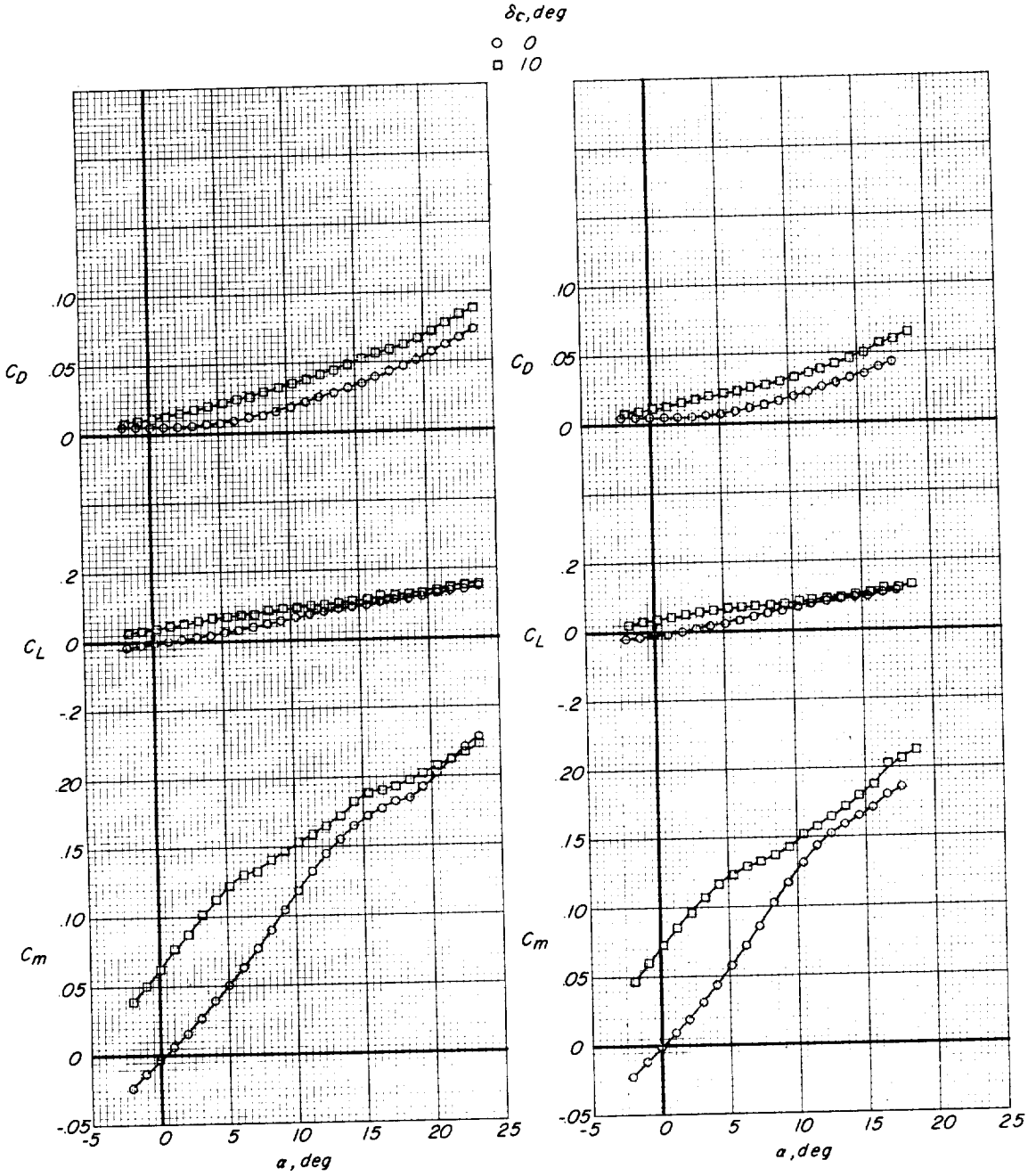

(a) M = 0.60 and 0.80.

Figure 18.- Static longitudinal stability characteristics for canard model less wing with two control deflections of medium canard surface (FV_1C_1). Transition free.

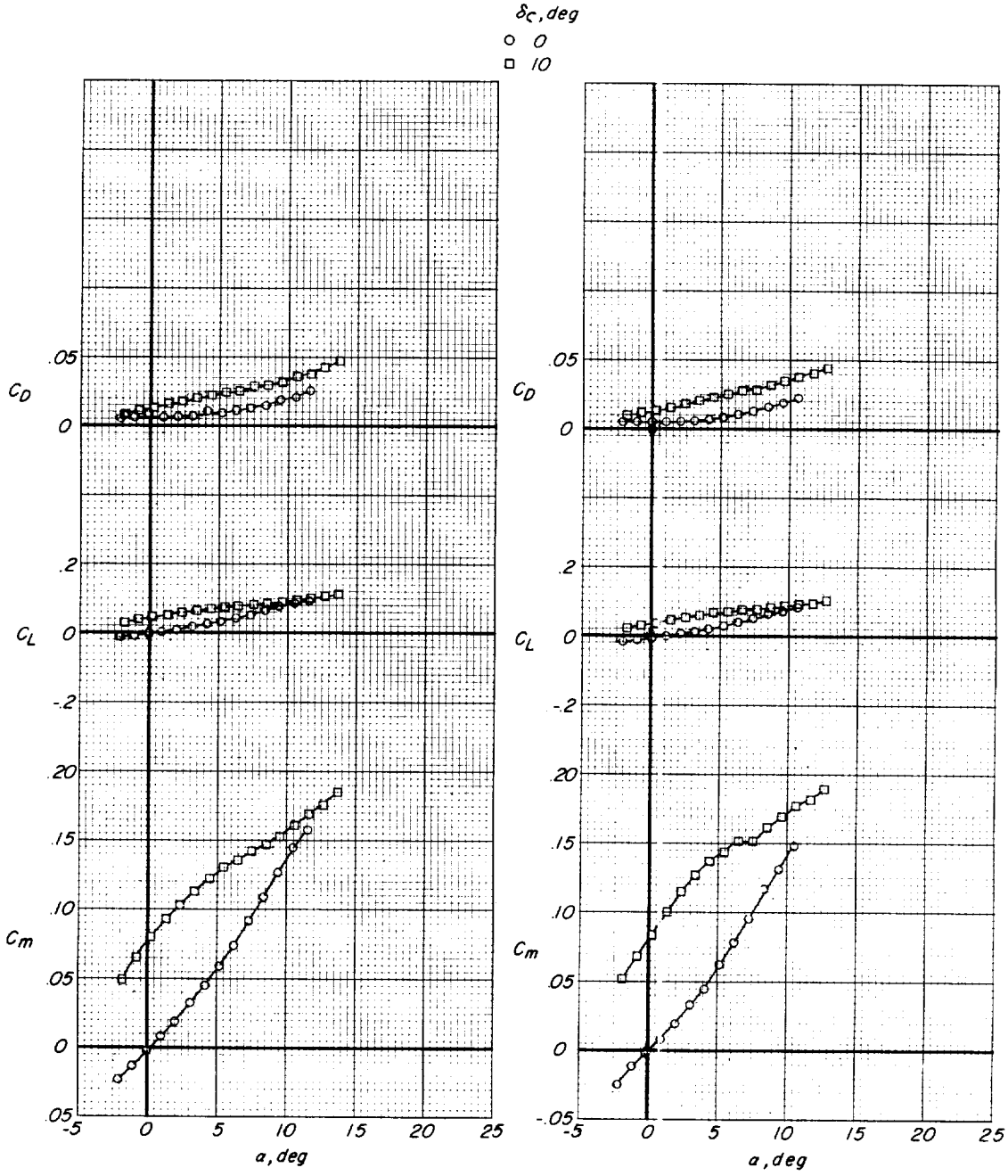

(b) M = 0.90 and 0.95.

Figure 18.- Concluded.

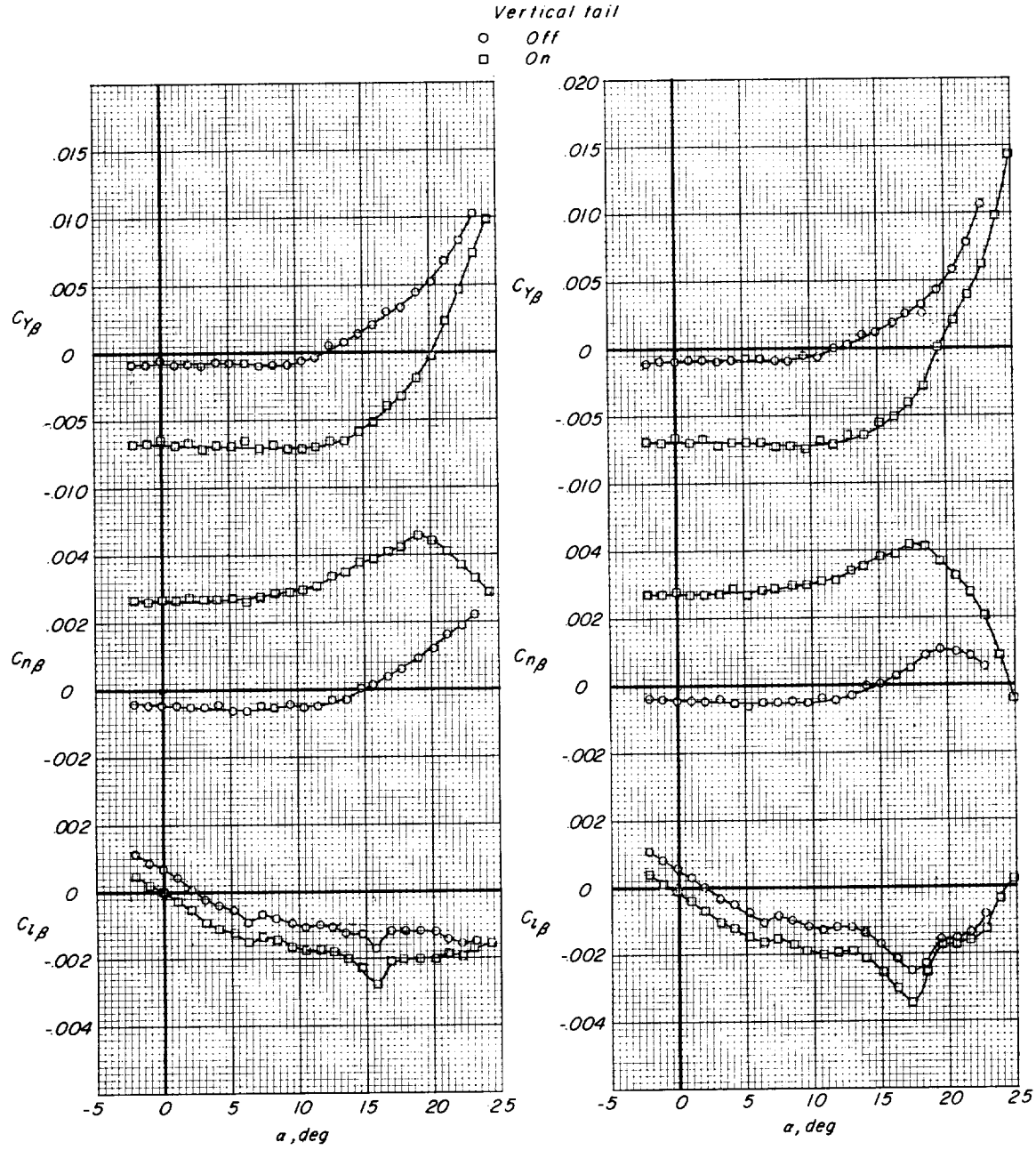

(a) M = 0.60 and 0.80.

Figure 19.- Variation of static lateral stability derivatives with angle of attack for canard model with and without vertical tail. Transition free; canard surface off.

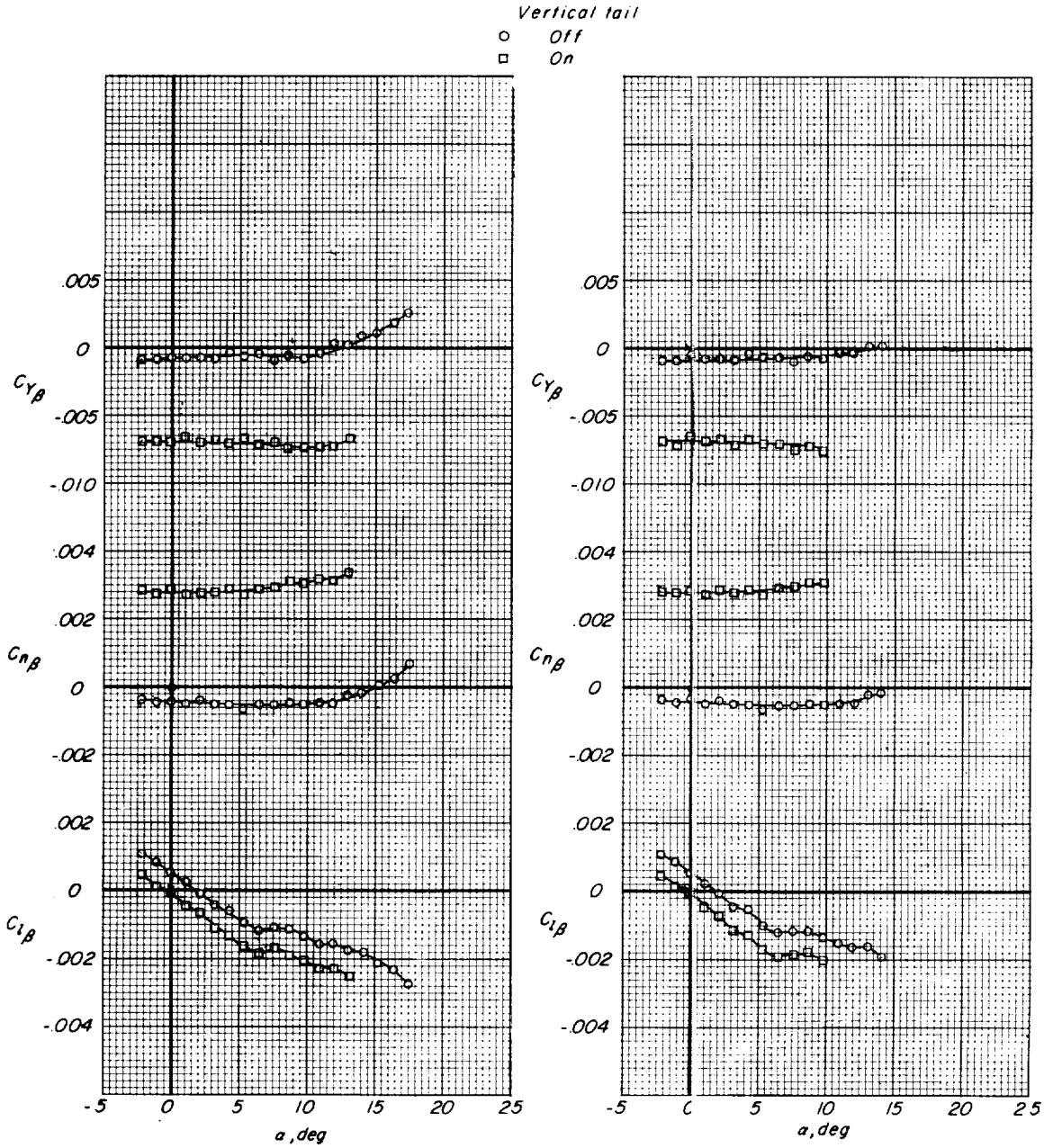

(b) M = 0.90 and 0.95.

Figure 19.- Concluded.

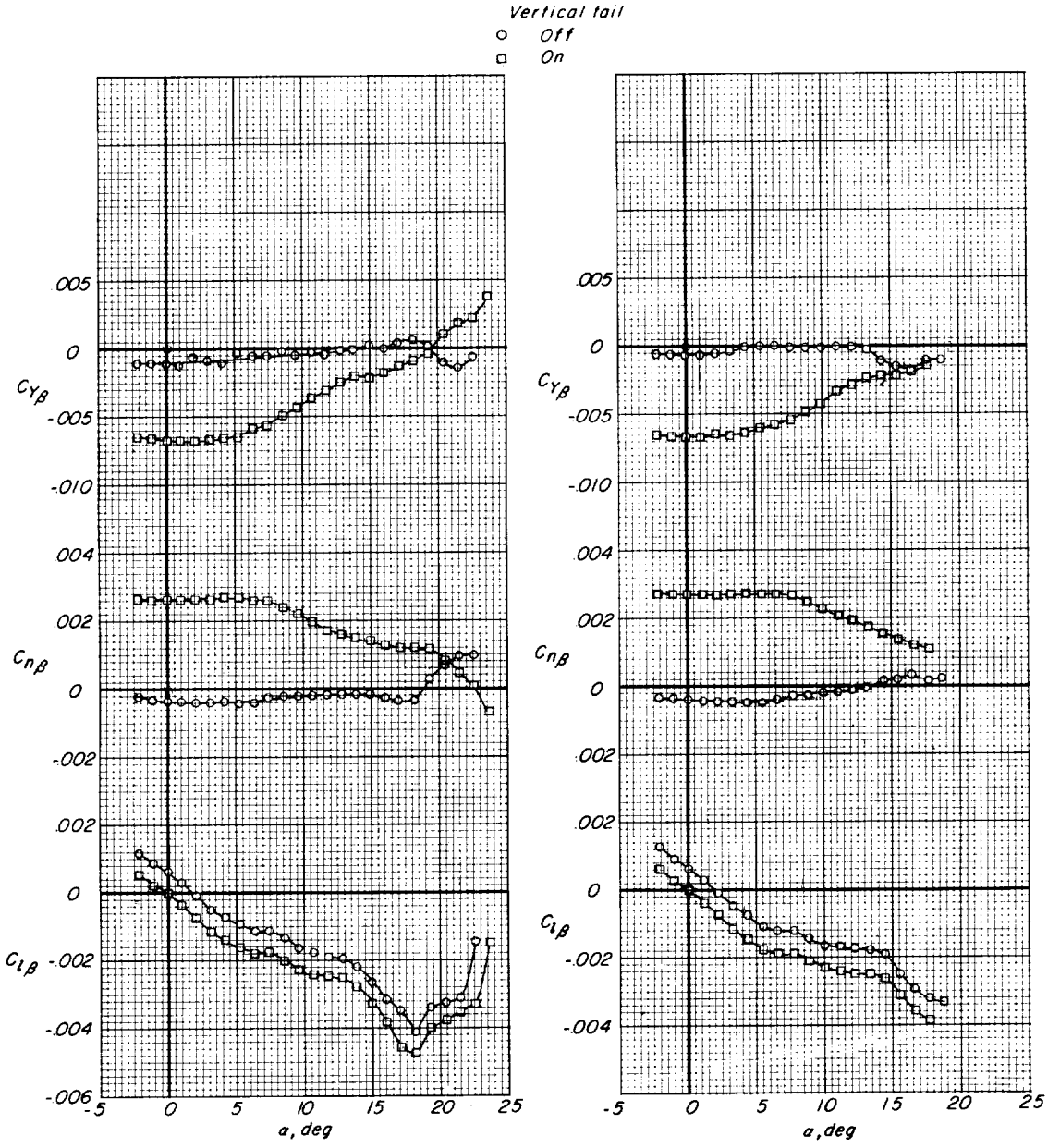

(a) M = 0.60 and 0.80.

Figure 20.- Variation of static lateral stability derivatives with angle of attack for the canard model with the medium canard surface and with and without vertical tail. Transition free; $\delta_c = 0^o$.

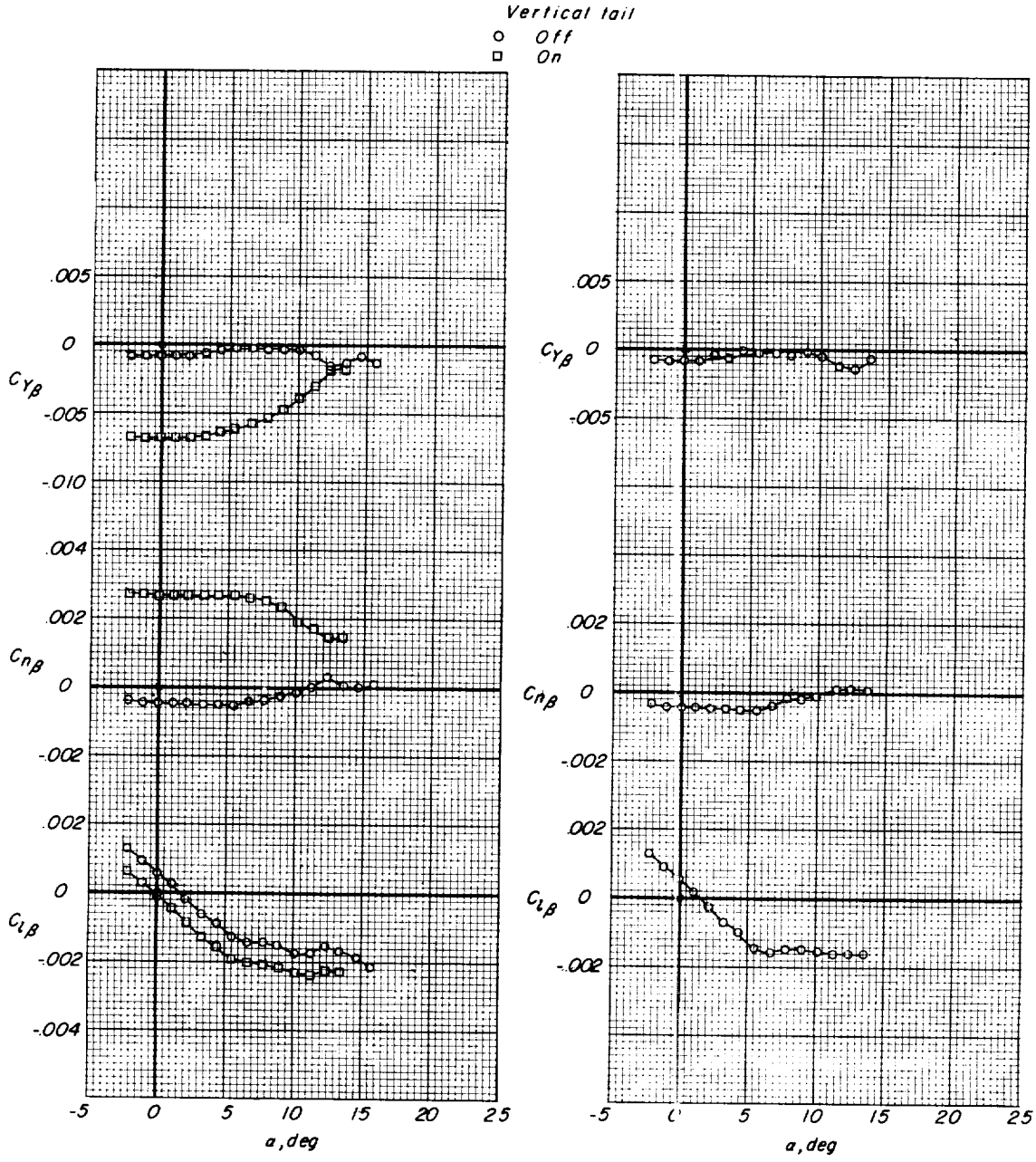

(b) M = 0.90 and 0.95.

Figure 20.- Concluded.

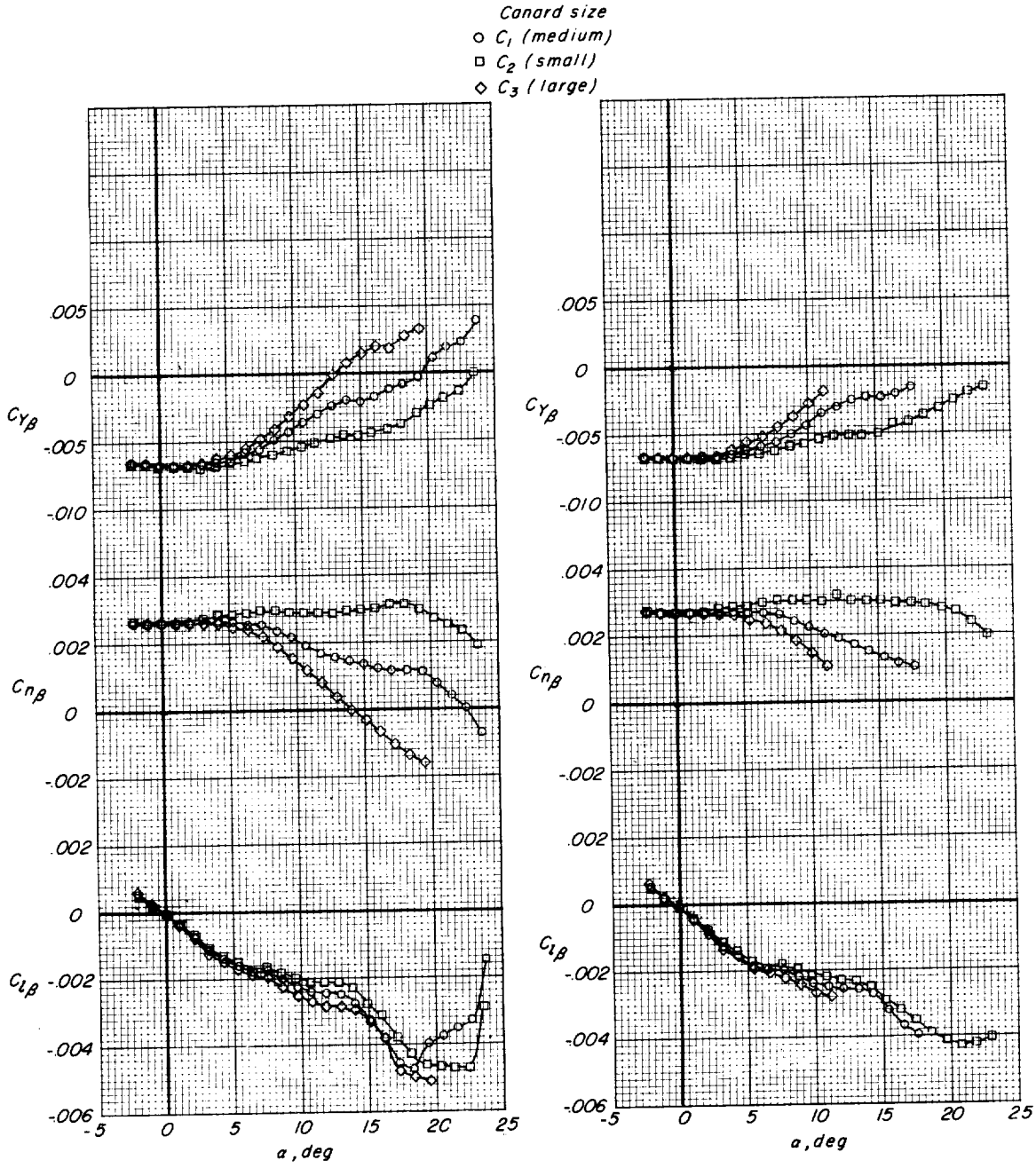

(a) M = 0.60 and 0.80.

Figure 21.- Variation of static lateral stability derivatives with angle of attack for complete canard model with three canard-surface sizes. Transition free; $\delta_c = 0^o$.

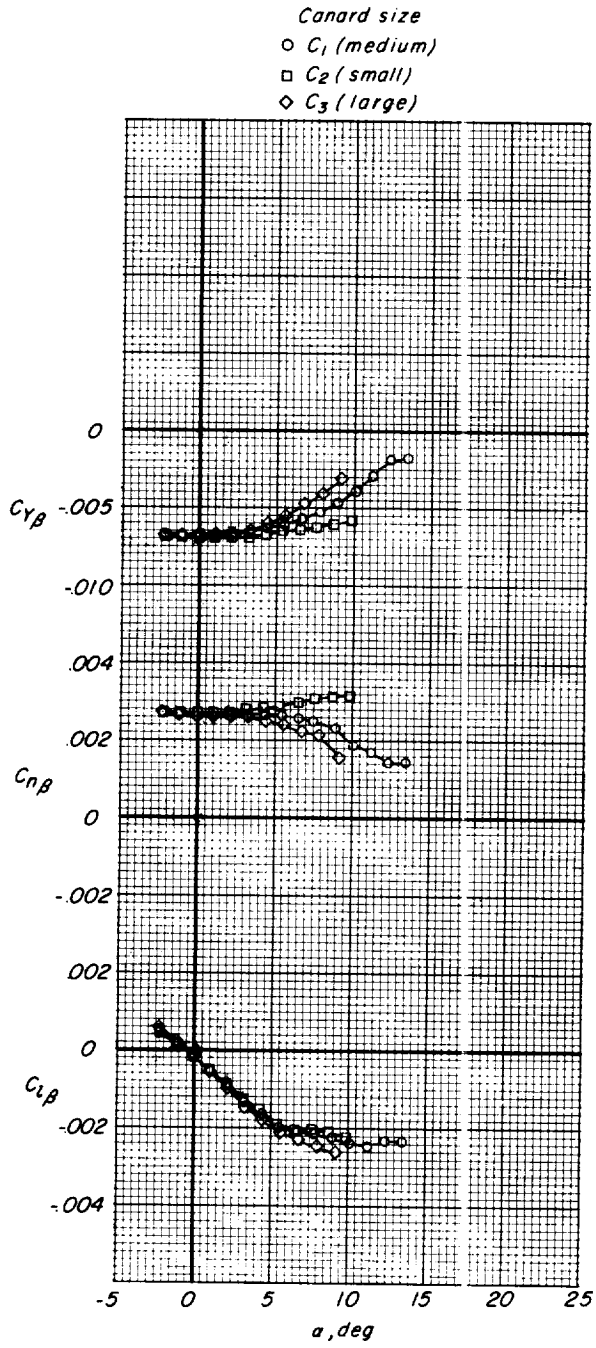

(b) M = 0.90.

Figure 21.- Concluded.

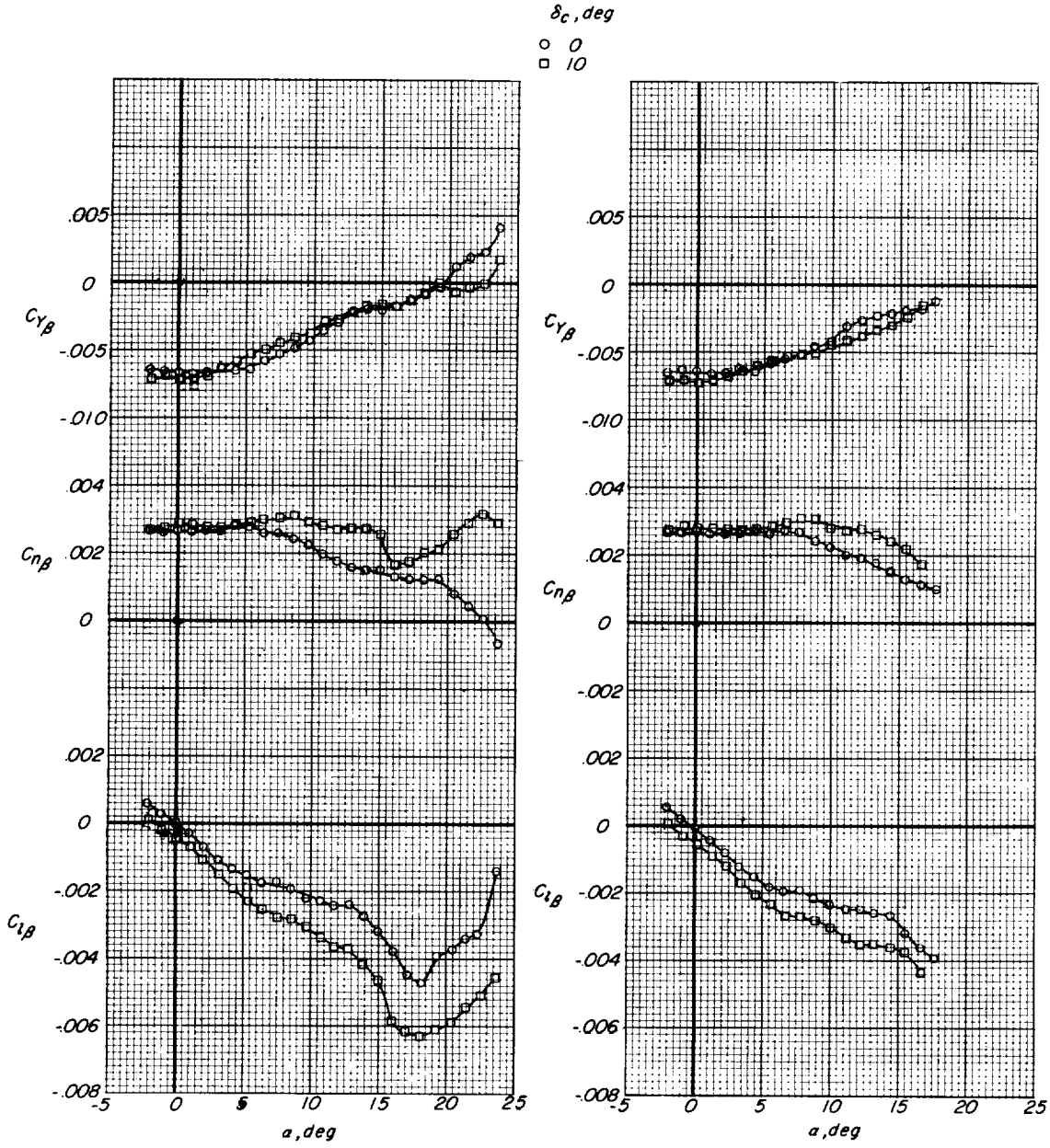

(a) M = 0.60 and 0.80.

Figure 22.- Variation of static lateral stability derivatives with angle of attack of canard model with medium canard surface deflected at two angles ($W_1FV_1C_1$). Transition free.

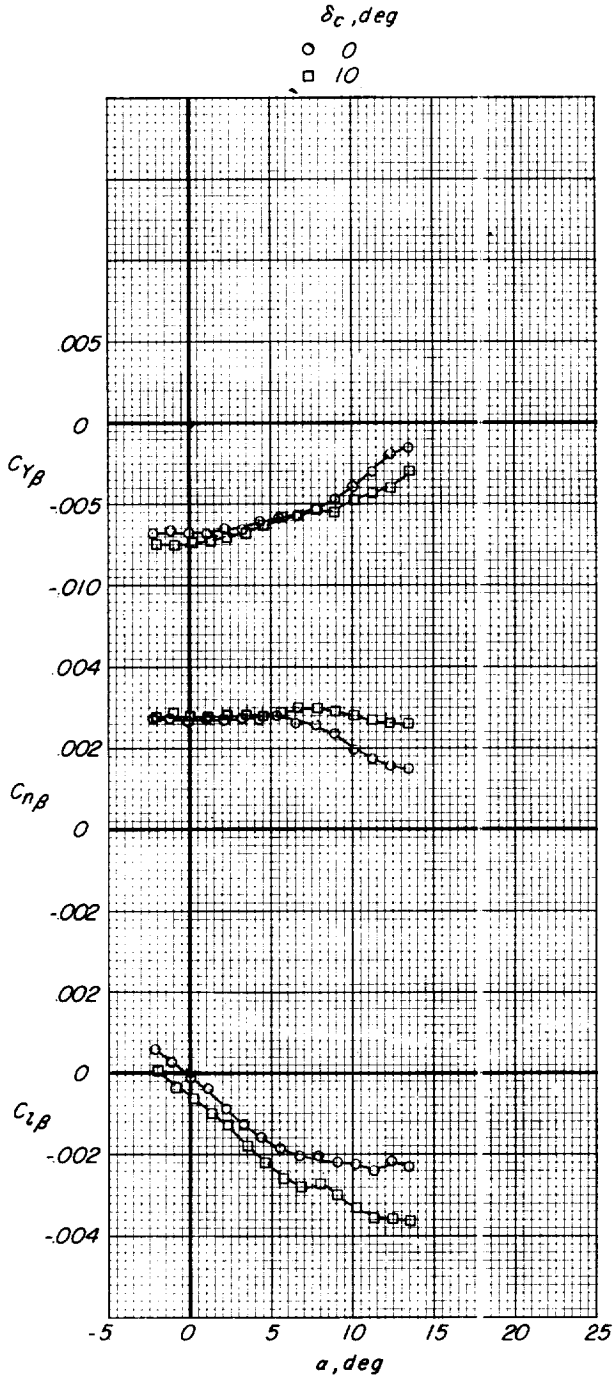

(b) M = 0.90.

Figure 22.- Concluded.

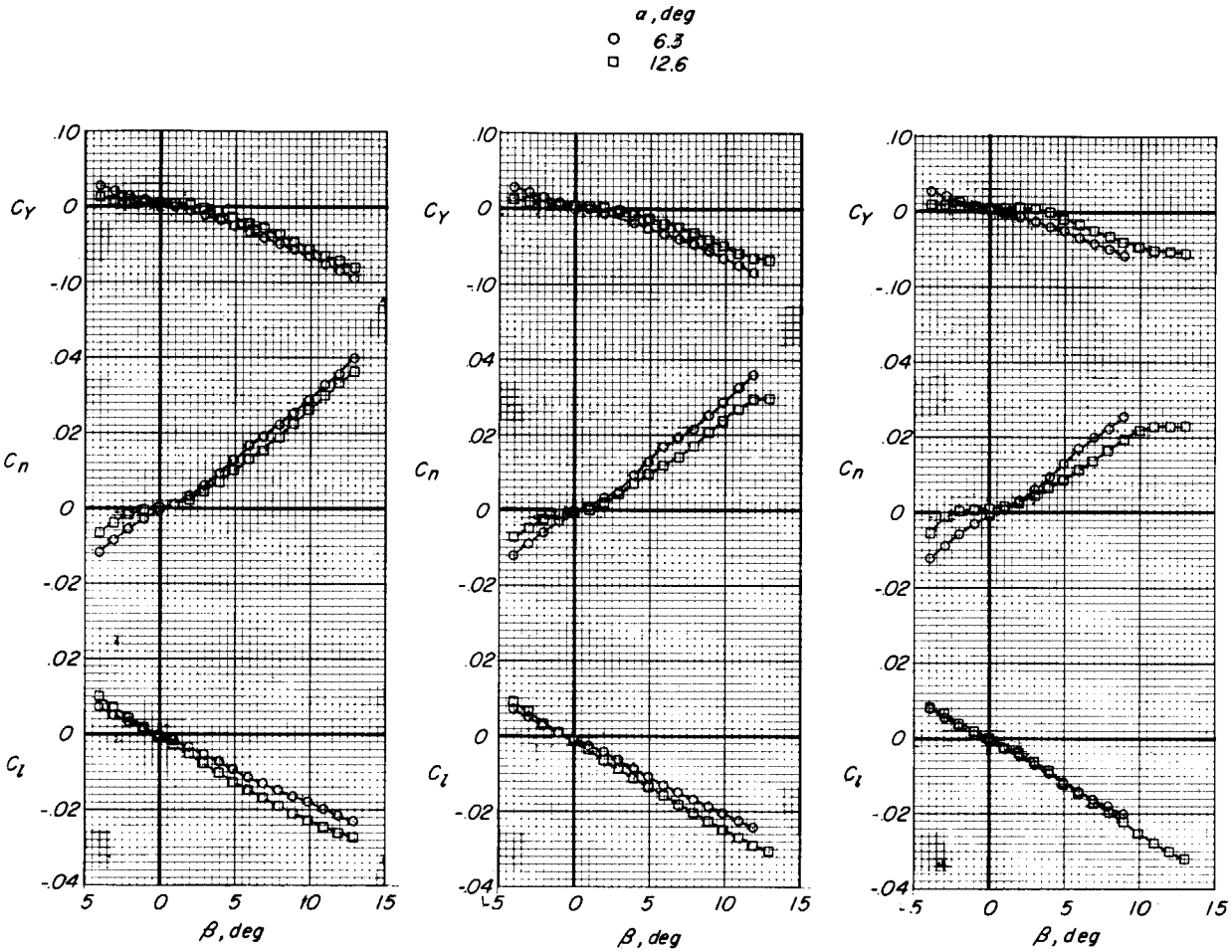

(a) M = 0.60. (b) M = 0.80. (c) M = 0.90.

Figure 23.- Static lateral stability characteristics for canard model with medium canard surface at two angles of attack ($W_1FV_1C_1$). Transition free; $\delta_c = 0^o$.